

JUNE 1990

LIDS-P-1985

$H_\infty$  OPTIMAL CONTROL FOR THE ATTITUDE CONTROL AND  
MOMENTUM MANAGEMENT OF THE SPACE STATION

by

A. Pothiwala  
M.A. Dahleh

Laboratory for Information and Decision Systems  
Massachusetts Institute of Technology  
Cambridge, MA 02139

---

This research is partially supported by the U.S. Army Research Office,  
contract DAAL03-86-K-0171 (Center for Intelligent Control Systems),  
and by the National Science Foundation grant NSF 8810178-ECS.

# **$H_\infty$ Optimal Control for the Attitude Control and Momentum Management of the Space Station**

## **ABSTRACT**

The basic problem in designing control systems is the ability to achieve good performance in the presence of uncertainties such as output disturbances, measurement noise or unmodelled dynamics (i.e. robust controllers). Recent development in the area has been directed towards developing a consistent design methodology within this uncertain environment. Examples of these are  $H_2$ ,  $H_\infty$ , and  $L^1$  optimization problems.

The attitude control/momentum management of the space station poses a typical problem in an uncertain environment (mass properties of the Space Station and environmental disturbances). The objective of this research is to use the  $H_\infty$  optimality criterion to design a controller for the linearized set of Space Station dynamics equations. Besides studying the various closed-loop properties of the resulting linear system, we would like to examine the robustness properties of this controller i.e. how well it performs in the presence of unmodelled dynamics, non-linearities and disturbances. Furthermore, we will compare and contrast the control action of the  $H_\infty$  controller with that of the LQR controllers.

# I INTRODUCTION

## OVERVIEW

Considered here is the attitude control and momentum management of the space station.

The space station will employ CMGs (control moment gyros) as a primary actuating device during normal flight mode operation. The objective of the CMG flight control system is to hold the space station at a fixed attitude relative to the LVLH frame. In the presence of continuous environmental disturbances CMGs will absorb momentum in an attempt to maintain the Space Station at a desired attitude. The CMGs will eventually saturate, resulting in loss of effectiveness of the CMG system as a control effector. Some kind of momentum management scheme (MMS) is necessary to allow the CMGs to hold a desired attitude profile and at the same time prevent CMG saturation. In the performance of momentum management, the Space Station user requirements should be met, and the momentum storage requirements should be minimized. Since the CMGs are momentum exchange devices, external control torques must be used to desaturate the CMGs, that is, bring the momentum back to nominal value. Some methods for unloading CMG momentum include the use of magnetic torques, reaction jets, and gravity gradient torque. For the space station, the gravity gradient torque approach is preferred since it requires no consumables or external hardware. For this reason, various schemes using gravity gradient torque have been developed.

Two approaches to momentum management using gravity gradient torque are possible. The first of these is a "discrete" or "periodic" momentum control approach which is basically a feedforward open-loop control scheme [6]. This scheme utilizes appropriate samples of CMG momentum, with the sampling frequency of the same order as the orbital frequency. This approach, as well as the "predictive" approach, can handle expected momentum changes; however, it requires accurate inertia matrix properties and environmental models to generate the proper attitude steering command. In the "discrete" or "periodic" approach, the attitude controller, with a much higher control bandwidth, is designed

independently.

The second approach to CMG momentum management, which will be considered here, is the "continuous" approach. Using a continuous time control scheme permits us to integrate the attitude control and momentum management of the space station into one control problem. In this continuous, closed-loop control of both the CMG momentum and station attitude, the design objective is to establish a proper tradeoff between station pointing and CMG momentum management, while satisfying the specific mission requirements.

Expanding on this "continuous" approach, we intend to present a different scheme to the space station momentum management and attitude control. The proposed controller, derived from the  $H_\infty$  optimality criterion, will provide a proper disturbance accommodation. As a result, the cyclic peak of the station attitude and CMG momentum oscillation caused by aerodynamic torque is minimized. For the purpose of this research, CMGs will be considered as ideal torquers; however, the CMG gimbal dynamics as well as the CMG steering law should be included in the further development of an efficient control law for the overall system. Structural flexibility of the space station is neglected because of the low bandwidth nature of the integrated momentum/attitude controller. It is assumed that a strapdown inertial reference system provides relatively noise-free estimates of all states and that the body-axis components of the CMG momentum can be measured. Practical multivariable controller synthesis can also be accomplished by employing various techniques such as the classical control approaches, linear-quadratic-regulator (LQR) synthesis technique [10], asymptotic disturbance rejection, decentralized (partial state feedback) control, and robust eigensystem assignment techniques.

## **OBJECTIVES OF ATTITUDE CONTROL/MOMENTUM MANAGEMENT**

1. to minimize excursions of the station body frame from the LVLH frame
2. to minimize peak cyclic momentum
3. to remove accumulated momentum

The objective of a MMS is to utilize available environmental torques

(aerodynamic or gravity gradient) acting on the Space Station to control and maintain CMG angular momentum. Given that environmental torques act continuously on the station, the CMGs must produce, on the average, torques on the station equal and opposite to the undesired portion of the environmental disturbance torques. If, however, the environmental torques can be properly altered by Space Station attitude manipulation, then the required CMG torques can be zeroed. Although this can not be accomplished exactly, the torque demands on the CMGs can be significantly reduced by utilizing environmental torques.

## ENVIRONMENTAL DISTURBANCE TORQUES

### GRAVITY GRADIENT TORQUES

Body axes gravity gradient torques are a function of the vehicle orbital rate, the inertia matrix, and the angles between the LVLH frame and the body reference frame. Over the life of the Space Station, there will be large changes in mass properties, different prescribed vehicle attitudes, and different orbit attitudes. All these significantly change the gravity gradient torques acting on the Space Station. For the case with no articulating surfaces and constant attitude, the gravity gradient torques are constant body axes torques causing momentum to accumulate about the inertial direction perpendicular to the orbital plane (inertial y direction), and cyclic momentum relative to inertial axes in the orbital plane (x and z inertial axes). Articulating masses, such as solar panels and radiator rotation, have the effect of super imposing a sinusoidal component onto the constant torque component. Assuming small angles and negligible cross products of inertia ( $I_{xy}, I_{yz}, I_{xz} = 0$ ) :

$(\psi, \theta, \phi)$  : yaw, pitch, and roll euler angles  
 $(I_x, I_y, I_z)$  : moment of inertia about the x, y and z axes

$$g_x = 1.5\omega_o^2 \left[ (I_z - I_y) s 2\Phi c^2\theta - 2I_{yz} c^2\theta c 2\Phi - I_{xz} s 2\theta s\Phi + I_{xy} s 2\theta c\Phi \right] \quad (1.1)$$

$$g_y = 1.5\omega_o^2 \left[ (I_z - I_x) s 2\theta c\Phi - 2I_{xz} (s^2\theta - c^2\Phi c^2\theta) + I_{yz} s 2\theta s\Phi + I_{xy} s 2\Phi c^2\theta \right] \quad (1.2)$$

$$g_z = 1.5\omega_o^2 \left[ (I_x - I_y) s 2\theta s\Phi - 2I_{xy} (s^2\Phi c^2\theta - s^2\theta) - I_{xz} s 2\Phi c^2\theta - I_{yz} c\Phi s 2\theta \right] \quad (1.3)$$

Since the gravity gradient torques are a function of station attitude relative to LVLH, they can be changed by changing the station attitude, and thus can be utilized for CMG desaturation. It is for this reason that angular perturbations can not be totally eliminated ( $g_x$ ,  $g_y$ ,  $g_z$  can not be zero since needed for desaturation).

## AERODYNAMIC TORQUES

The aerodynamic disturbance is a bias (i.e. non zero average over one orbit) plus a cyclic torque in the body reference frame, and causes accumulated momentum as well as cyclic momentum relative to the inertial frame. The time varying aerodynamic torque profile is due to a combination of a varying density around the orbit and articulating surfaces. Because of the diurnal bulge, the torques are cyclic around an offset, but not symmetric about that offset. That is, the torque profile is biased to one side of the offset. In the torque profiles where there are articulating solar panels and radiators, there are sharp peaks in the profile due to the rotation of the solar panels. This type of profile would be difficult to explicitly model. Aerodynamic torques result in an accumulated momentum in all three inertial axes. Most of the accumulated momentum about x and z is due to the rotating atmosphere, while most of the accumulated momentum about the y axes is due to center of pressure/center of gravity offset.

## LITERATURE SURVEY

Both discrete and continuous attitude adjustment strategies have been developed for gravity gradient management of CMG momentum. Discrete methods command specific offset attitudes for limited time intervals, while continuous strategies constantly regulate attitude offsets. Linear quadratic regulator derived gains as well as others have been used as an efficient basis for feedback design [10].

Studies applied to proposed NASA Space Station designs have used both continuous and discrete momentum management features. All schemes focus on approximate maintenance of torque equilibrium attitude (TEA). Offsets from true local vertical must vary with time to deal with atmospheric density variations and articulating saturation parts.

Methods to adaptively seek TEA, using momentum state feedback, have been devised to avoid disturbance estimation [11]. In a specific variation of this approach considered earlier by a Space Station program contractor, an active, continuous TEA seeking, closed-loop controller is applied while fixing yaw [12]. Pitch and roll control are decoupled in the momentum manager which generates maneuver commands executed by the attitude controller to keep total average momentum centered. Another contractor concept accommodates "fading in" of a discrete, fixed TEA maintenance momentum management strategy when disturbances reach an equilibrium. This would follow phases of vehicle/controller TEA self seeking, and tuning [13]. TEA adjustments are determined by sensing CMG momentum, and using gravity gradient and inertial environmental model data.

Several challenges are encountered by the momentum management strategies above and other proposals for the Space Station. Included are: development of appropriate dynamics decoupling strategies when dealing with large mass property variations and vehicle flight orientations during buildup; limiting maximum attitude excursions from true local vertical to allow instrument pointing; limiting momentum dumping maneuver magnitudes over short time intervals to avoid high maneuver rates. Two momentum management algorithms have been studied extensively, jointly by NASA and Draper Laboratory to assess continuous and discrete

momentum management relative merits. Some challenges created by trying to adapt to Space Station buildup effects have also been identified in this work. The first method, developed at the Johnson Space Center (JSC) uses a discrete momentum dumping strategy [6]. The second method, developed at Draper, uses environment predictions and momentum state feedback to continuously manage stored momentum and reduce peak storage requirements [14].



## II HIGHLIGHTS OF THE $H_\infty$ DESIGN METHODOLOGY

### DEFINITION OF $H_\infty$

$H_\infty$  is a set of all matrix functions,  $G$ , that are analytic in the right half plane and whose  $\infty$  norm is bounded i.e.  $\|G\|_\infty \equiv \sup \sigma_{\max}[G(j\omega)] < \infty$ .  $G$  is "small" in  $H_\infty$  sense if the magnitude of the frequency response is small over all frequencies.

$H_\infty$  as 'Worst Case' Measure:

Suppose  $G(s) \in H_\infty$  with  $G(s) \in C^{m \times n}$ ;  $G(s)$  is linear time-invariant, has finite gain and is stable. Then there exists some constant  $\gamma > 0$  s.t

$$\|y\|_{L_2} = \|Gu\|_{L_2} \leq \gamma \|u\|_{L_2}$$

Thus,  $\gamma$  is a bound on the "L2 amplification" or "energy amplification".

Define the smallest such number,  $\gamma^*$ , as the "induced norm of  $G$ " or "gain of  $G$ ". Infact,  $\gamma^*$  is the infinity norm of  $G$  i.e.  $\gamma^* = \|G\|_{H_\infty}$

### MOTIVATION FOR THE $H_\infty$ DESIGN METHODOLOGY

The  $H_\infty$  design methodology, especially after recent results by Glover and Doyle [2] has demonstrated great potential as a multivariable control tool. The main reasons for choosing this optimality criterion as a design tool are cited below :

- Since its a relatively new design methodology, we would like to see how well it performs in comparison to LQR methodology..
- It provides a more general framework since this methodology can be

applied to all systems regardless of whether their outputs to be regulated are measurable or not.

- This methodology guarantees robustness to expected disturbances and plant uncertainty. The expected disturbances are specified through the weights chosen in the open loop model of the system.
- The objective of the space station control problem is to minimize the energy of the outputs for bounded energy disturbances. This induces the  $H_\infty$  optimality criterion.
- The  $H_\infty$  methodology will yield an optimal controller as long as the disturbances are of bounded energy. This is a much broader framework when compared to the  $H_2$ , or LQG, where the disturbances are white gaussian noise. Also  $H_\infty$  controllers are more robust in general compared to LQG compensators.

## GENERAL STRUCTURE

The general interconnection structure of a feedback system can be represented as in figure 1 where

$M(s)$ :	finite dimensional LTI system
$K(s)$ :	compensator
$w$ :	exogenous input vector (commands, disturbances, sensor noise etc.)
$z$ :	regulated output (any signal of interest; weighted errors, controls etc.)
$y$ :	measured output vector
$u$ :	control input vector

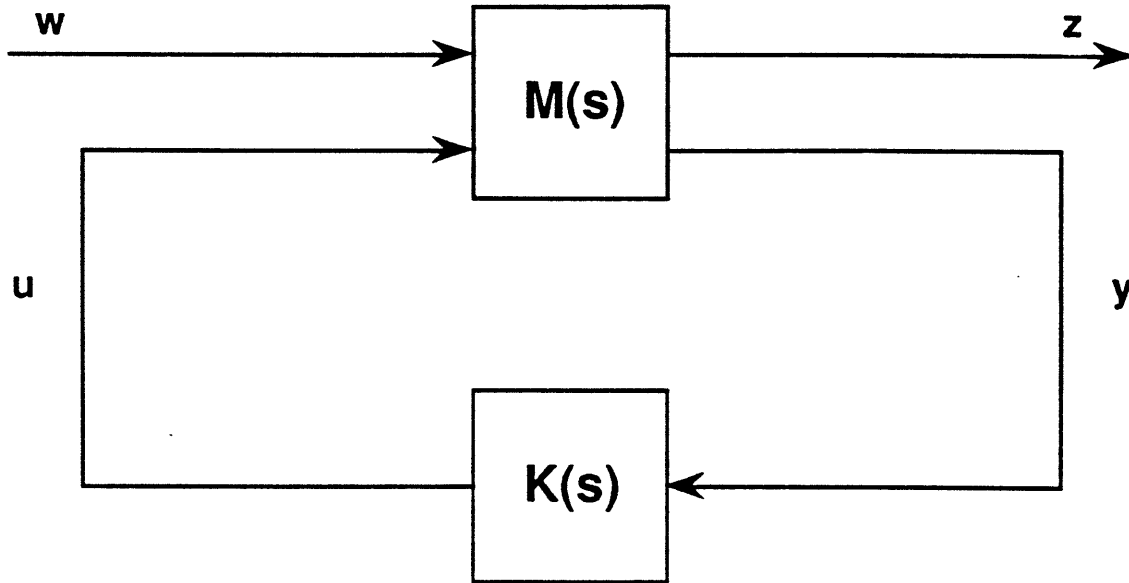


Fig. 1 General Framework

The objective in the  $H_\infty$  methodology is to find a stabilizing compensator,  $K(s)$ , such that the infinity norm of the transfer function  $H_{zw}(s)$  from  $w$  to  $z$  is minimized i.e.

$$\min_{\text{stabilizing } K(s)} \|H_{zw}(s)\|_\infty = \min_{\text{stabilizing } K(s)} \left( \sup_{\omega} \sigma_{\max} [H_{zw}(j\omega)] \right)$$

This can be interpreted in the time domain as minimizing the worst case energy of the output  $z$  ( $L_2$  norm) when the energy of the input  $w$  ( $L_2$  norm) is bounded. Viewing it in the frequency domain, this minimization implies that the worst case steady state amplitude of the output  $z$  is minimized when the input  $w$  is a bounded amplitude sinusoid.

The specifications can be used to condition the outputs (and/or inputs) with (stable) weights that are absorbed in the general system  $M(s)$ . Figure 2 shows the standard feedback loop transformed to the general framework.

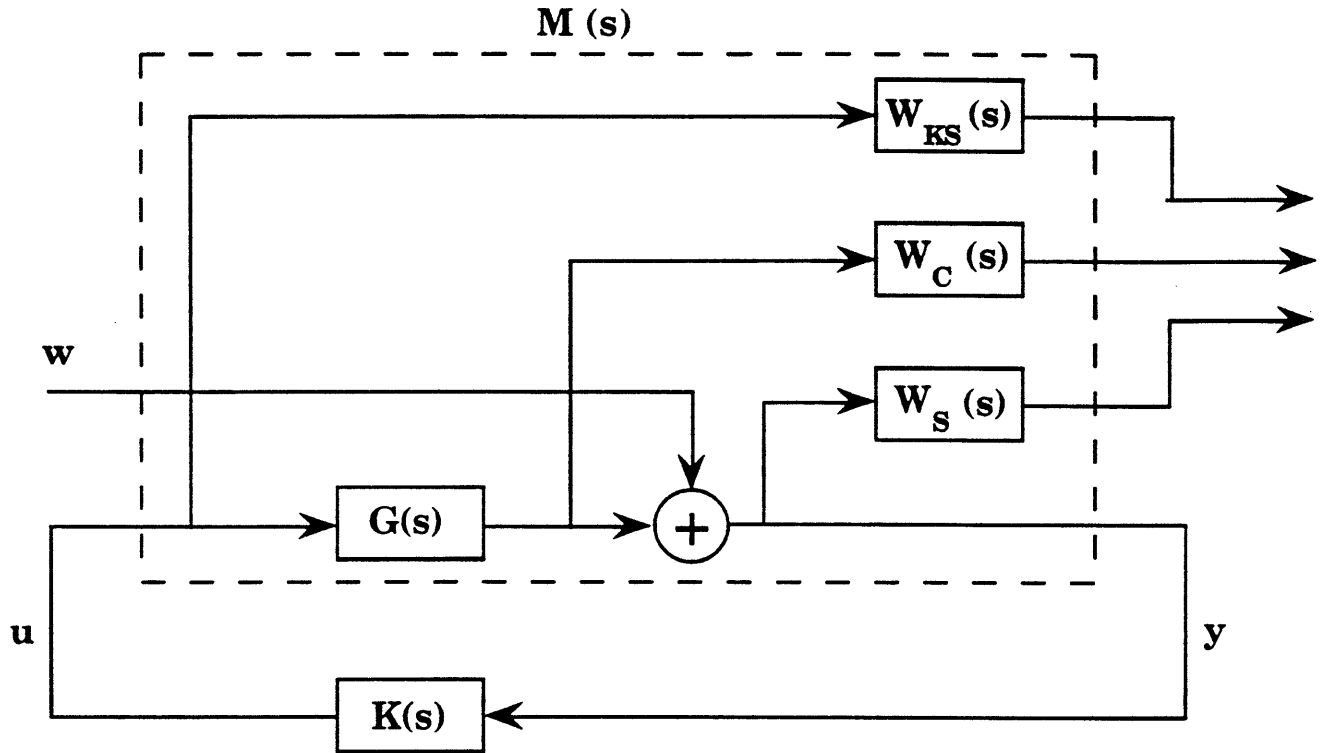


Fig. 2 : Standard feedback loop transformed to the general framework

In general, the solution of the  $H_\infty$  problem cannot be computed directly. However, a high level algorithm,  $g$  - iteration , can be used to find solutions arbitrarily close to the optimal. In particular, this iterative approach consists of finding stabilizing compensators that guarantee

$$\| H_{zw}(s) \|_\infty < \gamma \quad (2.1)$$

with

$$\gamma > \gamma_{\text{opt}} = \min_{\text{stabilizing } K(s)} ( \| H_{zw}(s) \|_\infty )$$

## GLOVER/DOYLE ALGORITHM

Recent results in the area of  $H_\infty$  synthesis by Doyle and Glover [15] provide a convenient method to solve the problem above by essentially solving two Riccati equations. This method is demonstrated below.

Let  $M(s)$  be partitioned as :

$$M(s) = \begin{bmatrix} M_{11}(s) & M_{12}(s) \\ M_{21}(s) & M_{22}(s) \end{bmatrix}$$

with each element having the state space representation

$$M_{ij}(s) = [A, B_j, C_i, D_{ij}] \quad ij = 1,2$$

The transfer functions  $M_{11}(s)$ ,  $M_{22}(s)$  must be strictly proper i.e.  $D_{11}$ ,  $D_{22}$  should be zero. If this is not the case, then high frequency poles must be added. Also  $M_{12}(s)$ ,  $M_{21}(s)$  should be proper but not strictly proper.

**Step 1 :** Guess a level of achievable performance  $\gamma$

**Step 2 :** Scale  $w$  and/or  $z$  so that the upper bound in (2.1) is 1 i.e

$$\| \tilde{H}_w(s) \|_\infty \leq 1 \quad \text{where } \tilde{H}_w(s) \text{ is appropriately scaled}$$

**Step 3 :** Scale  $u$  and  $y$  so that

$$D_{12}^T D_{12} = I \quad (2.2)$$

$$D_{21} D_{21}^T = I \quad (2.3)$$

Step 4 : The stabilizing compensator that achieves  $\| \tilde{H}_{zw}(s) \|_{\infty} \leq 1$  and, consequently,  $\| H_{zw}(s) \|_{\infty} \leq \gamma$  is given in figure 3

where

$Q(s)$  any stable system with

$$\| Q(s) \|_{\infty} < 1$$

and  $J(s)$  is given by the state space representation

$$J(s) = [A_J, B_J, C_J, D_J]$$

with

$$A_J = A \cdot K_F C_2 \cdot B_2 K_C + Y_{\infty} C_1^T (C_1 \cdot D_{12} K_C)$$

$$B_J = [K_F \quad K_{F1}]$$

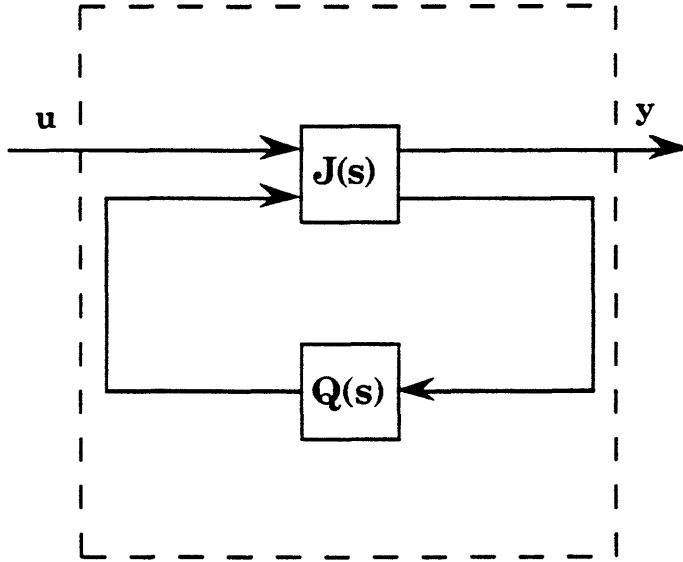


Fig. 3 : The  $H_{\infty}$  compensator structure

$$C_J = \begin{bmatrix} -K_C \\ K_{C1} \end{bmatrix}$$

$$D_J = \begin{bmatrix} 0 & -I \\ I & 0 \end{bmatrix}$$

$$K_C = (B^T X_\infty + D_{12}^T C_1)(I - Y_\infty X_\infty)^{-1}$$

$$K_{C1} = (D_{12} B_1^T - C_2)(I - Y_\infty X_\infty)^{-1}$$

Where  $X_\infty$  is the unique, real, symmetric solution of the Algebraic Riccati equation

$$(A - B_2 D_{12}^T C_1)^T X_\infty + X_\infty (A - B_2 D_{12}^T C_1) - X_\infty (B_2 B_2^T - B_1 B_1^T) X_\infty + C_1^T C_1 = 0$$

with

$$C_1 = (I - D_{12} D_{12}^T) C_1$$

$$K_F = (Y_\infty C_2^T + B_1 D_{21}^T)$$

$$K_{F1} = (Y_\infty C_1^T D_{12} + B_2)$$

and  $Y_\infty$  is the unique, real, symmetric solution of the Algebraic Riccati equation

$$(A - B_1 D_{21}^T C_2) Y_\infty + Y_\infty (A - B_1 D_{21}^T C_2)^T - Y_\infty (C_2^T C_2 - C_1^T C_1) Y_\infty + B_1 B_1^T = 0$$

with

$$B_1 = B_1 (I - D_{21}^T D_{21})$$

Initial  $\gamma$  is achievable if

$$X_\infty \geq 0$$

$$Y_\infty \geq 0$$

$$\lambda_{\max}(X_\infty Y_\infty) \leq 1$$

**Step 5:** Scale back  $u$  and  $y$  to their initial (before Step 3) scales.

A legitimate choice of  $Q(s)$  is  $Q(s) = 0$ . This choice of  $Q(s)$  will be used in the design. Thus a minimizing feedback might never be found, however we can get arbitrarily close to optimal.

### III SYSTEM DESCRIPTION AND MODEL DEVELOPMENT

#### BASIC RELATIONS

The basic relations required in the development of the attitude control and momentum management scheme are presented here.

Variables used :

$(\psi, \theta, \phi)$  : yaw, pitch, and roll euler angles.

$(I_x, I_y, I_z)$  : moment of inertia about the x, y, and z axes

$(h_x, h_y, h_z)$  : angular momentum of CMG system  
(roll axis momentum, pitch axis momentum, yaw axis momentum)

$(u_x, u_y, u_z)$  : reaction torque on space station from CMG system  
(control torques)

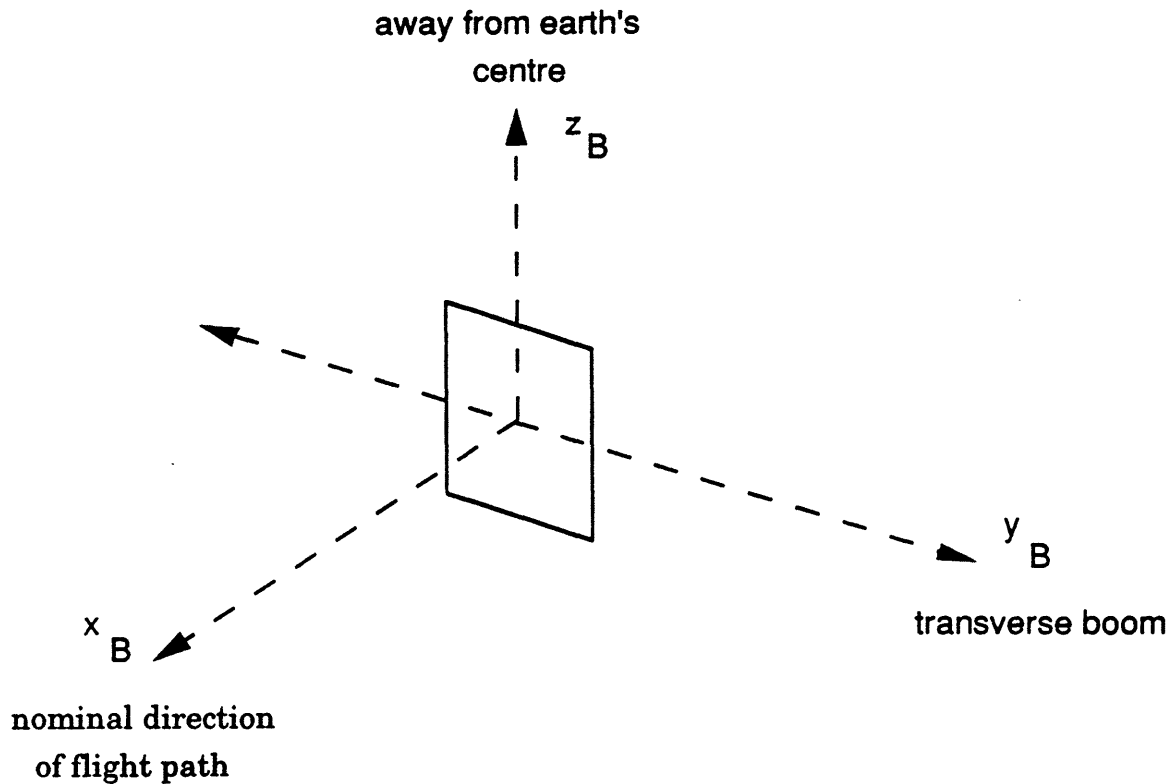
$(T_x, T_y, T_z)$  : aerodynamic disturbance torques

$w_0$  : orbital rate of the LVLH frame

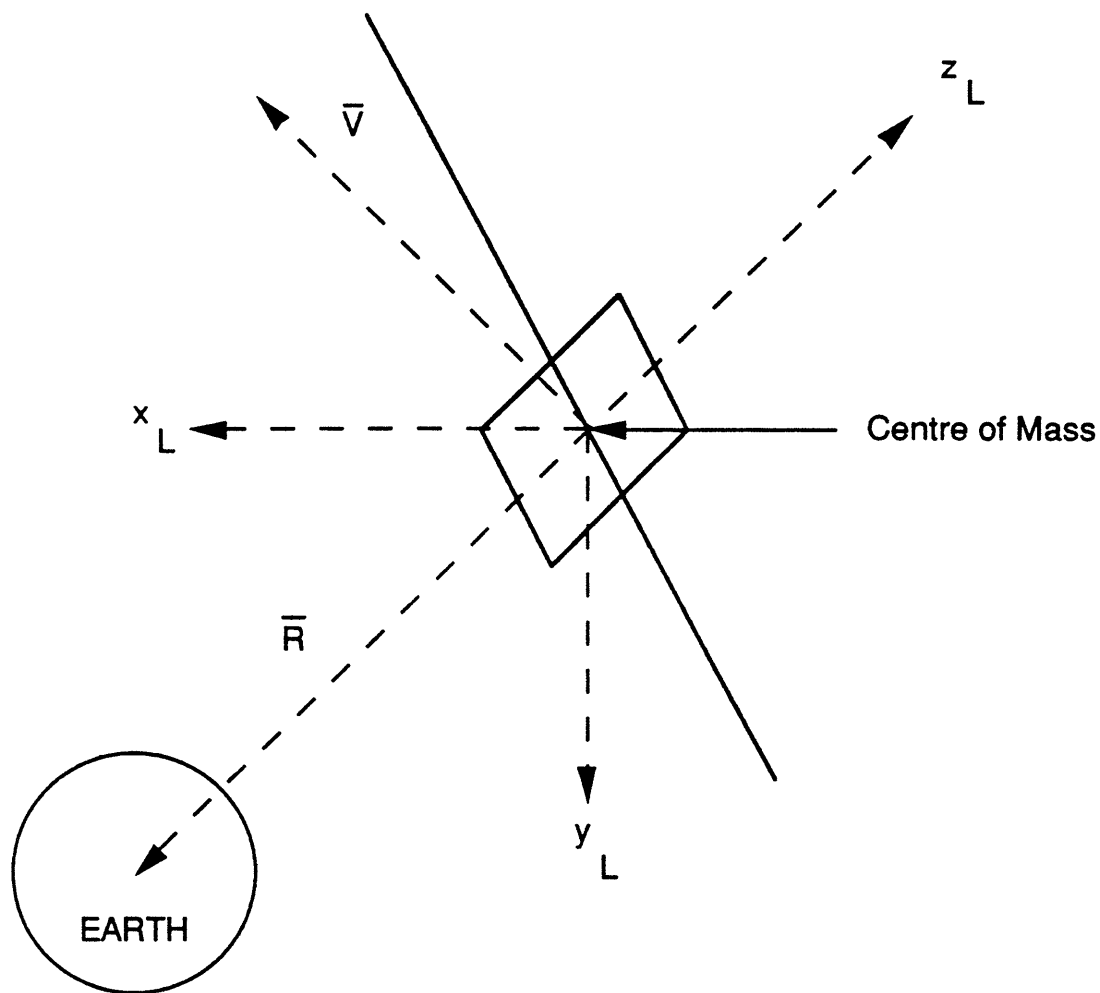
#### COORDINATE FRAMES

Two coordinate frames are utilized in this paper; a body axes (B) frame, and





a local vertical local horizontal (LVLH) frame.  $(x_B, y_B, z_B)$  are the coordinate axes for the body reference frame.  $(x_L, y_L, z_L)$  are the coordinate axes for the LVLH frame. The body frame is fixed relative to the "core" of the station (non-articulating part of the vehicle) with the origin at the center of the station composite center of mass. The  $x_B$  axis is perpendicular to the plane of the dual keel and positive in the nominal direction of flight. The  $z_B$  axis is parallel to the vertical centerline of the dual keel and positive upward (away from the center of the earth). The  $y_B$  axis is parallel to the centerline of the transverse boom and positive in the direction completing a right-handed coordinate system. The LVLH coordinate system has the vehicle center of mass as the origin. The  $z_L$  axis lies along the geocentric



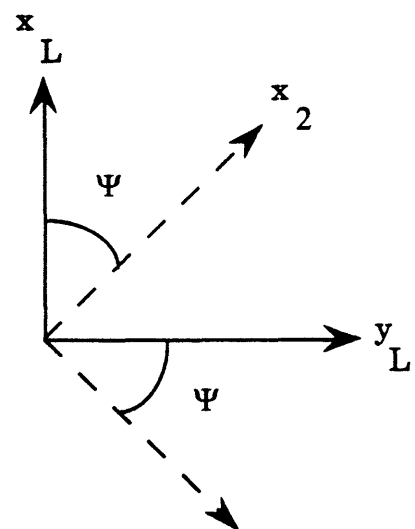
radius vector to the vehicle center of mass and is positive away from the center of the earth. The  $y_L$  axis is perpendicular to the vehicle velocity and radius vectors and is positive in the  $\vec{R} \times \vec{V}$  direction. The  $x_L$  axis completes a right handed coordinate system. The reason for multiple reference frames is that different quantities are most easily represented in different frames. For example, torques are most easily described in the body frame since they are acting on the body, whereas the LVLH frame is most convenient for describing station motion since the spacecraft is to maintain a constant orientation relative to the LVLH coordinates.

## COORDINATE TRANSFORMATIONS

Let  $s=\sin$  and  $c=\cos$ . Assuming a yaw ( $\Psi$ ), pitch ( $\theta$ ), roll ( $\Phi$ ) sequence, the transformation from the LVLH frame to the body frame can be broken up into the following steps :

LVLH to Body reference frame coordinate transformation  
following a yaw, pitch, roll sequence

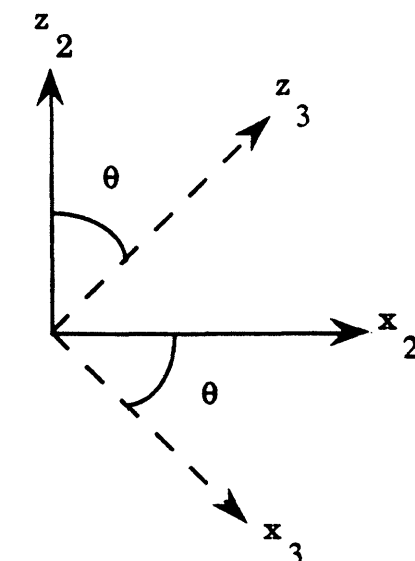
Step 1



$$\begin{bmatrix} x_2 \\ y_2 \\ z_2 \end{bmatrix} = \begin{bmatrix} c\Psi & s\Psi & 0 \\ -s\Psi & c\Psi & 0 \\ 0 & 0 & 1 \end{bmatrix} \begin{bmatrix} x_L \\ y_L \\ z_L \end{bmatrix}$$

$C_1$

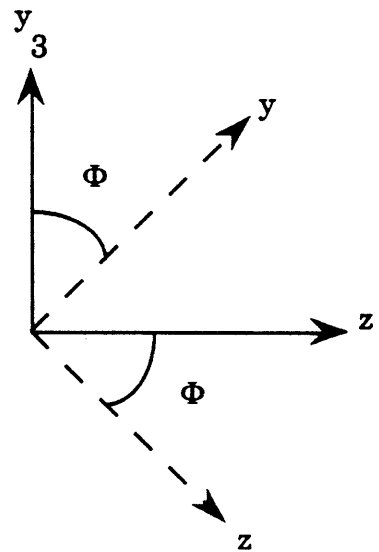
Step 2



$$\begin{bmatrix} x_3 \\ y_3 \\ z_3 \end{bmatrix} = \begin{bmatrix} c\theta & 0 & -s\theta \\ 0 & 1 & 0 \\ s\theta & 0 & c\theta \end{bmatrix} \begin{bmatrix} x_2 \\ y_2 \\ z_2 \end{bmatrix}$$

$C_2$

Step 3



$$\begin{bmatrix} x \\ y \\ z \end{bmatrix} = \begin{bmatrix} 1 & 0 & 0 \\ 0 & c\Phi & s\Phi \\ 0 & -s\Phi & c\Phi \end{bmatrix} \begin{bmatrix} x_3 \\ y_3 \\ z_3 \end{bmatrix}$$

$C_3$

∴ The transformation matrix to go from  $\begin{bmatrix} x_L \\ y_L \\ z_L \end{bmatrix} \Rightarrow \begin{bmatrix} x_B \\ y_B \\ z_B \end{bmatrix}$

$$= C_3 * C_2 * C_1$$

$$= \begin{bmatrix} c\theta c\psi & c\theta s\psi & -s\theta \\ (s\Phi s\theta c\psi) - (c\Phi s\psi) & (s\theta s\Phi s\psi) + (c\Phi c\psi) & s\Phi c\theta \\ (c\Phi s\theta c\psi) + (s\Phi s\psi) & (c\Phi s\theta s\psi) - (s\Phi c\psi) & c\Phi c\theta \end{bmatrix}$$

## DERIVATION OF SPACE STATION DYNAMICS

Derivation of torque expression :

The net torque is the sum of the CMG reaction torque(control), the gravity gradient torque, and the aerodynamic disturbance torque.

$$\sum T = T_{CMG} + T_{gravity\ gradient} + T_{disturbance}$$

$$\Rightarrow \sum T = \begin{bmatrix} L \\ M \\ N \end{bmatrix} = \begin{bmatrix} u_x + g_x + T_x \\ u_y + g_y + T_y \\ u_z + g_z + T_z \end{bmatrix}$$

Let inertia matrix,  $I_B = \begin{bmatrix} I_x & -I_{xy} & -I_{xz} \\ -I_{yx} & I_y & -I_{yz} \\ -I_{zx} & -I_{zy} & I_z \end{bmatrix}$

Recall the expressions for gravity gradient torque stated in (1.4.1)

$$g_x = 1.5\omega_o^2 \left[ (I_z - I_y) s^2 \Phi c^2 \theta - 2I_{yz} c^2 \theta c^2 \Phi - I_{xz} s^2 \theta s \Phi + I_{xy} s^2 \theta c \Phi \right]$$

$$g_y = 1.5\omega_o^2 \left[ (I_z - I_x) s^2 \theta c \Phi - 2I_{xz} (s^2 \theta - c^2 \Phi c^2 \theta) + I_{yz} s^2 \theta s \Phi + I_{xy} s^2 \Phi c^2 \theta \right]$$

$$g_z = 1.5\omega_o^2 \left[ (I_x - I_y) s^2 \theta s \Phi - 2I_{xy} (s^2 \Phi c^2 \theta - s^2 \theta) - I_{xz} s^2 \Phi c^2 \theta - I_{yz} c \Phi s^2 \theta \right]$$

Let the angular rates in the body axis frame be  $\omega_B = \begin{bmatrix} p \\ q \\ r \end{bmatrix}$

Let the system angular momentum be  $h_B = \begin{bmatrix} h_x \\ h_y \\ h_z \end{bmatrix}$

By the theorem of angular momentum torque can be related to angular rate and momentum as :

$$\text{Torque} = \dot{h}_B + \omega_B \otimes h_B$$

$$h_B = I_B \omega_B + \text{rotor terms}$$

Since we are assuming rigid body dynamics and no time varying inertias, the rotor terms and the time derivative of the inertia matrix can be neglected

$$\Rightarrow \dot{h}_B = \dot{I}_B \omega_B + I_B \dot{\omega}_B + \tilde{\omega}_B I_B \omega_B$$

$$\Rightarrow \sum T = \begin{bmatrix} L \\ M \\ N \end{bmatrix} = \begin{bmatrix} I_x & -I_{xy} & -I_{xz} \\ -I_{yx} & I_y & -I_{yz} \\ -I_{zx} & -I_{zy} & I_z \end{bmatrix} \begin{bmatrix} \dot{p} \\ \dot{q} \\ \dot{r} \end{bmatrix} + \begin{bmatrix} 0 & -r & q \\ r & 0 & -p \\ -q & p & 0 \end{bmatrix} [I_B] \begin{bmatrix} p \\ q \\ r \end{bmatrix}$$

Carrying out the matrix algebra we have,

$\Rightarrow$

$$L = I_x \dot{p} + I_{yz}(r^2 - q^2) + I_{xz}(-\dot{r} - pq) + I_{xy}(-\dot{q} + pr) - (I_y - I_z)qr \quad (3.1)$$

$$M = I_y \dot{q} + I_{xz}(p^2 - r^2) + I_{xy}(-\dot{p} - qr) + I_{yz}(-\dot{r} + pq) - (I_z - I_x)rp \quad (3.2)$$

$$N = I_z \dot{r} + I_{xy}(q^2 - p^2) + I_{yz}(-\dot{q} - rp) + I_{xz}(-\dot{p} + qr) - (I_x - I_y)pq \quad (3.3)$$

The objective now, is to express the angular rate,  $\omega_B$ , in terms of the euler angles  $(\Psi, \theta, \Phi)$  :

$$\begin{bmatrix} p \\ q \\ r \end{bmatrix} = \begin{bmatrix} \dot{\Phi} \\ \dot{\theta} \\ \dot{\Psi} \end{bmatrix} \quad \text{resolved to body axis} + \omega_L \quad \text{resolved to body axes}$$

Recollecting the step by step transformation procedure that was carried out earlier,

$$= C_3^* C_2^* \begin{bmatrix} 0 \\ 0 \\ \dot{\Psi} \end{bmatrix} + C_3^* \begin{bmatrix} 0 \\ \dot{\theta} \\ 0 \end{bmatrix} + \begin{bmatrix} \dot{\Phi} \\ 0 \\ 0 \end{bmatrix} + C_3^* C_2^* C_1^* \begin{bmatrix} \omega_{XL} \\ \omega_{YL} \\ \omega_{ZL} \end{bmatrix}$$

$$\Rightarrow \begin{bmatrix} p \\ q \\ r \end{bmatrix} = \begin{bmatrix} 1 & 0 & -s\theta \\ 0 & c\Phi & s\Phi c\theta \\ 0 & -s\Phi & c\Phi c\theta \end{bmatrix} \begin{bmatrix} \dot{\Phi} \\ \dot{\theta} \\ \dot{\psi} \end{bmatrix} + C_3^* C_2^* C_1^* \begin{bmatrix} \omega_{XL} \\ \omega_{YL} \\ \omega_{ZL} \end{bmatrix}$$

Now, to maintain an attitude relative to LVLH,  $\omega_L = \begin{bmatrix} 0 \\ \omega_O \\ 0 \end{bmatrix}$

where  $\omega_O$  is the orbital rate.

$$\Rightarrow \begin{bmatrix} p \\ q \\ r \end{bmatrix} = \begin{bmatrix} 1 & 0 & -s\theta \\ 0 & c\Phi & s\Phi c\theta \\ 0 & -s\Phi & c\Phi c\theta \end{bmatrix} \begin{bmatrix} \dot{\Phi} \\ \dot{\theta} \\ \dot{\psi} \end{bmatrix} + C_3^* C_2^* C_1^* \begin{bmatrix} 0 \\ \omega_O \\ 0 \end{bmatrix}$$

$$\Rightarrow p = -\dot{\psi}s\theta + \dot{\Phi} + \omega_O + \omega_O c\theta s\psi \quad (3.4)$$

$$q = \dot{\psi}s\Phi c\theta + \dot{\theta}c\Phi + \omega_O [s\Phi s\theta s\psi + c\Phi c\psi] \quad (3.5)$$

$$r = \dot{\psi}c\Phi c\theta - \dot{\theta}s\Phi + \omega_O [c\Phi s\theta s\psi - s\Phi c\psi] \quad (3.6)$$

Taking the time derivative of the above set of equations we have,

$$\begin{bmatrix} \dot{p} \\ \dot{q} \\ \dot{r} \end{bmatrix} = \begin{bmatrix} 1 & 0 & -s\theta \\ 0 & c\Phi & s\Phi c\theta \\ 0 & -s\Phi & c\Phi c\theta \end{bmatrix} \begin{bmatrix} \ddot{\Phi} \\ \ddot{\theta} \\ \ddot{\psi} \end{bmatrix} + \begin{bmatrix} -c\theta & 0 & 0 \\ -s\Phi s\theta & -s\Phi & c\theta c\Phi \\ -c\Phi s\theta & -c\Phi & -c\theta s\Phi \end{bmatrix} \begin{bmatrix} \dot{\psi}\dot{\theta} \\ \dot{\Phi}\dot{\theta} \\ \dot{\Phi}\dot{\psi} \end{bmatrix} \\ + \omega_O \begin{bmatrix} 0 & -s\psi s\theta & c\psi c\theta \\ s\psi s\theta c\Phi - c\psi s\Phi & s\Phi s\psi c\theta & s\Phi c\psi s\theta - s\psi c\Phi \\ -s\psi s\theta s\Phi - c\psi c\Phi & c\Phi s\psi c\theta & s\Phi s\psi + c\Phi c\psi s\theta \end{bmatrix} \begin{bmatrix} \dot{\Phi} \\ \dot{\theta} \\ \dot{\psi} \end{bmatrix} \quad (3.7)$$

### Linearizing the Space Station dynamics for controller synthesis :

The equations governing the space station dynamics are derived from

the principle of angular momentum [3, 7]. It is essential that we have a linear set of equations in order to design a compensator using the  $H_\infty$  optimality criterion. The small angle approximation ( $\sin\theta \approx \theta$  &  $\cos\theta \approx 1$ ) is used on the nonlinear set of equations to obtain the LTI equations on which basis the  $H_\infty$  compensator will be designed. Given that the steady state attitude of the space station will be "close" to LVLH (i.e. LVLH and B frame nearly coincident), it can be assumed that  $\psi$ ,  $\theta$  and  $\phi$  are small angles. Since the space station is planned to orbit in an LVLH attitude and the body frame excursions away from the LVLH frame are small, the small angle approximation is reasonable

Furthermore, most practical situations of interest with small products of inertia ( $I_{xy}$ ,  $I_{xz}$ ,  $I_{yz} \approx 0$ ) permit simplification in such a way that pitch motion is uncoupled from roll/yaw motion. Hence, pitch control is often treated separately from coupled roll/yaw motion. This partially decoupled dynamics is also helpful since it allows the problem to be broken into two independent problems, each of a lower order than the original. This simplifies both the controller design and analysis.

In lines of the above stated assumptions, and neglecting the higher powers and products of states (angle and momentum), eqs(3.4 - 3.6) can be approximated as follows :

$$p \approx \dot{\Phi} + \omega_o \psi$$

$$q \approx \dot{\theta} + \omega_o$$

$$r \approx \dot{\psi} - \omega_o \Phi$$

$\Rightarrow$

$$\dot{p} \approx \ddot{\Phi} + \omega_o \dot{\psi}$$

$$\dot{q} \approx \ddot{\theta}$$

$$\dot{r} \approx \ddot{\psi} - \omega_o \dot{\Phi}$$

Similarly, the gravity gradient torque expressions can be simplified to :

$$g_x \approx 3\omega_o^2(I_z - I_y)\Phi$$



$$g_y \approx 3\omega_o^2(I_z - I_x)\theta$$

$$g_z \approx 0$$

Substituting the above expressions into the torque equations derived in (3.1 - 3.3), and neglecting the cross products of inertia we have :

$$\begin{aligned} L &\approx I_x \dot{p} - (I_y - I_z)qr \\ &= I_x(\ddot{\Phi} + \omega_o \dot{\Psi}) - (I_y - I_z)(\omega_o \dot{\Psi} - \omega_o^2 \Phi) \end{aligned}$$

$$\begin{aligned} M &\approx I_y \dot{q} - (I_z - I_x)rp \\ &= I_y(\ddot{\theta}) \end{aligned}$$

$$\begin{aligned} N &\approx I_z \dot{r} - (I_x - I_y)pq \\ &= I_z(\ddot{\Psi} - \omega_o \dot{\Phi}) - (I_x - I_y)(\omega_o \dot{\Phi} + \omega_o^2 \Psi) \end{aligned}$$

Recall,

$$L = u_x + g_x + T_x$$

$$I_x(\ddot{\Phi} + \omega_o \dot{\Psi}) - (I_y - I_z)(\omega_o \dot{\Psi} - \omega_o^2 \Phi) = u_x + 3\omega_o^2(I_z - I_y)\Phi + T_x$$

$$\Rightarrow I_x \ddot{\Phi} = 4\omega_o^2(I_z - I_y)\Phi - I_x \omega_o \dot{\Psi} + I_y \omega_o \dot{\Psi} - I_z \omega_o \dot{\Psi}$$

$$\Rightarrow \ddot{\Phi} = \frac{4\omega_o^2(I_z - I_y)\Phi}{I_x} + \frac{(I_y - I_x - I_z)}{I_x} \omega_o \dot{\Psi} + \frac{u_x}{I_x} + \frac{T_x}{I_x}$$

The above second order differential LTI equation governs the roll axis attitude kinematics of the space station. A similar derivation can be carried out for the pitch and yaw axes .

For the pitch axes :

$$M = u_y + g_y + T_y$$

$$I_y \ddot{\theta} = 3\omega_o^2(I_z - I_x)\theta + u_y + T_y$$

$$\Rightarrow \ddot{\theta} = \frac{3\omega_o^2(I_z - I_x)\theta}{I_y} + \frac{u_y}{I_y} + \frac{T_y}{I_y}$$

and finally for the yaw axis :

$$N = u_z + g_z + T_z$$

$$I_z(\ddot{\psi} - \omega_o \dot{\Phi}) - (I_x - I_y)(\omega_o \dot{\Phi} + \omega_o^2 \psi) = u_z + T_z + 0$$

$$\Rightarrow I_z \ddot{\psi} = \omega_o(I_z + I_x - I_y)\dot{\Phi} + \omega_o^2 \psi(I_x - I_y) + u_z + T_z$$

$$\Rightarrow \ddot{\psi} = \frac{\omega_o(I_z + I_x - I_y)\dot{\Phi}}{I_z} + \frac{\omega_o^2 \psi(I_x - I_y)}{I_z} + \frac{u_z}{I_z} + \frac{T_z}{I_z}$$

Derivation of CMG momentum equations :

The reaction torques from the CMG are used for control input. They can be expressed as:

$$T_{CMG} = -[\dot{h}_B + (\omega_B \otimes h_B)]$$

Putting the above equation in matrix form we have:

$$\begin{bmatrix} u_x \\ u_y \\ u_z \end{bmatrix} = \begin{bmatrix} \dot{h}_x \\ \dot{h}_y \\ \dot{h}_z \end{bmatrix} + \begin{bmatrix} 0 & -r & q \\ r & 0 & -p \\ -q & p & 0 \end{bmatrix} \begin{bmatrix} h_x \\ h_y \\ h_z \end{bmatrix}$$

Carrying out the matrix algebra we have:

$$u_x = \dot{h}_x - r h_y + q h_z$$

$$u_y = \dot{h}_y + r h_x - p h_z$$

$$u_z = \dot{h}_z - q h_x + p h_y$$

Substituting for the body axes rates in terms of euler angles , the momentum equations can be expressed as :

$$u_x = -\dot{h}_x - \omega_o h_z \quad (3.8)$$

$$u_y = -\dot{h}_y \quad (3.9)$$

$$u_z = -\dot{h}_z + \omega_o h_x \quad (3.10)$$

## MATHEMATICAL MODEL FOR CONTROLLER SYNTHESIS

Given below are the set of linearized equations describing the space station dynamics . It is based upon these equations that a  $H_\infty$  optimal controller will be derived.

Attitude Kinematics:

$$\Rightarrow \ddot{\Phi} = \frac{4\omega_o^2(I_z - I_y)\Phi}{I_x} + \frac{(I_y - I_x - I_z)}{I_x}\omega_o\dot{\psi} + \frac{u_x}{I_x} + \frac{T_x}{I_x} \quad (3.11)$$

$$\Rightarrow \ddot{\theta} = \frac{3\omega_o^2(I_z - I_x)\theta}{I_y} + \frac{u_y}{I_y} + \frac{T_y}{I_y} \quad (3.12)$$

$$\Rightarrow \ddot{\Psi} = \frac{\omega_o(I_z + I_x - I_y)\dot{\Phi}}{I_z} + \frac{\omega_o^2\Psi(I_x - I_y)}{I_z} + \frac{u_z}{I_z} + \frac{T_z}{I_z} \quad (3.13)$$

CMG Momentum Equations:

$$u_x = -\dot{h}_x - \omega_o h_z$$

$$u_y = -\dot{h}_y$$

$$u_z = -\dot{h}_z + \omega_o h_x$$

Space Station parameters :

The following space station parameters were obtained from the paper by Wei [?]

$I_x$	50.28E6 slug ft <sup>2</sup>
$I_y$	10.8E6 slug ft <sup>2</sup>
$I_z$	58.57E6 slug ft <sup>2</sup>
orbital rate $w_o$	0.0011 rad/sec ( 1 orbit is approximately 5712 sec)

Allowable CMG momentum peak 20,000 ft.lb.sec

Allowable CMG torque demand 150 ft.lb.sec

Substituting the space station parameters , we have for the attitude kinematics :

$$\ddot{\Phi} = 4.598 \times 10^{-6} \Phi - 2.145 \times 10^{-3} \dot{\psi} + 1.894 \times 10^{-7} u_x + 1.894 \times 10^{-7} T_x \quad (3.14)$$

$$\ddot{\theta} = 2.786 \times 10^{-6} \theta + 9.26 \times 10^{-8} T_y + 9.26 \times 10^{-8} u_y \quad (3.15)$$

$$\ddot{\psi} = 1.842 \times 10^{-3} \dot{\Phi} + 8.167 \times 10^{-7} \dot{\psi} + 1.707 \times 10^{-8} u_z + 1.707 \times 10^{-8} T_z \quad (3.16)$$

and for the CMG momentum equations we have :

$$u_x = -\dot{h}_x - 0.0011 h_z \quad (3.17)$$

$$\dot{h}_y = -u_y \quad (3.18)$$

$$u_z = -\dot{h}_z + 0.0011 h_x \quad (3.19)$$

## APPLICATION OF THE $H_\infty$ DESIGN METHODOLOGY TO THE SPACE STATION

The  $H_\infty$  optimal controller is derived using state space techniques. Hence, it is essential to have a description of the space station dynamics in the state space domain. The following is the application of the general framework to

the linearized model of the space station dynamics.

General State Space representation :

$$\begin{aligned}\dot{\mathbf{x}} &= \mathbf{A} \mathbf{x} + \mathbf{B}_1 \mathbf{w} + \mathbf{B}_2 \mathbf{u} \\ \mathbf{z} &= \mathbf{C}_1 \mathbf{x} + \mathbf{D}_{11} \mathbf{w} + \mathbf{D}_{12} \mathbf{u} \\ \mathbf{y} &= \mathbf{C}_2 \mathbf{x} + \mathbf{D}_{21} \mathbf{w} + \mathbf{D}_{22} \mathbf{u}\end{aligned}$$

Definitions, Notations and Units

STATES :

$(\psi, \theta, \Phi)$	yaw, pitch, roll angles (rad)
$(\dot{\psi}, \dot{\theta}, \dot{\Phi})$	yaw, pitch, roll angular rates (rad/sec)
$(h_x, h_y, h_z)$	CMG momentum (ft.lb.sec)
$(\int h_x, \int h_y, \int h_z)$	Accumulated CMG momentum (ft.lb)

CONTROL INPUT :

$(u_x, u_y, u_z)$	CMG (control) reaction torques (ft.lb)
-------------------	--

EXOGENOUS INPUTS :

$(T_x, T_y, T_z)$	Aerodynamic torques (ft.lb)
$(n_1, n_2, \dots, n_{12})$	Noise (fictitious ; included to satisfy eqs 2.2, 2.3)

OUTPUTS :

Measured outputs (y)	all states
Regulated Outputs (z)	angles, CMG momentum, accumulated momentum, and CMG control torques.

PITCH AXIS STATE SPACE REPRESENTATION :

Equation (2 & 5), which are linearized and uncoupled from the roll/yaw equations, are used as the basis for pitch control analysis and design. The pitch axis momentum management/attitude control loop is similar to the general block diagram shown in Fig. 4. Putting the pitch axis

attitude/momentum governing equations into the general state space form we have :

$$\dot{\mathbf{x}} = \begin{bmatrix} 0 & 1 & 0 & 0 \\ 2.786 \times 10^{-6} & 0 & 0 & 0 \\ 0 & 0 & 0 & 0 \\ 0 & 0 & 1 & 0 \end{bmatrix} \mathbf{x} + \begin{bmatrix} 0 & 1 & 0 & 0 \\ 9.26 \times 10^{-8} & 0 & 0 & 0 \\ 0 & 0 & 0 & 0 \\ 0 & 0 & 1 & 0 \end{bmatrix} \mathbf{w} + \begin{bmatrix} 0 \\ 9.26 \times 10^{-8} \\ -1 \\ 0 \end{bmatrix} \mathbf{u}$$

$$\mathbf{z} = \begin{bmatrix} 1 & 0 & 0 & 0 \\ 0 & 0 & 1 & 0 \\ 0 & 0 & 0 & 1 \\ 0 & 0 & 0 & 0 \end{bmatrix} \mathbf{x} + \begin{bmatrix} 0 & 1 & 0 & 0 & 0 \\ 0 & 0 & 0 & 1 & 0 \\ 0 & 0 & 0 & 0 & 1 \\ 0 & 0 & 0 & 0 & 0 \end{bmatrix} \mathbf{w} + \begin{bmatrix} 0 \\ 0 \\ 0 \\ 1 \end{bmatrix} \mathbf{u}$$

$$\mathbf{y} = \begin{bmatrix} 1 & 0 & 0 & 0 \\ 0 & 1 & 0 & 0 \\ 0 & 0 & 1 & 0 \\ 0 & 0 & 0 & 1 \end{bmatrix} \mathbf{x} + \begin{bmatrix} 0 & 1 & 0 & 0 & 0 \\ 0 & 0 & 1 & 0 & 0 \\ 0 & 0 & 0 & 1 & 0 \\ 0 & 0 & 0 & 0 & 1 \end{bmatrix} \mathbf{w} + \begin{bmatrix} 0 \\ 0 \\ 0 \\ 0 \end{bmatrix} \mathbf{u}$$

where ,

$$\mathbf{x} = \mathbf{y} = \begin{bmatrix} \theta \\ \dot{\theta} \\ h_y \\ \int h_y \end{bmatrix} \quad \mathbf{z} = \begin{bmatrix} \theta \\ h_y \\ \int h_y \\ u_y \end{bmatrix}$$

$$\mathbf{w} = \begin{bmatrix} T_y \\ n_1 \\ n_2 \\ n_3 \\ n_4 \end{bmatrix} = \begin{bmatrix} T \\ N \end{bmatrix}$$

$$\mathbf{u} = \mathbf{u}_y$$

The open loop poles of the pitch axis "plant" are :

- Unstable pitch modes @  $s = \pm 1.5n$  where  $n$  is 0.0011 rad/sec
- Momentum mode with double pole at  $s = 0$ .

## ROLL/YAW AXES STATE SPACE REPRESENTATION :

A design procedure similar to that of the pitch axis design is followed for the roll/yaw controller. Once again, the control loop is of the same format as the general block diagram shown in Fig. 4. Transformed to the general state space representation the system matrices describing the attitude/momentum governing equations are given below

System matrix  $A(8 \times 8)$  :

$$A = \begin{bmatrix} 0 & 0 & 1 & 0 & 0 & 0 & 0 & 0 \\ 0 & 0 & 0 & 1 & 0 & 0 & 0 & 0 \\ 4.598 \times 10^{-6} & 0 & 0 & -2.145 \times 10^{-3} & 0 & 0 & 0 & 0 \\ 0 & 8.16 \times 10^{-7} & 1.8415 \times 10^{-3} & 0 & 0 & 0 & 0 & 0 \\ 0 & 0 & 0 & 0 & 0 & -1.1 \times 10^{-3} & 0 & 0 \\ 0 & 0 & 0 & 0 & 1.1 \times 10^{-3} & 0 & 0 & 0 \\ 0 & 0 & 0 & 0 & 0 & 1 & 0 & 0 \\ 0 & 0 & 0 & 0 & 0 & 0 & 1 & 0 \end{bmatrix}$$

Open loop poles of the roll/yaw axes plant are :

$$(\pm 1.05 \pm 0.7j) \times n, \pm nj, 0, 0$$

Once again the angular modes are unstable in open loop.

Disturbance gain matrix  $B_1 (8 \times 10)$  :

$$B_1 = \begin{bmatrix} 0 & 0 & 0 & 0 & 0 & 0 & 0 & 0 & 0 & 0 \\ 0 & 0 & 0 & 0 & 0 & 0 & 0 & 0 & 0 & 0 \\ 1.894 \times 10^{-7} & 0 & 0 & 0 & 0 & 0 & 0 & 0 & 0 & 0 \\ 0 & 1.707 \times 10^{-8} & 0 & 0 & 0 & 0 & 0 & 0 & 0 & 0 \\ 0 & 0 & 0 & 0 & 0 & 0 & 0 & 0 & 0 & 0 \\ 0 & 0 & 0 & 0 & 0 & 0 & 0 & 0 & 0 & 0 \\ 0 & 0 & 0 & 0 & 0 & 0 & 0 & 0 & 0 & 0 \\ 0 & 0 & 0 & 0 & 0 & 0 & 0 & 0 & 0 & 0 \end{bmatrix}$$

Input gain matrix  $B_2$  (8x2) :

$$B_2 = \begin{bmatrix} 0 & 0 \\ 0 & 0 \\ 1.894 \times 10^{-7} & 0 \\ 0 & 1.707 \times 10^{-8} \\ -1 & 0 \\ 0 & -1 \\ 0 & 0 \\ 0 & 0 \end{bmatrix}$$

Regulated output matrix  $C_1$  (8x8) :

$$C_1 = \begin{bmatrix} 1 & 0 & 0 & 0 & 0 & 0 & 0 & 0 \\ 0 & 1 & 0 & 0 & 0 & 0 & 0 & 0 \\ 0 & 0 & 0 & 0 & 1 & 0 & 0 & 0 \\ 0 & 0 & 0 & 0 & 0 & 1 & 0 & 0 \\ 0 & 0 & 0 & 0 & 0 & 0 & 1 & 0 \\ 0 & 0 & 0 & 0 & 0 & 0 & 0 & 1 \\ 0 & 0 & 0 & 0 & 0 & 0 & 0 & 0 \\ 0 & 0 & 0 & 0 & 0 & 0 & 0 & 0 \end{bmatrix}$$



Measured output matrix  $C_2$  (8x8)

$$C_2 = \begin{bmatrix} 1 & 0 & 0 & 0 & 0 & 0 & 0 & 0 \\ 0 & 1 & 0 & 0 & 0 & 0 & 0 & 0 \\ 0 & 0 & 1 & 0 & 0 & 0 & 0 & 0 \\ 0 & 0 & 0 & 1 & 0 & 0 & 0 & 0 \\ 0 & 0 & 0 & 0 & 1 & 0 & 0 & 0 \\ 0 & 0 & 0 & 0 & 0 & 1 & 0 & 0 \\ 0 & 0 & 0 & 0 & 0 & 0 & 1 & 0 \\ 0 & 0 & 0 & 0 & 0 & 0 & 0 & 1 \end{bmatrix}$$

Matrix  $D_{11}$  (8x10) :

$$D_{11} = \begin{bmatrix} 0 & 0 & 1 & 0 & 0 & 0 & 0 & 0 & 0 & 0 \\ 0 & 0 & 0 & 1 & 0 & 0 & 0 & 0 & 0 & 0 \\ 0 & 0 & 0 & 0 & 0 & 0 & 1 & 0 & 0 & 0 \\ 0 & 0 & 0 & 0 & 0 & 0 & 0 & 1 & 0 & 0 \\ 0 & 0 & 0 & 0 & 0 & 0 & 0 & 0 & 1 & 0 \\ 0 & 0 & 0 & 0 & 0 & 0 & 0 & 0 & 0 & 1 \\ 0 & 0 & 0 & 0 & 0 & 0 & 0 & 0 & 0 & 0 \\ 0 & 0 & 0 & 0 & 0 & 0 & 0 & 0 & 0 & 0 \end{bmatrix}$$

Matrix  $D_{12}$  (8x2) :

$$D_{12} = \begin{bmatrix} 0 & 0 \\ 0 & 0 \\ 0 & 0 \\ 0 & 0 \\ 0 & 0 \\ 0 & 0 \\ 1 & 0 \\ 0 & 1 \end{bmatrix}$$

Matrix D<sub>21</sub> (8x10) :

$$D_{21} = \begin{bmatrix} 0 & 0 & 1 & 0 & 0 & 0 & 0 & 0 & 0 & 0 \\ 0 & 0 & 0 & 1 & 0 & 0 & 0 & 0 & 0 & 0 \\ 0 & 0 & 0 & 0 & 1 & 0 & 0 & 0 & 0 & 0 \\ 0 & 0 & 0 & 0 & 0 & 1 & 0 & 0 & 0 & 0 \\ 0 & 0 & 0 & 0 & 0 & 0 & 1 & 0 & 0 & 0 \\ 0 & 0 & 0 & 0 & 0 & 0 & 0 & 1 & 0 & 0 \\ 0 & 0 & 0 & 0 & 0 & 0 & 0 & 0 & 1 & 0 \\ 0 & 0 & 0 & 0 & 0 & 0 & 0 & 0 & 0 & 1 \end{bmatrix}$$

Matrix D<sub>22</sub> (8x2) :

$$D_{22} = \begin{bmatrix} 0 & 0 \\ 0 & 0 \\ 0 & 0 \\ 0 & 0 \\ 0 & 0 \\ 0 & 0 \\ 0 & 0 \\ 0 & 0 \end{bmatrix}$$

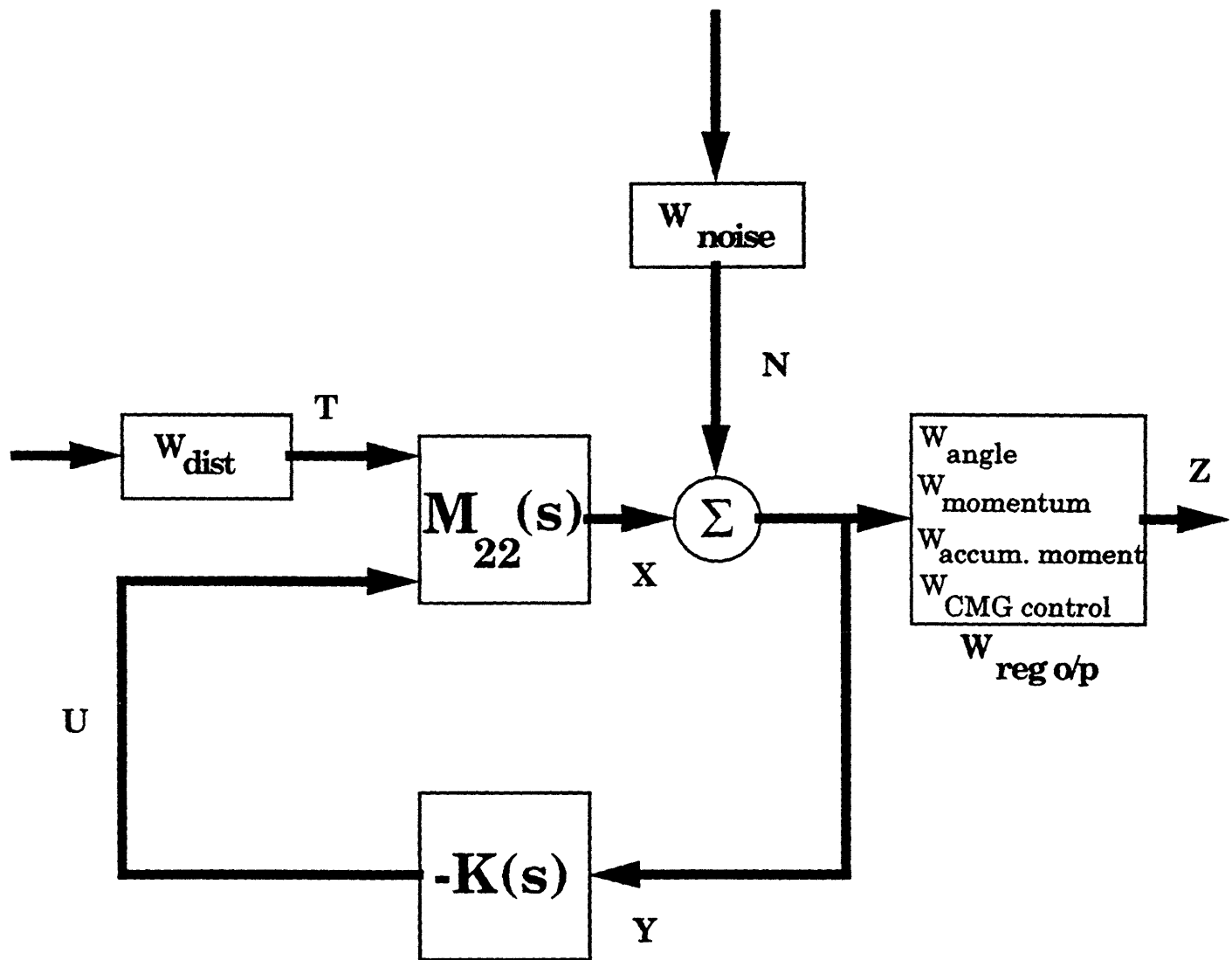


Fig. 4 : General Momentum / attitude control loop

#### SELECTION OF WEIGHTS/SCALING :

The selection of weights is one of the most important steps in the  $H_{\infty}$  methodology. They are used to emphasize one frequency range over another , and in the case of regulated outputs, they can be used to scale variables so that they are "comparable". It must be kept in mind that the selection of weights reflects engineering judgement and, thus, a poor

selection of these weights may result in poor designs. For example, posing a heavy penalty on the sensitivity via  $W_s(s)$  (fig 2) and on the complimentary sensitivity, via,  $W_c(s)$  in the same frequency region, does not make a lot of sense since

$$C(s) + S(s) = I$$

It should also be noted that the complexity of the compensator, namely its order, is equal to the sum of the orders of the plant, the weights, and of the parameter  $Q(s)$ . Therefore, high order weights will result in a high order compensator.

Scaling of chosen regulated outputs plays a vital role in the selection of appropriate weights. For example, posing penalties on CMG momentum and pitch angle without scaling them so that they have comparable magnitudes doesn't make sense. The maximum allowable magnitude for angular excursion is of the order of  $10^0$ , for the CMG momentum it's of the order of  $10^3$ , and the magnitude of the integral of CMG momentum is of the order of  $10^5$ . So scaling the weight on the angle by 10, the weight on momentum by 0.01 and the weight on the integral of momentum by 0.0001 permits us to compare these quantities in our performance index.

In this design the output  $z$  was considered as the weighted error signal  $e$  and the weighted control torque  $u$ . By minimizing  $\| H_{zw}(s) \|_\infty$ , we will minimize

$$\| W_s(s) e(s) \|_{L_2}^2 + \| W_{KS}(s) u(s) \|_{L_2}^2$$

which represents a tradeoff between bandwidth and control action.

**$W_{dist}$  : WEIGHT TO MODEL AERODYNAMIC DISTURBANCE TORQUES**

This weight basically "models" the expected aerodynamic disturbance torque. They are modelled as bias plus cyclic terms in the body fixed control axes.

$$w(t) = \text{Bias} + A_n \sin(nt + \Phi_n) + A_{2n} \sin(2nt + \Phi_{2n})$$

where  $n$  is the orbital rate = 0.0011 rad/sec. The cyclic component at orbital rate is due to the diurnal bulge effect, while the cyclic torque at twice the orbital rate is caused by the rotating solar panels. The magnitudes and phases of aerodynamic torque in each axis are assumed unknown for control design.  $W_1(s)$  should reflect this description of the disturbance torque. Since poles on the  $j\omega$  axis are not permissible, an  $\epsilon$  damping term is introduced.

$$W_1(s) = \frac{N(s)}{(s^2 + \epsilon s + n^2) (s^2 + \epsilon s + (2n)^2)}$$

where  $\epsilon = 2 \times 10^{-6}$ , and  $N(s)$  is the numerator that preserves the stability of the overall closed loop system and incorporates the bias term into the weight.

This will result in disturbance rejection at frequencies  $n$  and  $2n$ . ( $n$  is the orbital rate = 0.0011 rad/sec)

WEIGHTS ON REGULATED OUTPUTS,  $W_{reg\ o/p}$  :

In order to account for the bias term in the expected aerodynamic disturbance, a pole sufficiently close to is included i.e. at  $\epsilon = 2 \times 10^{-5}$ . This will ensure a zero error to constant inputs (for control  $u$  and CMG momentum  $h$ ).

$$W_s(s) = \frac{s + 0.02}{(s + 2 \times 10^{-5}) \left(\frac{s}{10} + 1\right)}$$

Due to the requirements of the Glover/Doyle algorithm, the high frequency pole at  $s = -10$  was selected so that  $D_{11} = 0$ . ( $D_{22} = 0$  since  $M_{22}$  is strictly proper). The zero at  $s = -0.02$  indicates the desired bandwidth over which performance sought.

WEIGHT ON CMG CONTROL TORQUE,  $W_{ks}(s)$  :

Here we must consider satisfying the conditions of Doyle's algorithm (weight should be proper with high frequency gain = 1) in addition to

limiting CMG torque to 150 ft.lb. Furthermore, we would like  $K(s)S(s)$  to roll off in order to prevent excessive control action. This implies that the weighting should be heavier as frequency increases. Having this in mind,  $W_{ks}(s)$  would have to be high pass.

$$W_{KS}(s) = \frac{s + 1}{s + 100}$$

The "fast" pole at  $s = -100$  is inserted to make  $W_{ks}(s)$  proper. The pole at  $s = -1$  indicates the bandwidth over which the control action should not be excessive

### CONTROLLER SYNTHESIS :

The state space model of the open loop system is constructed using the above representation describing the pitch and coupled roll/yaw axes plant , the weights/scaling chosen for the regulated outputs, and the weights describing the expected aerodynamic disturbance torques. The  $H_\infty$  controller is obtained using existing software ("DOYLE" compiled by Dragon Obradavic) that essentially is the equivalent of the procedure outlined in Chapter 3. This program accepts the system description as input, sets up and solves the  $H_\infty$  problem and returns the controller description,  $[AK,BK,CK,DK]$ , as output. In addition to stabilizing the resulting closed loop system, the compensator is expected to provide appropriate disturbance rejection, necessarily bounded outputs and some degree of stability robustness.

#### IV CLOSED LOOP SYSTEM ANALYSIS :

The closed loop system analysis and simulations are carried out using Pro-Matlab on the Digital Vax System. The computer code compiled to do this is presented in Appendix A. Presented here is the derivation of the state space representation of the closed loop system,  $[Acl, Bcl, Ccl, Dcl]$ .

##### STATE SPACE OF CLOSED LOOP SYSTEM :

Let the state space of the open loop plant (without the weights) be  $[Ap, Bp, Cp, Dp]$ . In deriving this representation states of the pitch axis plant and the roll/yaw axis plant are augmented as follows :

$$\begin{bmatrix} \dot{x}_p \\ \dot{x}_{ry} \end{bmatrix} = \begin{bmatrix} A_p & 0 \\ 0 & A_{ry} \end{bmatrix} \begin{bmatrix} x_p \\ x_{ry} \end{bmatrix} + \begin{bmatrix} B1_p & 0 \\ 0 & B1_{ry} \end{bmatrix} \begin{bmatrix} T_y \\ T_x \\ T_z \end{bmatrix} + \begin{bmatrix} B2_p & 0 \\ 0 & B2_{ry} \end{bmatrix} \begin{bmatrix} u_y \\ u_x \\ u_z \end{bmatrix}$$

$$\begin{bmatrix} z_p \\ z_{ry} \end{bmatrix} = \begin{bmatrix} C1_p & 0 \\ 0 & C1_{ry} \end{bmatrix} \begin{bmatrix} x_p \\ x_{ry} \end{bmatrix} + \begin{bmatrix} D11_p & 0 \\ 0 & D11_{ry} \end{bmatrix} \begin{bmatrix} T_y \\ T_x \\ T_z \end{bmatrix} + \begin{bmatrix} D12_p & 0 \\ 0 & D12_{ry} \end{bmatrix} \begin{bmatrix} u_y \\ u_x \\ u_z \end{bmatrix}$$

$$\begin{bmatrix} y_p \\ y_{ry} \end{bmatrix} = \begin{bmatrix} C2_p & 0 \\ 0 & C2_{ry} \end{bmatrix} \begin{bmatrix} x_p \\ x_{ry} \end{bmatrix} + \begin{bmatrix} D21_p & 0 \\ 0 & D21_{ry} \end{bmatrix} \begin{bmatrix} T_y \\ T_x \\ T_z \end{bmatrix} + \begin{bmatrix} D22_p & 0 \\ 0 & D22_{ry} \end{bmatrix} \begin{bmatrix} u_y \\ u_x \\ u_z \end{bmatrix}$$

Note that the fictitious noise included in the open loop system for controller synthesis is not included in the closed loop system formulation. Fictitious noise was included only to satisfy conditions (eqs 2.2, 2.3) of the Glover/Doyle algorithm.

Let the compensator dynamics be described by the following state space representation, where  $x_{kp}$  are the pitch axis compensator states and  $x_{kry}$  are the roll/yaw axis compensator states :

$$\begin{bmatrix} \dot{x}_{kp} \\ \dot{x}_{kry} \end{bmatrix} = \begin{bmatrix} A_{kp} & 0 \\ 0 & A_{kry} \end{bmatrix} \begin{bmatrix} x_{kp} \\ x_{kry} \end{bmatrix} + \begin{bmatrix} B_{kp} & 0 \\ 0 & B_{kry} \end{bmatrix} \begin{bmatrix} u_{kp} \\ u_{kry} \end{bmatrix}$$

$$\begin{bmatrix} y_{kp} \\ y_{kry} \end{bmatrix} = \begin{bmatrix} C_{kp} & 0 \\ 0 & C_{kry} \end{bmatrix} \begin{bmatrix} x_{kp} \\ x_{kry} \end{bmatrix}$$

Now the input to the plant is the output of the controller, i.e  $u_p = y_k$   
 Developed here is the state space for the closed loop transfer function  $H_{zw}$   
 from disturbance to the regulated outputs :

$$\dot{x}_p = A_p x_p + B_{p1} w + B_{p2} u_p$$

$$z_p = C_{p1} x_p + D_{p11} w + D_{p12} u_p$$

Recall,

$$u_p = y_k = C_k x_k$$

$$\Rightarrow \dot{x}_p = A_p x_p + B_{p1} w + B_{p2} [C_k x_k]$$

$$z_p = C_{p1} x_p + D_{p12} [C_k x_k]$$

with negative feedback,

$$u_k = -y_p = -C_{p2} x_p - D_{p21} w$$

$$\Rightarrow \dot{x}_k = A_k x_k + B_k [-C_{p2} x_p] + B_k [-D_{p21} w]$$

$$y_k = C_k x_k$$

Augmenting the states of the plant and the compensator states, we have the representation for the closed loop system :

$$\text{Let } x_{cl} = \begin{bmatrix} x_p \\ x_k \end{bmatrix}$$

$$\dot{x}_{cl} = \begin{bmatrix} A_p & B_{p2} * C_k \\ -B_k * C_{p2} & A_k \end{bmatrix} x_{cl} + \begin{bmatrix} B_{p1} \\ -B_k * D_{p21} \end{bmatrix} \begin{bmatrix} T_y \\ T_x \\ T_z \end{bmatrix}$$



$$z = \begin{bmatrix} z_p \\ z_{ry} \end{bmatrix} = [Cp1 \ Dp12*Ck] x_{cl}$$

Time and frequency domain simulations of the closed loop system are performed using the above derived state space representation.

## LINEAR SIMULATIONS :

In addition to having bounded outputs, some degree of nominal performance in presence of expected aerodynamic disturbance is guaranteed by  $H_\infty$  controllers. This is verified by the time and frequency domain simulation of the closed loop system.

### PITCH AXIS :

#### a) Time Domain :

The transient responses are satisfactory, while the cyclic aerodynamic disturbance,  $4 + 2*\sin(nt) + 0.5*\sin(2*nt)$ , causes the periodic response of both pitch attitude and pitch axis CMG momentum. The momentum is bounded with zero mean value while the pitch angle is oscillating with respect to  $7.5^\circ$  pitch TEA. The CMG momentum peak and control torque demand are both well below their allowable limits of about 20,000 ft.lb.sec and 150 ft.lb respectively. Profiles of the time responses are shown in (Figs. B.1 through B.4 in Appendix B)

#### b) Frequency Domain :

- Bode Plots :

The  $H_\infty$  compensator does accommodate for disturbance rejection as can be seen from the bode plot of  $\theta_2 / w_2$  and  $h_2 / w_2$  (Fig. C.1 & C.2) and their corresponding transmission zeros. These zeros are near  $s = +nj, -nj$  and  $s = 2nj, -2nj$  (poles of the disturbance dynamics). This results in reducing the effects of sinusoidal disturbance to the regulated outputs by minimizing the cyclic peak of the CMG momentum and pitch attitude.

- Singular value plots:

Recall that  $\gamma$  is a bound on the "L2 amplification" or "energy amplification". Furthermore, the smallest such number,  $\gamma^*$ , is the induced norm of the closed loop transfer function from disturbances to outputs,  $H_{zw}$ , or gain of  $H_{zw}$

$$\text{i.e. } \gamma^* = \|H_{zw}\|_{H_\infty}$$

Using the " $\gamma$ -iteration algorithm",  $\gamma^*$  for the transfer function  $H_{zw}$  is  $9.35 \times 10^6$ .

$$\text{i.e. } \sigma_{\max}(H_{zw}) \leq 9.35 \times 10^6 \quad \text{or} \quad \sigma_{\max}(H_{zw}) \leq 139.42 \text{ dB}$$

From the maximum singular value plot of  $H_{zw}$  it can be seen that

$$\sigma_{\max}(H_{zw}) \leq 190 \text{ dB}$$

This is the maximum singular value that results from the closed loop transfer function from disturbance to pitch angle  $\theta$  as can be seen in the singular value plot in Fig.C.11. It must be noted that in the open loop system (for which the controller was designed), the low frequency gain of the weight/scaling imposed on the pitch angle is

$$10 \times \frac{0.02}{2 \times 10^{-5}} = 10^4 = 80 \text{ dB}$$

This additional gain must be accounted for in order to make a correct evaluation of  $\sigma_{\max}(H_{zw})$ . Subtracting the 80 dB (additional gain in open loop system that doesn't appear in the closed loop system),

$$\sigma_{\max}(H_{zw}) = 190 \text{ dB} - 80 \text{ dB} = 110 \text{ dB}.$$

This satisfies the condition  $\sigma_{\max}(H_{zw}) \leq 139.42 \text{ dB}$

## ROLL/YAW AXES :

### a) Time Domain :

The regulated outputs for the coupled roll/yaw dynamics are all well within their prescribed limits. The roll angle oscillates about a  $2.8^\circ$  TEA, whereas the yaw angle has a  $1.1^\circ$  average value. CMG momentum about the roll/yaw axes have a zero mean value and the CMG reaction torque (control) is not excessive. The time domain profiles of the roll/yaw axes regulated outputs in response to aerodynamic disturbances can be seen in

Figs. B.5 through B.12.

Frequency Domain :

- Bode Plots:

From the bode plots shown in Figs C.3 through C.10 it is apparent that the transmission zeros at  $s = +nj, -nj$  and  $s = 2nj, -2nj$  appear in all channels from  $w_1, w_3$  to the regulated outputs. This results in minimization of cyclic peaks in response to sinusoidal type disturbances. This was precisely the type of disturbance rejection that was sought through the choice of weights and scaling in the open loop model.

- Singular Value Plots :

For the roll/yaw axes closed loop system  $\gamma^*$  is  $9.65 \times 10^6$

i.e.  $\sigma_{\max}(H_{zw}) \leq 9.65 \times 10^6$  or  $\sigma_{\max}(H_{zw}) \leq 139.69 \text{ dB}$

It is seen from Fig.C.14 that  $\sigma_{\max}(H_{zw}) < 226 \text{ dB}$ . Once again the additional gain in the disturbance to roll angle channel that does not appear in the closed loop system must be accounted for. The low frequency gain of the weight/scaling for the roll angle is

$$10 \times \frac{0.02}{2 \times 10^{-6}} = 10^5 = 100 \text{ dB}$$

Hence,  $\sigma_{\max}(H_{zw}) = 226 \text{ dB} - 100 \text{ dB} = 126 \text{ dB} < 139.69 \text{ dB}$ .

## NON-LINEAR SYSTEM SIMULATION :

A consequence of the linear design model is that the system actually being controlled is not identical to the system for which the controller was designed. Particularly, consider the nominal system shown in Fig.5(a). The linearized model is represented by  $P_0$  and the compensator by  $C$ .

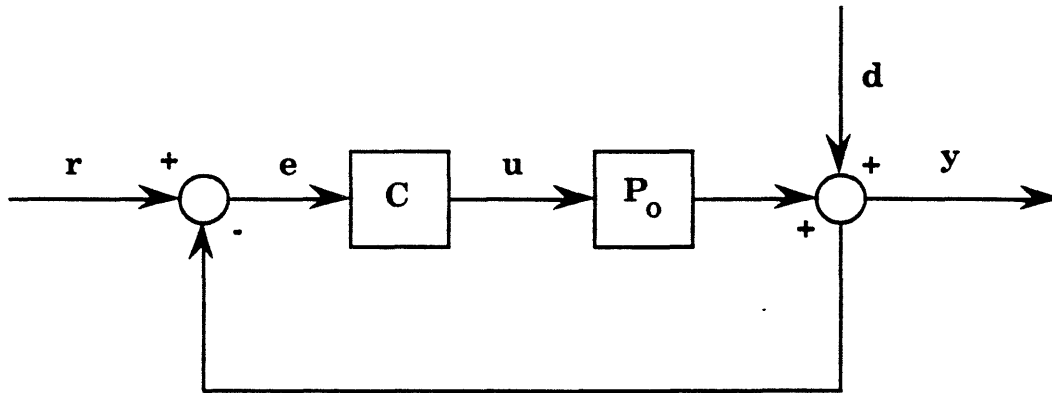


Fig. : Nominal system control loop

The actual system can be represented as shown in Fig.5(b) where  $\Delta$  is a stable, bounded perturbation describing various unmodeled dynamics and modeling errors in the linear model. The controller  $C$  is identical in both cases. It is desired that given  $r \in B_1^2$  and  $d \in B_1^2$ ,  $u, y$ , and  $e$  are all bounded.

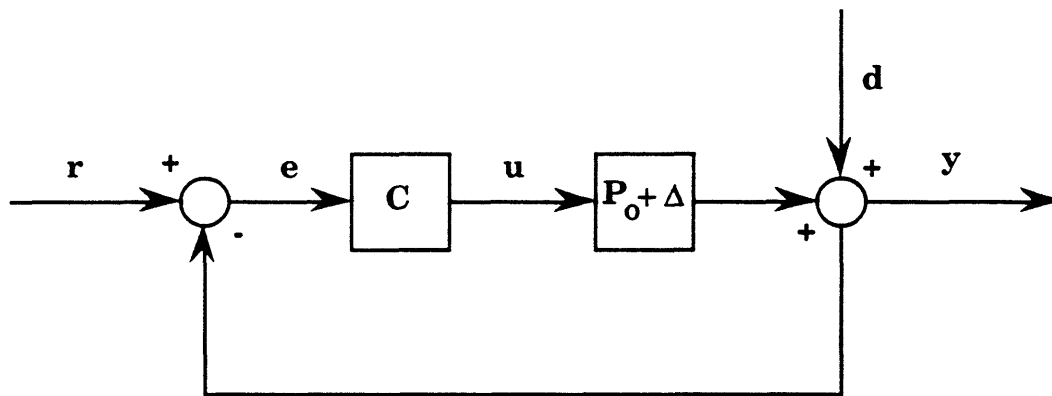


Fig. : Control loop of Actual system

Although the controller stabilizes the nominal system (linearized space station dynamics), the actual system (including the unmodeled dynamics) will perform differently when coupled with the same controller. A robust controller will retain satisfactory performance in presence of unmodeled

effects. Derived below, is the nonlinear model of the space station dynamics for those situations where the pitch angle can not be considered negligible. Through the simulation of these equations, a certain degree of stability robustness of  $H_\infty$  controllers will be established.

#### DERIVATION OF THE NON LINEAR SPACE STATION DYNAMICS :

Certain configurations of the space station may need a large pitch TEA because of the small gravity gradient torque available in the pitch axis. Under such conditions a small angle approximation for the pitch angle is not reasonable. So applying the small angle approximation only to the roll and yaw axes, eqs(3.4 - 3.6) become :

$$p = -\dot{\psi} \sin \theta + \dot{\Phi} + \omega_o \psi \cos \theta$$

$$q = \dot{\theta} + \omega_o$$

$$r = \dot{\psi} \cos \theta - \omega_o \Phi + \omega_o \psi \sin \theta$$

Taking the derivative with respect to time we have :

$$\dot{p} = -(\ddot{\psi} \sin \theta + \dot{\psi} \cos \theta) + \ddot{\Phi} + \omega_o(\dot{\psi} \cos \theta - \psi \sin \theta)$$

$$\dot{q} = \ddot{\theta}$$

$$\dot{r} = -\dot{\psi} \sin \theta + \ddot{\psi} \cos \theta - \omega_o \dot{\Phi} + \omega_o(\psi \cos \theta + \dot{\psi} \sin \theta)$$

The gravity gradient equations are now expressed as,

$$g_x = 3\omega_o^2[(I_z - I_y)\cos^2\theta]\Phi$$

$$g_y = 3\omega_o^2(I_z - I_x)\sin\theta\cos\theta$$

$$g_z = 3\omega_o^2(I_x - I_y)\sin\theta\cos\theta$$

For the pitch axis attitude kinematics,

$$M = u_y + T_y + g_y$$

$$\begin{aligned}
M &= I_y \dot{q} - (I_z - I_x) r p = I_y \ddot{\theta} \\
\Rightarrow \ddot{\theta} &= \frac{3\omega_o^2 (I_z - I_x) \sin \theta \cos \theta}{I_y} + \frac{u_y}{I_y} + \frac{T_y}{I_y}
\end{aligned} \tag{4.1}$$

A similar derivation can be made, using the above substitutions, for the roll/yaw axes.

Roll axis :

$$\begin{aligned}
\ddot{\Phi} &= (1 + 3 \cos^2 \theta) \omega_o \left( \frac{I_z - I_y}{I_x} \right) \Phi + \omega_o \left( \frac{I_y - I_z - I_x}{I_x} \right) \dot{\Psi} \\
&\quad + 3 \frac{(I_z - I_y)}{I_x} \omega_o^2 \Psi \sin \theta \cos \theta + \frac{u_x}{I_x} + \frac{T_x}{I_x}
\end{aligned} \tag{4.2}$$

Yaw axis :

$$\begin{aligned}
\ddot{\Psi} &= (1 + 3 \sin^2 \theta) \omega_o^2 \left( \frac{I_x - I_y}{I_z} \right) \Psi + \omega_o \left( \frac{I_z + I_x - I_y}{I_z} \right) \dot{\Phi} \\
&\quad + 3 \frac{(I_x - I_y)}{I_z} \omega_o^2 \Phi \sin \theta \cos \theta + \frac{u_z}{I_z} + \frac{T_z}{I_z}
\end{aligned} \tag{4.3}$$

*It is evident that roll/yaw motion is now affected by pitch motion.*

## SOFTWARE DEVELOPMENT :

The nonlinear simulations of the above equations were carried out using the Advanced Continuous Simulation Language (ACSL) on the Digital VAX system. This language is designed for modelling and evaluating the performance of continuous systems described by time dependent, nonlinear differential equations.

The integration operator is the heart of the simulation system. In

building the space station dynamics model it is necessary to change differential operators into integration operators; this is accomplished by expressing the highest derivative of a state variable in terms of lower derivatives and other state variables. This process transforms the original set of differential equations to a set of first order differential equations which can be solved directly by integrating.

#### Integration Algorithm :

Runge-Kutta second order is the integration algorithm chosen. In general, Runge-Kutta routines evaluate the derivatives at various points across the calculation interval(integration step), and a weighted combination of these derivatives is used to step across the interval. Specifically, the second order routine makes one derivative evaluation at the beginning and two evaluations at a point two-thirds across a step.

The next state is calculated :

$$x_{n+1} = x_n + \frac{h}{3} (k_1 + 2k_2)$$

where :

x	=	state
h	=	step size(calculation interval)
k	=	derivative evaluation

#### RESULTS OF SIMULATIONS :

The results depicted in Fig. B.13 to Fig.B.14 show the nonlinear system response to the same disturbance profile used earlier. Note that the time axis is in seconds while the angles are in radians. Although initial transients seem to be worse than in the linearized case, the time domain profiles of the space station dynamics are all well within limits imposed on peak CMG control torque (150 ft.lb) and the system angular momentum (20,000 ft.lb.sec) for the pitch,roll and yaw axes. The huge initial transients are due to the fact that initial conditions on angle and angular rate are

zero. The mean of the steady state angular excursions for pitch, roll and yaw are approximately equal to those observed for the linearized system, while the amplitude of steady state oscillations for CMG control torque and momentum are smaller.

The above mentioned results clearly establish some of the stability robustness properties of closed loop systems with  $H_\infty$  compensators.



## V CONCLUSION

### COMPARISON OF $H_\infty$ AND LQR DESIGN METHODOLOGIES FOR THE SPACE STATION PROBLEM :

The LQR results [Wei (10)] served as a guideline to check the mathematical model of the linearized space station dynamics and the closed loop results obtained using the  $H_\infty$  optimality criterion. One of the key advantages of this design is that the outputs to be regulated need not be measurable. The trade-off seems to be the higher order of the derived controller (more complex) which could be impractical in some situations.

In terms of bounded outputs, the results obtained from the two design methodologies are very similar. However,  $H_\infty$  has produced a solution which possesses superior disturbance rejection and stability robustness properties.

### DISTURBANCE REJECTION:

From [10] it can be seen that LQR pitch axis control with cyclic disturbance rejection proposes a disturbance rejection filter of the form :

$$C(s) = \frac{N(s)}{(s^2 + n^2)(s^2 + (2n)^2)}$$

in only one of the channels, either attitude or momentum. The filter poles appear in the numerator (transmission zeros) of the closed loop transfer function  $\theta_2(s)/w_2(s)$  or  $h_2(s)/w_2(s)$  depending on mode selection. This results in asymptotic disturbance rejection at frequencies of  $n$  (orbital rate) and  $2n$  for either  $\theta_2$  or  $h_2$ . The other output oscillates about an average value (with higher cyclic peaks than in the  $H_\infty$  case). Similarly, it is

claimed in [10] that due to some inherent physical property of the coupled roll/yaw dynamics in terms of transmission zeros of a multivariable system, cyclic disturbance rejection at the orbital rate is not possible for roll attitude while it is possible for yaw attitude, using this method of LQR control. The reasoning given in [10] for this claim is not entirely understood and is taken as a fact .

In contrast, by selection of appropriate weights/scaling for disturbance modeling and regulated outputs when setting up the  $H_\infty$  problem (refer to Fig. 4) transmission zeros near  $s=+nj, -nj$  and  $s=+2nj, -2nj$  appear in all attitude ( $\psi, \theta, \phi$ ) channels and momentum ( $h_x, h_y, h_z$ ) channels. Although oscillations are not completely eliminated in either of the attitude or momentum outputs (which is not expected since the choice of weights/scaling does not imply this), the steady state oscillations are minimized to a greater extent than in the LQR with disturbance rejection filter case. In other words, there is more flexibility in terms of disturbance rejection in the  $H_\infty$  structure which permits a choice of regulated outputs and to what extent each is affected by extraneous inputs. Furthermore, the  $H_\infty$  controller can be designed for an arbitrary disturbance rather than for specific disturbances as in the case of the LQR methodology. As such, no assumptions need be made about the the disturbances other than they be of bounded energy ( $\epsilon B l^2$ ). Even if this is not the case ( as is the case here where aerodynamic disturbances are bounded magnitude,  $\epsilon B l^\infty$ , but persistent), a stabilizing solution can be found for the problem but it will in no sense be an optimal one. Even then, some degree of nominal performance is retained in presence of unknown disturbances and modeling errors.

## STABILITY ROBUSTNESS :

In Wei, [10], there is no evidence suggesting that the proposed controller can handle model nonlinearities or cross coupling of inertias. That is although the performance is acceptable with the nominal system ( $P_0$ ), it might be inadequate to handle the actual system ( $P_0 + \Delta$ ).

This property of stability robustness, however, is a consequence of the  $H_\infty$  optimization. The nonlinear space station model for those situations where pitch angle is not negligible retained satisfactory performance with the compensator designed for the nominal linear system.

### SUGGESTIONS FOR FUTURE STUDY:

The space station model has a certain degree of uncertainty which contributes to the robustness problem. The situation where the pitch angle is not negligible (Phase 3 of the space station build up) has been addressed. In addition, situations of movement inside the station, docking of vehicles at the station, and additional construction will vary the inertia matrix by possibly introducing some cross coupling of inertias. Although the  $H_\infty$  controller will satisfactorily handle a certain amount of  $I_{xx}$ ,  $I_{yy}$ ,  $I_{zz}$  perturbations, the problem of introduction of cross coupling of inertias ( $I_{xy}$ ,  $I_{xz}$ ,  $I_{yz}$ ) into the system model needs to be investigated.

The space station, especially in its build up stage, assumes various configurations. This tends to change the system parameters, the system and hence the required controller. Adaptive control employing self tuning and model referencing techniques might provide some good solutions to this type of a problem and should be looked into.

The  $H_\infty$  methodology arises from the problem of designing a stabilizing controller to minimize the energy of system output for arbitrary bounded energy disturbances. The aerodynamic disturbances acting on the space station are not of bounded energy but are rather bounded in magnitude ( $\epsilon B l^\infty$ ). This induces the  $l^1$  minimization problem where the disturbances are assumed to be persistent and bounded. Hence,  $l^1$  might provide a more optimal solution to this problem. Although preliminary work in this area has been completed in terms of software development of the resulting linear programming problem and some linear system analysis [16], stability robustness studies of the  $l^1$  controller for the space station nonlinearities is yet to be explored.

In conclusion,

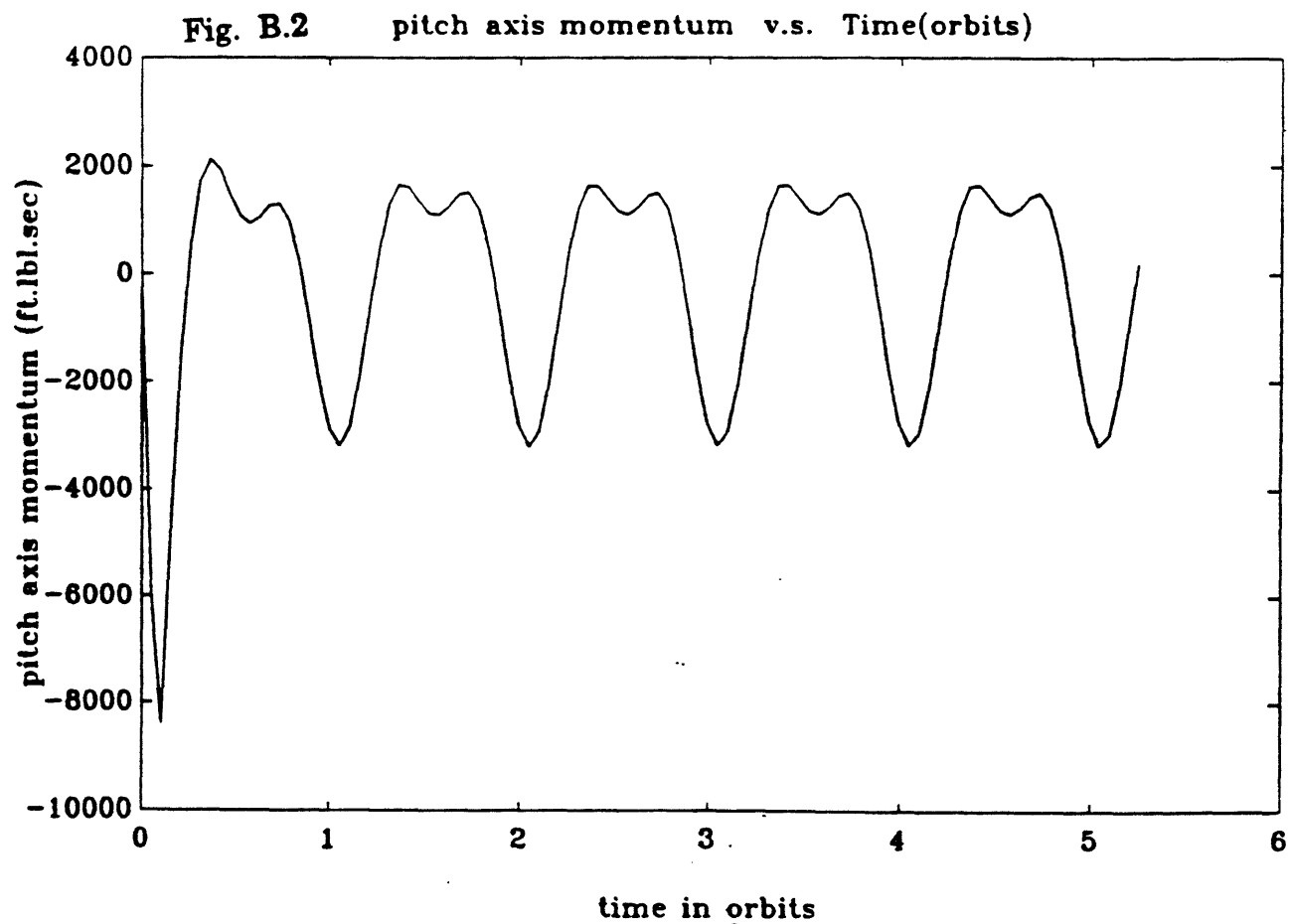
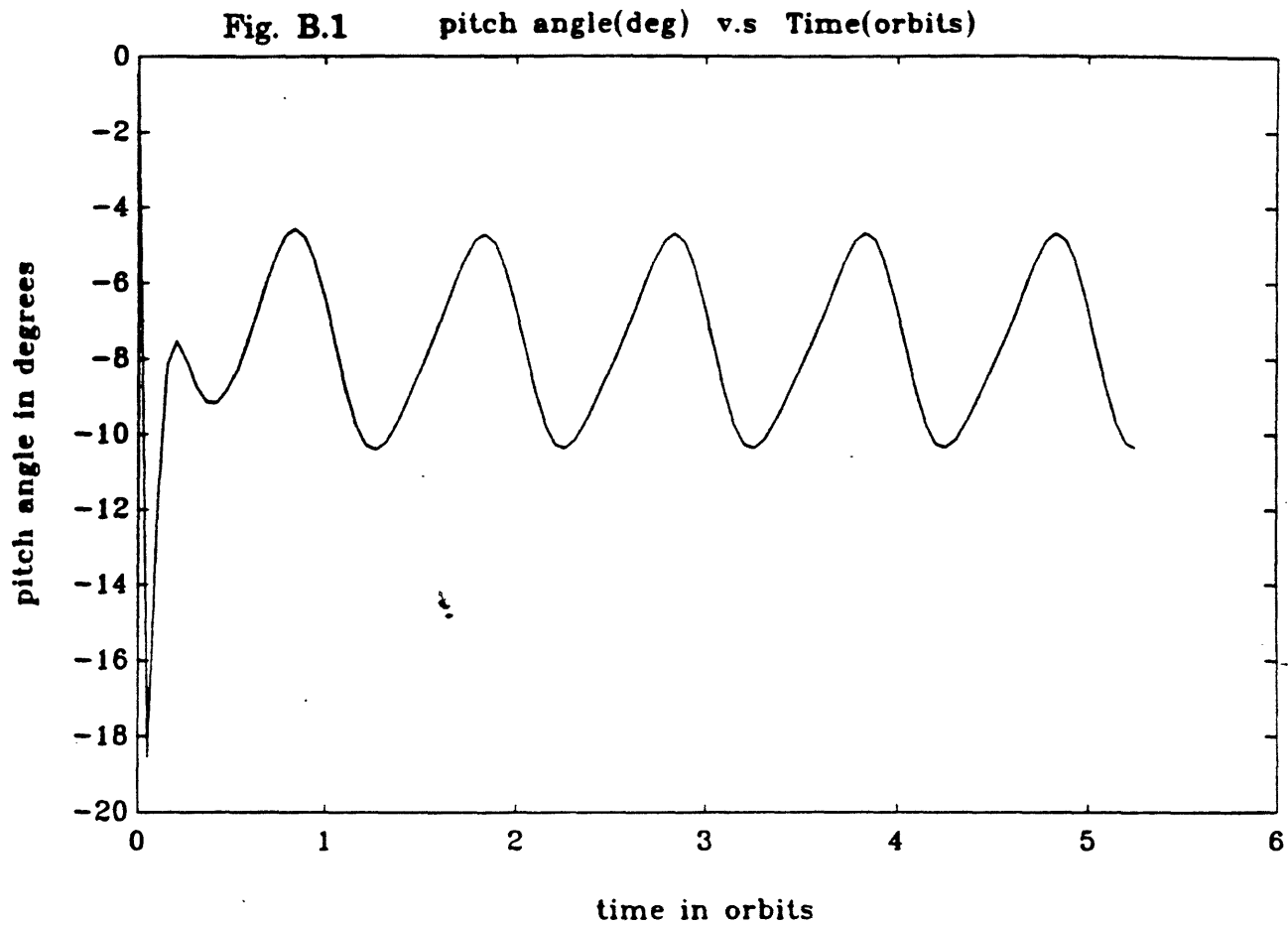
- it has been shown that disturbance rejection, bounded outputs and some degree of stability robustness are consequences of the  $H_\infty$  optimization problem.
- $H_\infty$  has provided a reasonably robust stabilizing solution for the space station attitude control/momentum management problem. But this is not an optimal solution since the disturbance characteristics do not comply with the  $H_\infty$  criteria (bounded energy) but fall into the criteria for  $l^1$  minimization (persistent and bounded magnitude).
- The main drawback of this methodology seems to be the complexity of the derived compensator. This arises from the fact that the order of the controller is the sum of the order of the plant and all the weights chosen to model disturbances and scale regulated outputs. Hence, for most applications today this may not provide a most practical or cost effective solution.

## REFERENCES

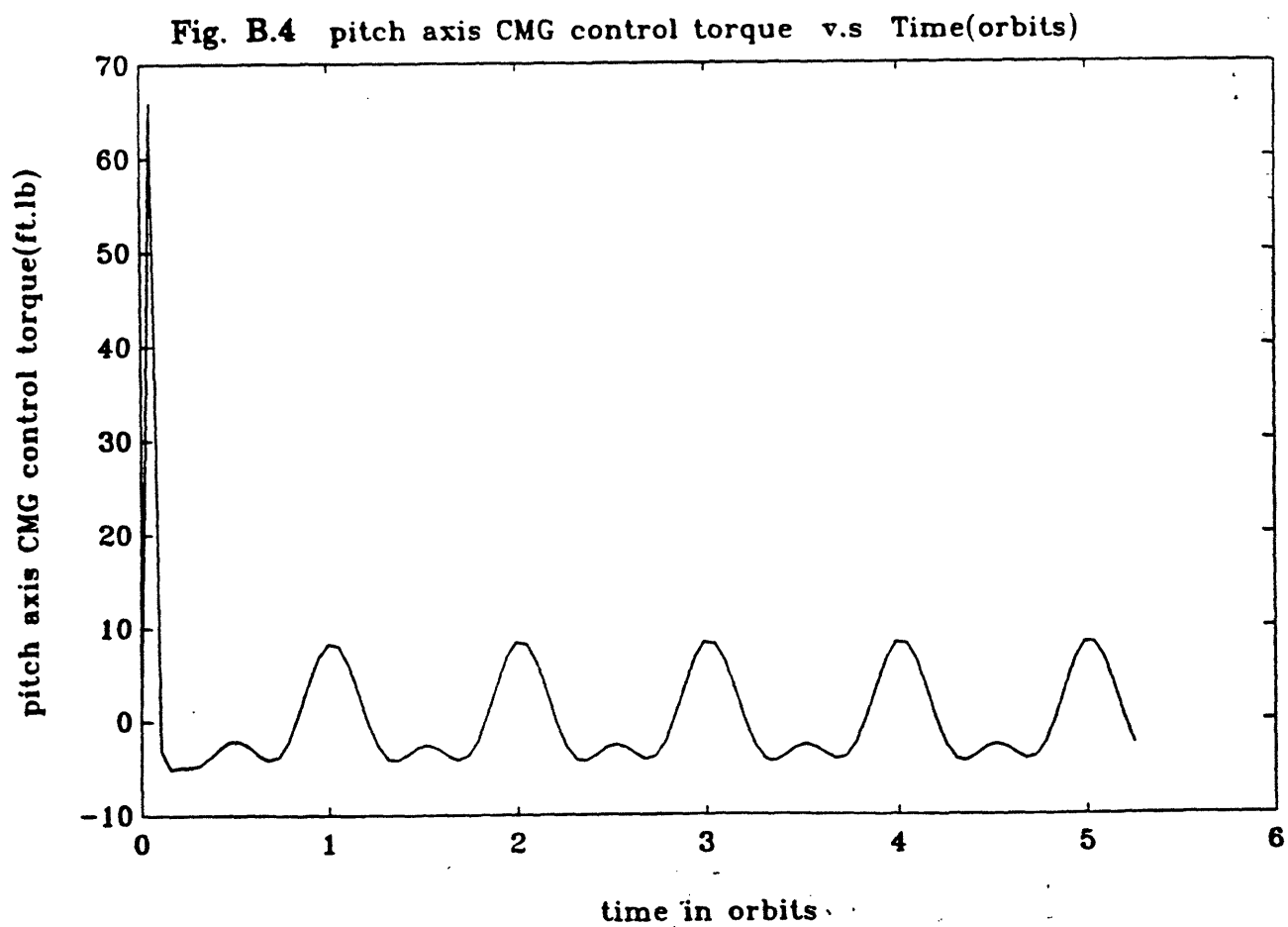
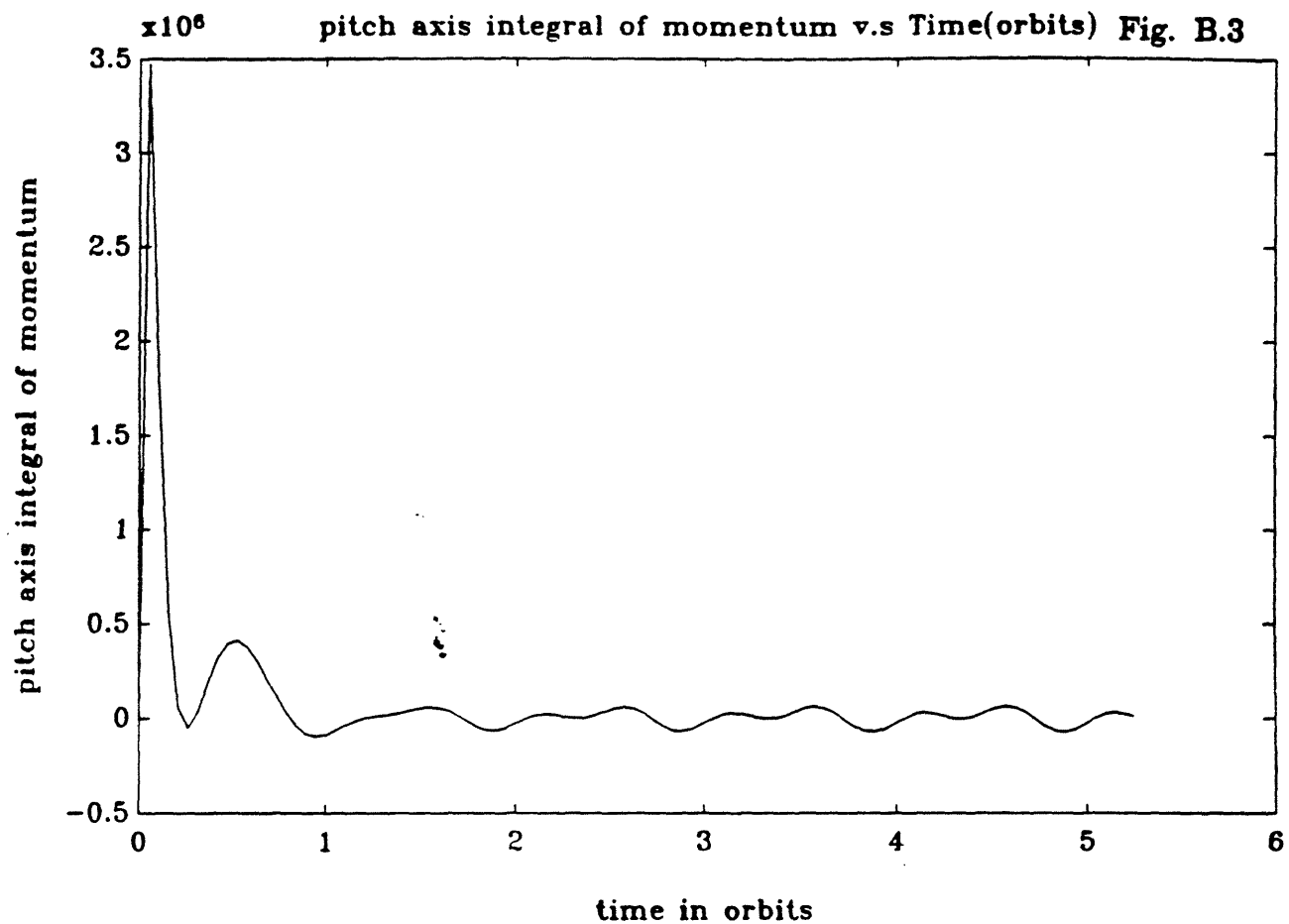
- [1] B.A. Francis, *A Course in  $H_\infty$  Control Theory*, Lecture Notes in Control and Information Sciences, Springer-Verlag, Berlin, 1987.
- [2] G. Stein, "Latest  $H_\infty$  Results", unpublished note, Oct. 1987.
- [3] B. Etkin, *Dynamics of Flight - Stability and Control*, New York, Wiley, 1982.
- [4] P. Voulgaris, High Performance Multivariable Control of the "Supermaneuverable" F18/HARV Fighter Aircraft, M.S. Thesis, M.I.T, May 1988.
- [5] C.D. Johnson and R.E. Skelton, "Optimal Desaturation of Momentum Exchange Control Systems", *AIAA Journal*, VOL 9, NO.1, Jan. 1971.
- [6] L.R. Bishop and K.L. Lindsay, "Proposed CMG Momentum Management Scheme for Space Station.", *AIAA Paper 87-2528*, Aug. 19, 1987.
- [7] Bong Wei, "Preliminary Analysis Results for Space Station Momentum and Attitude Control", unpublished note, Jan. 1987.
- [8] R.E. Oglevie, "Space Station Attitude Control Challenges and Options", *Annual Rocky Mountain Guidance and Control Conference*, Feb. 1983.
- [9] Lynda Bishop, Harvey Malchow and Philip Hattis, "Momentum Management Strategy During Space Station Buildup", *11<sup>th</sup> Annual AAS Guidance and Control Conference*, Jan 1988.
- [10] B. Wei and D. Geller, "A New Momentum Management Controller for the Space Station", *AIAA Journal of Guidance, Control, and Dynamics*, Jan 1988.

- [11] E.B. Shain and V.A. Spector, "Adaptive Torque Equilibrium Control of the Space Station", AIAA Paper 85-0028, Jan. 1985.
- [12] "Momentum Management Technical Exchange Meeting", McDonnell Douglas Presentation at the Johnson Space Center, Feb. 14, 1986.
- [13] H.H. Woo et al, "Momentum Management Concepts for a Space Station", AIAA Paper 86-2047, Aug. 20, 1986.
- [14] P.D. Hattis, "Predictive Momentum Management for the Space Station", J. Guid., Contr. and Dynam., Vol. 9, No. 4, July-Aug., 1986, pp. 454-461.
- [15] J.C. Doyle, Lecture Notes, 1984 ONR/Honeywell Workshop on Advances in Multivariable Control, Minn. MN, Oct. 1984.
- [16] D. Richards, <sup>1</sup> - Optimal Control : Solution Software and Design Examples, S.M. Thesis, MIT July, 1989.

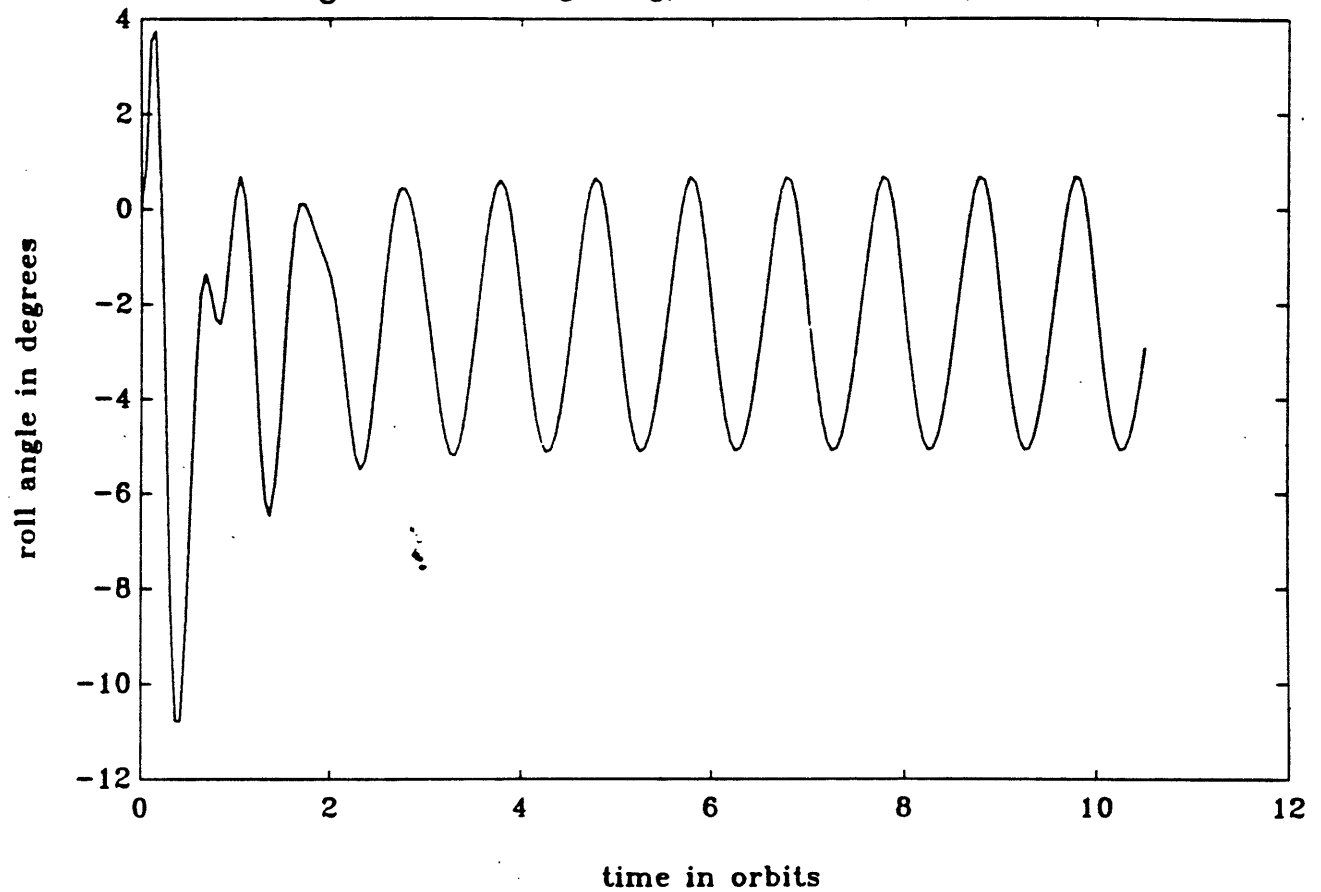
## **LINEAR SIMULATIONS**



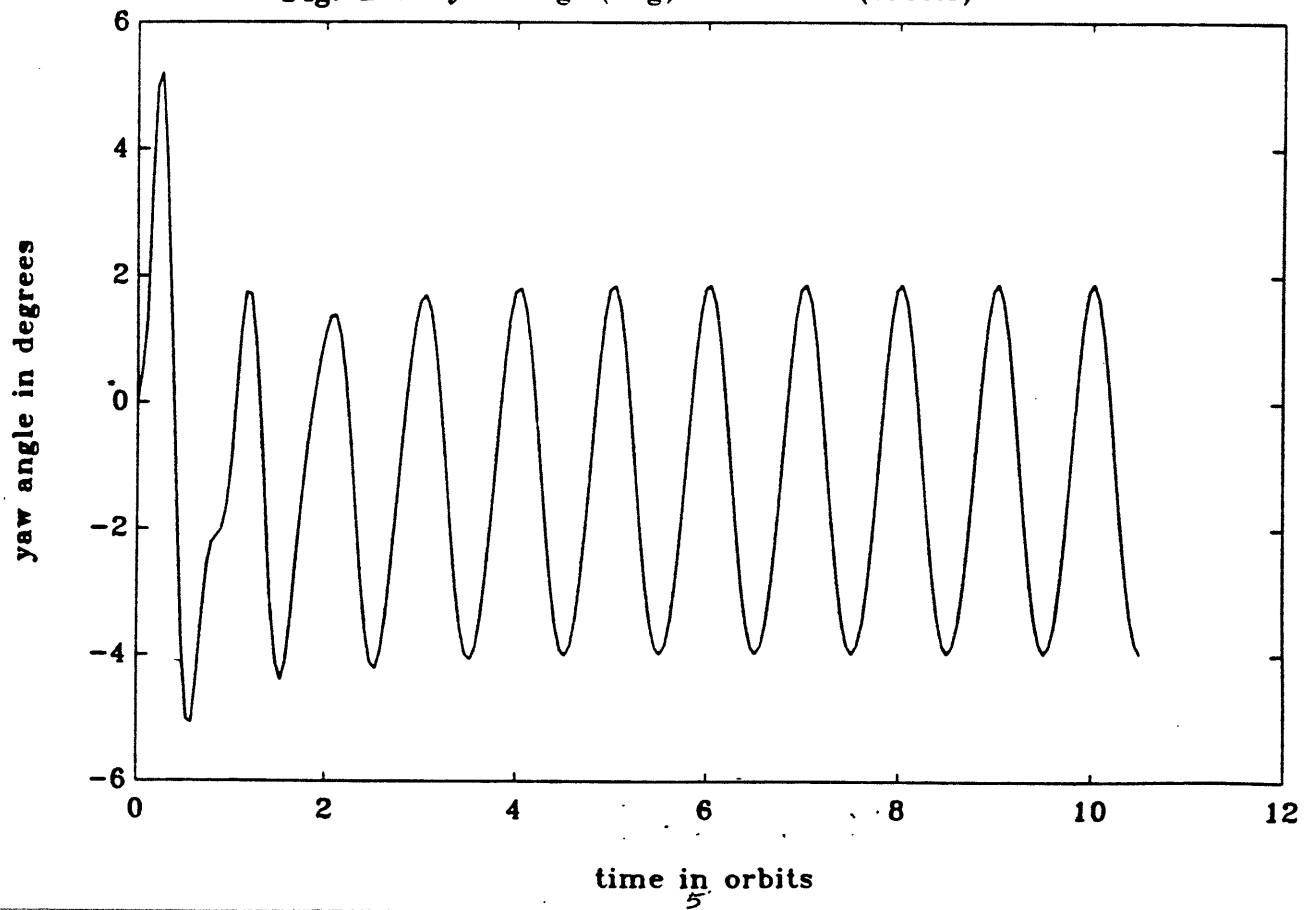




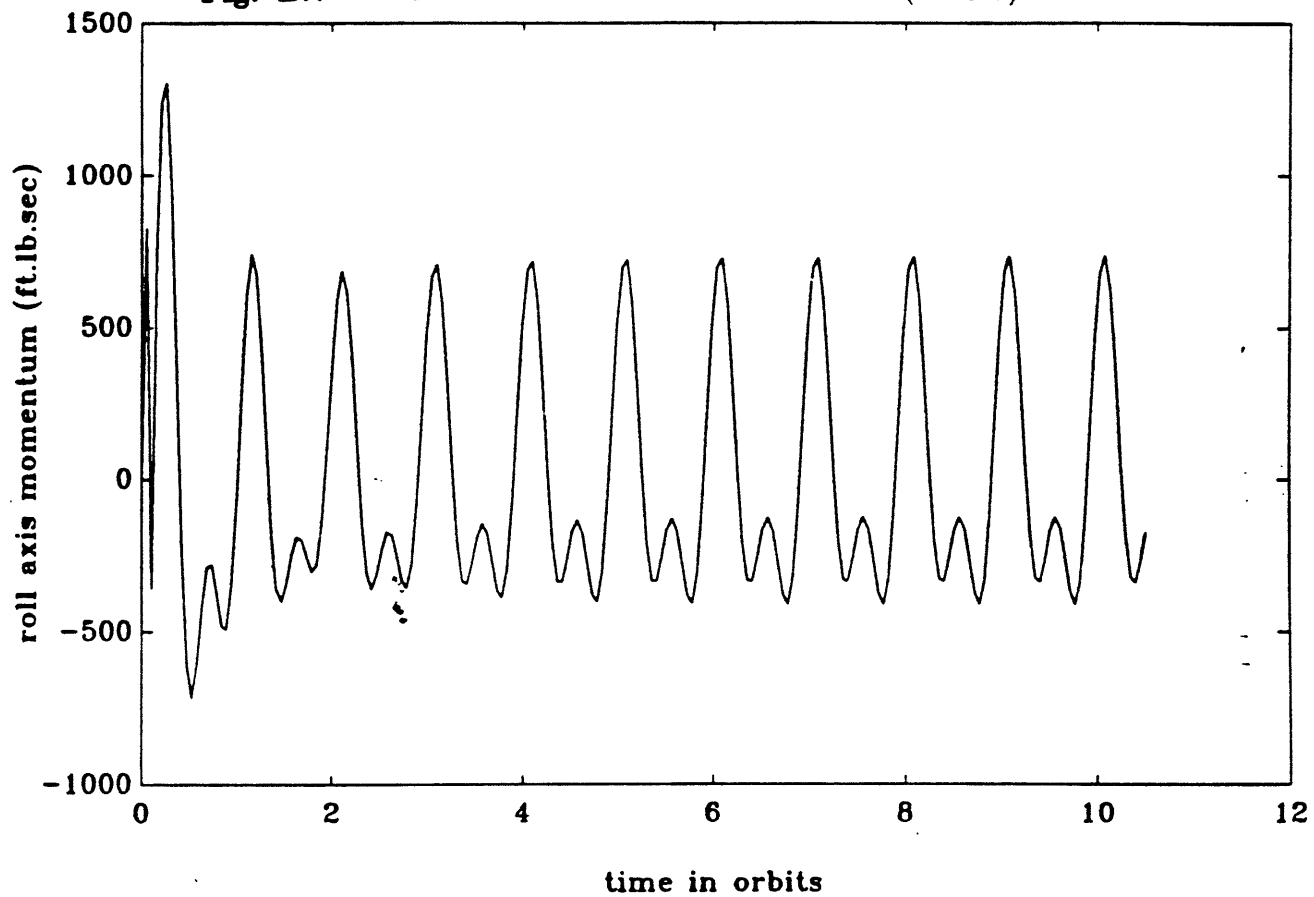
**Fig. B.5** roll angle(deg) v.s. Time(orbits)



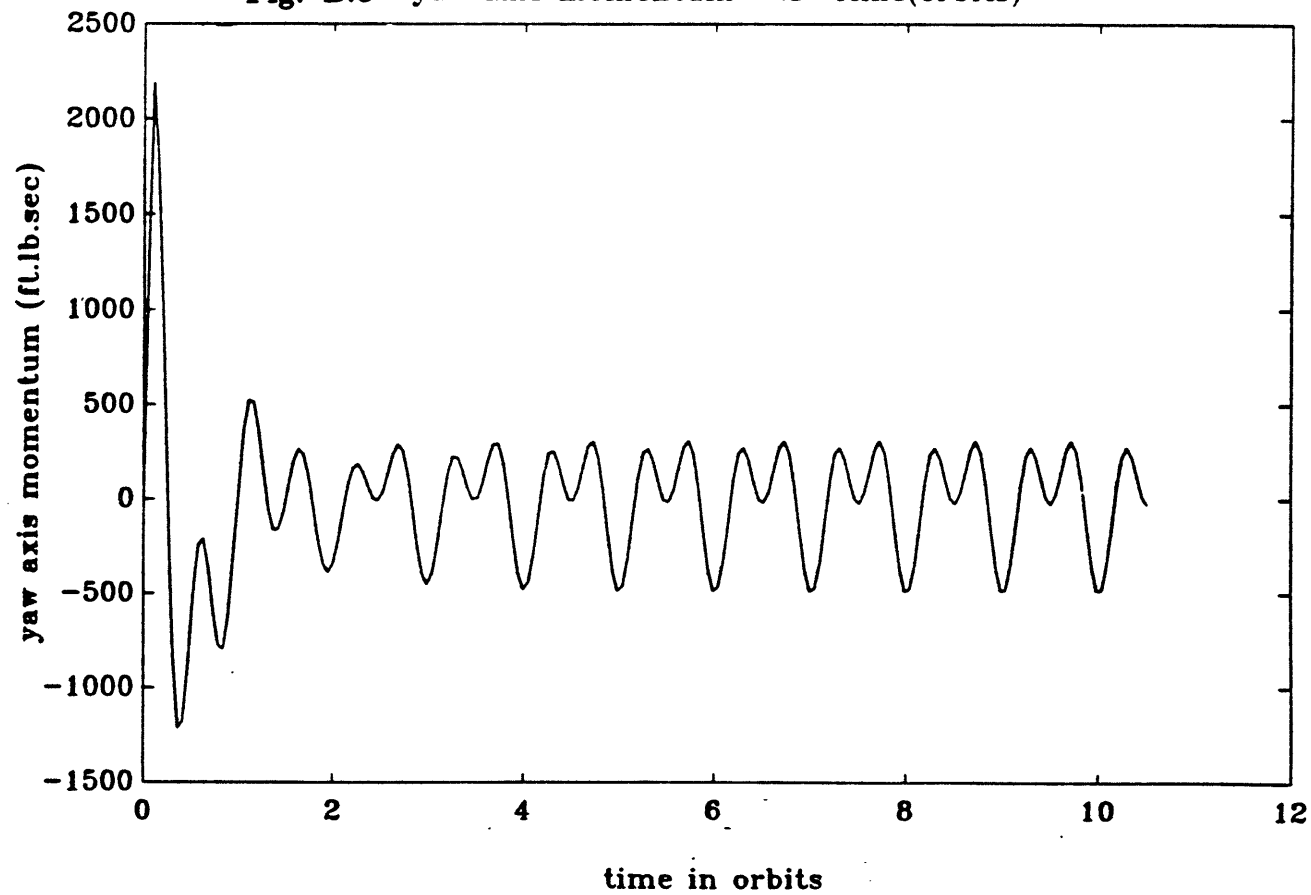
**Fig. B.6** yaw angle(deg) v.s. Time(orbits)



**Fig. B.7** roll axis momentum v.s Time(orbits)



**Fig. B.8** yaw axis momentum v.s Time(orbits)



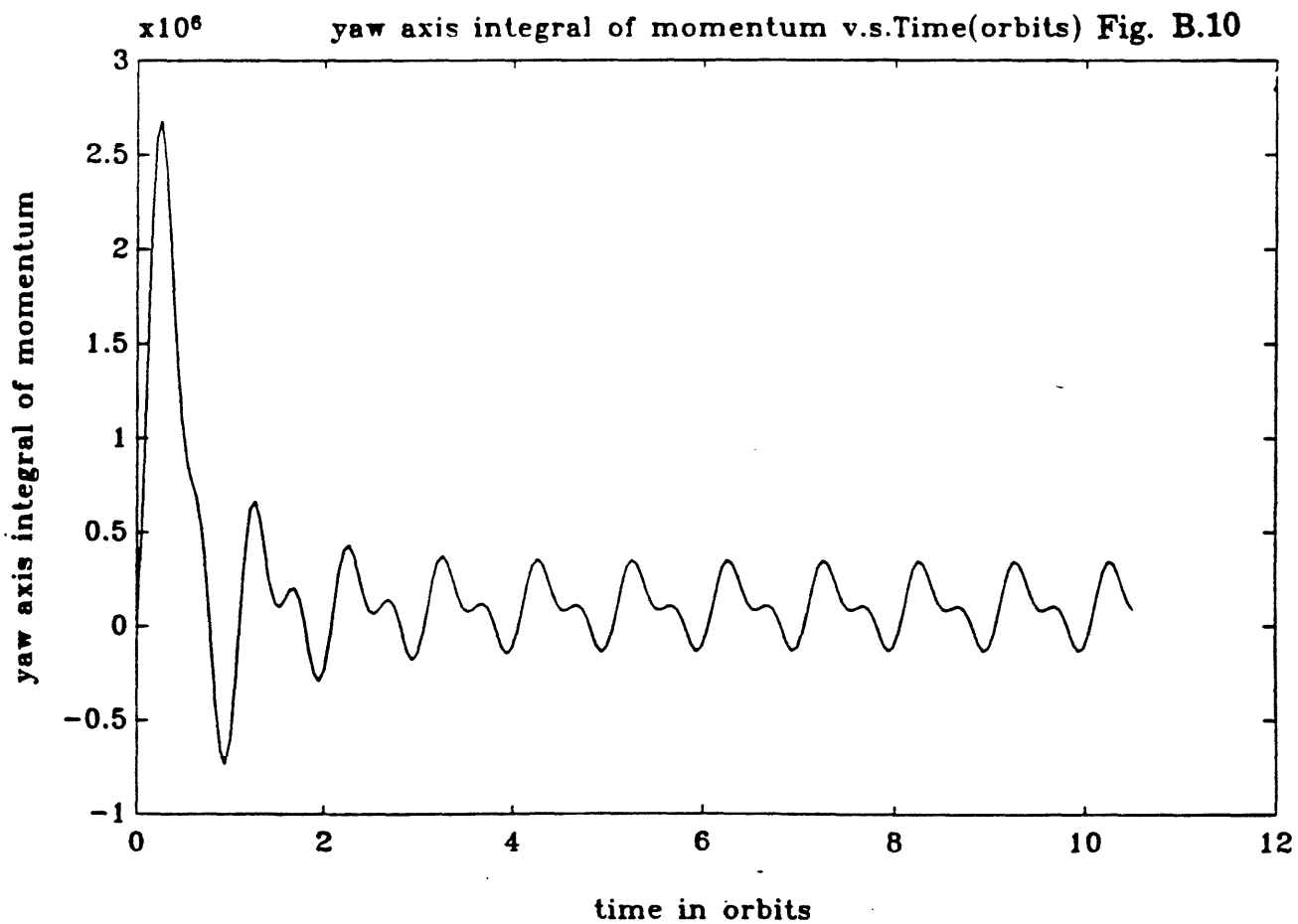
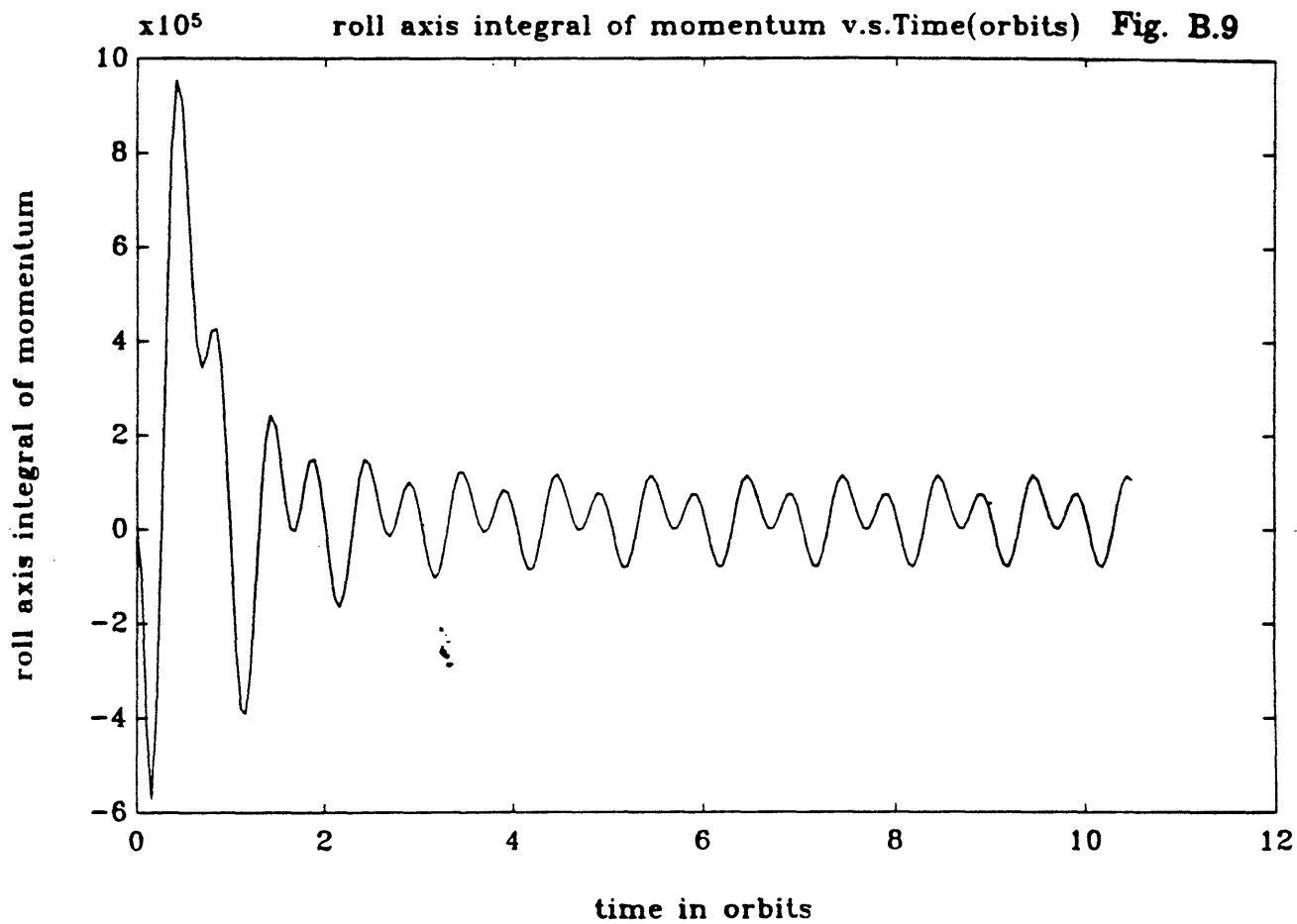


**Fig. B.11** roll axis CMG control torque v.s. Time(orbits)

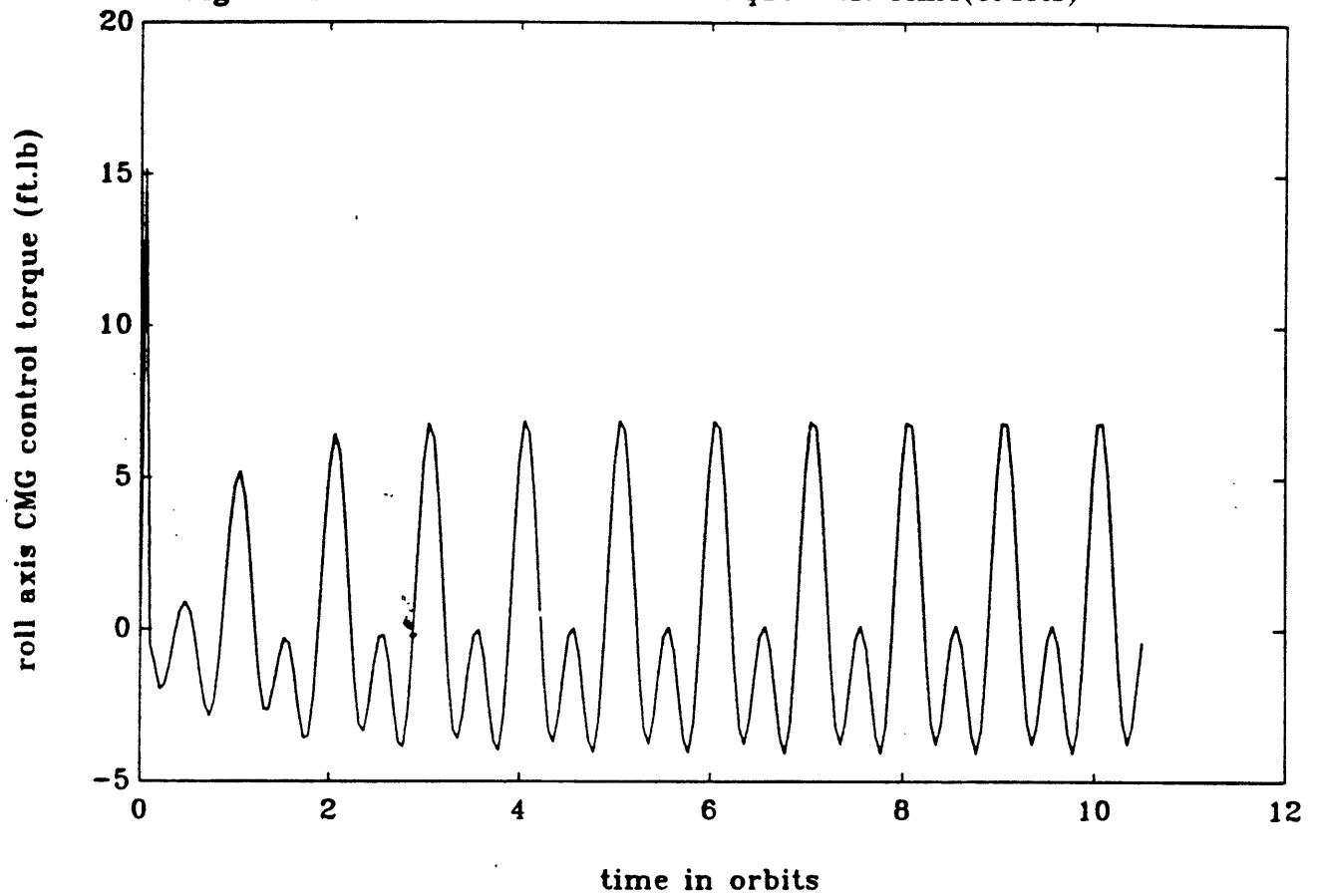
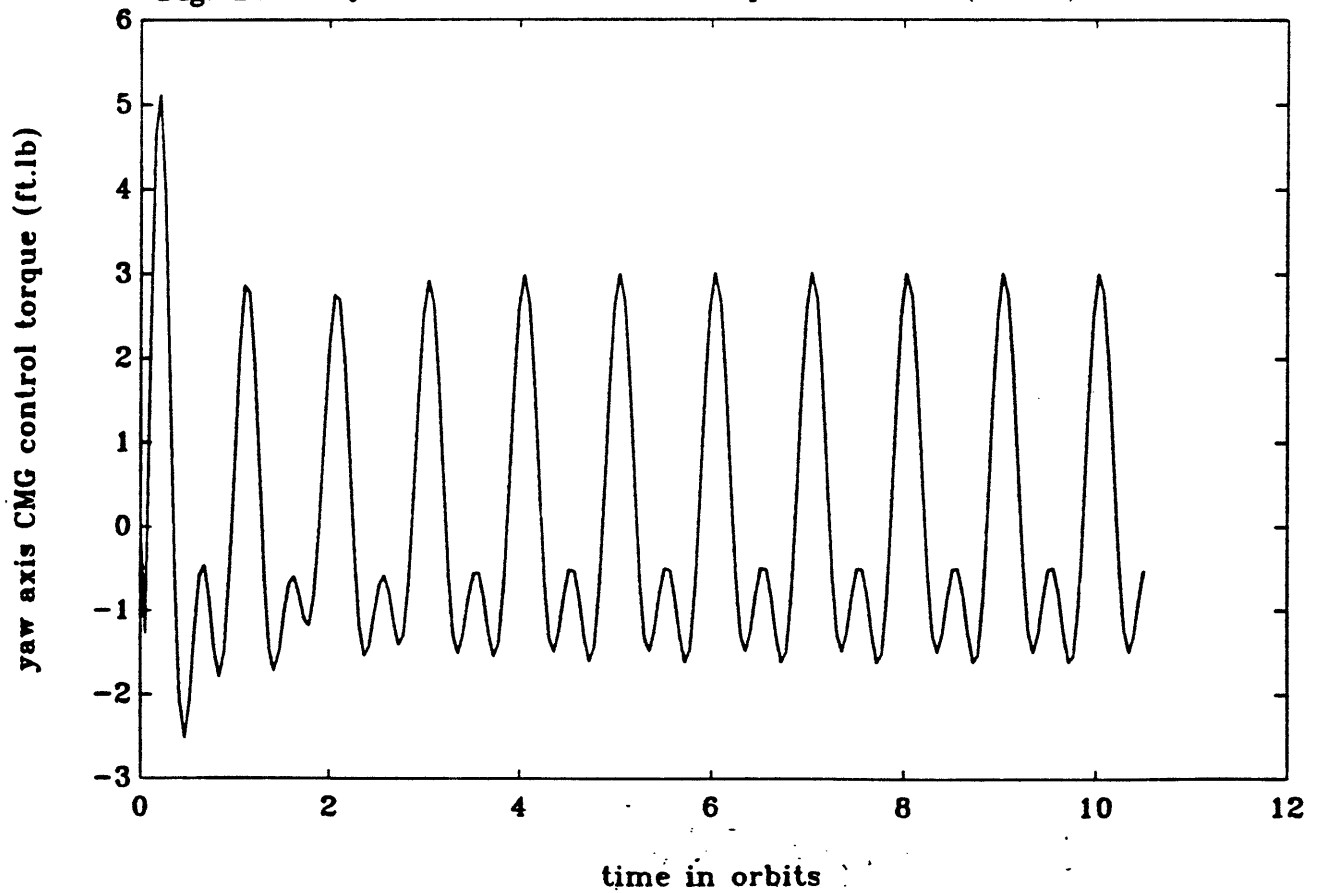


**Fig. B.12** yaw axis CMG control torque v.s. Time(orbits)



## **NON LINEAR SIMULATIONS**

Fig. B.14 Pitch axis momentum (ft.lb.sec) v.s Time (sec)

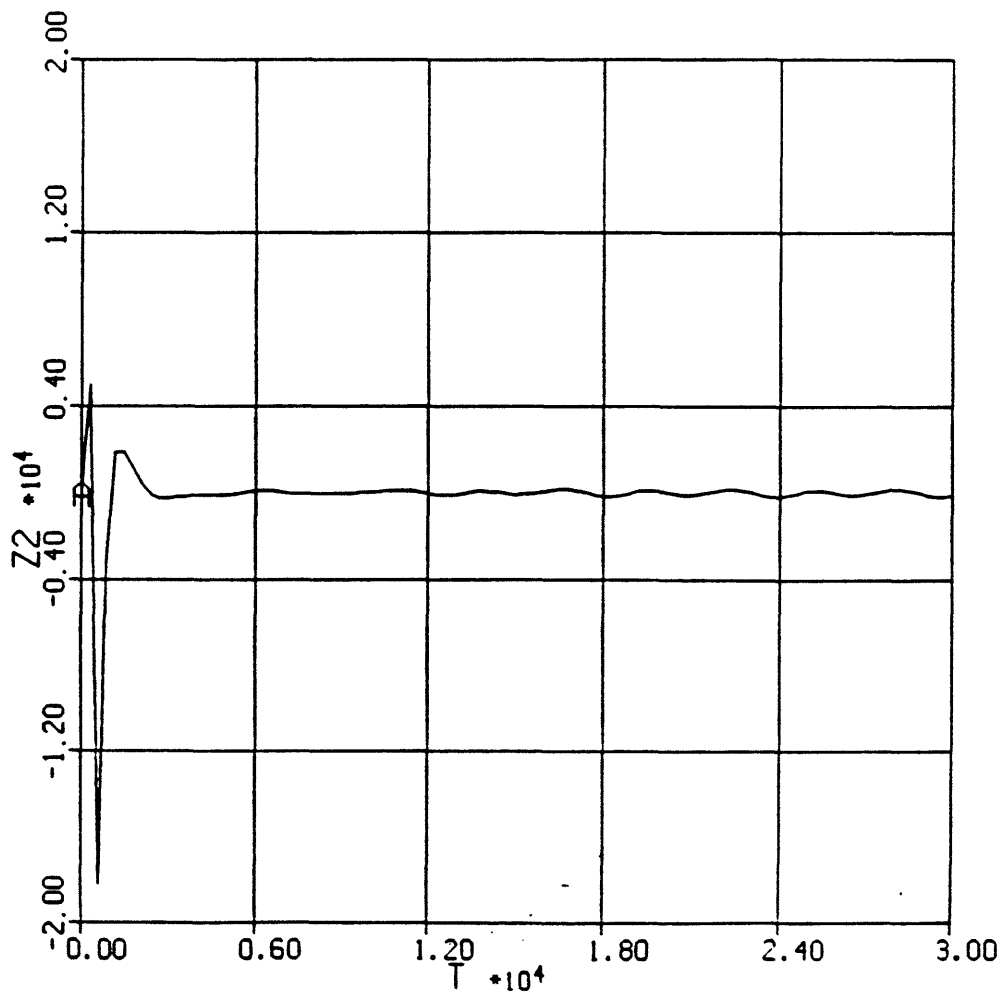


Fig. B.13 Pitch angle (rad) v.s Time (sec)

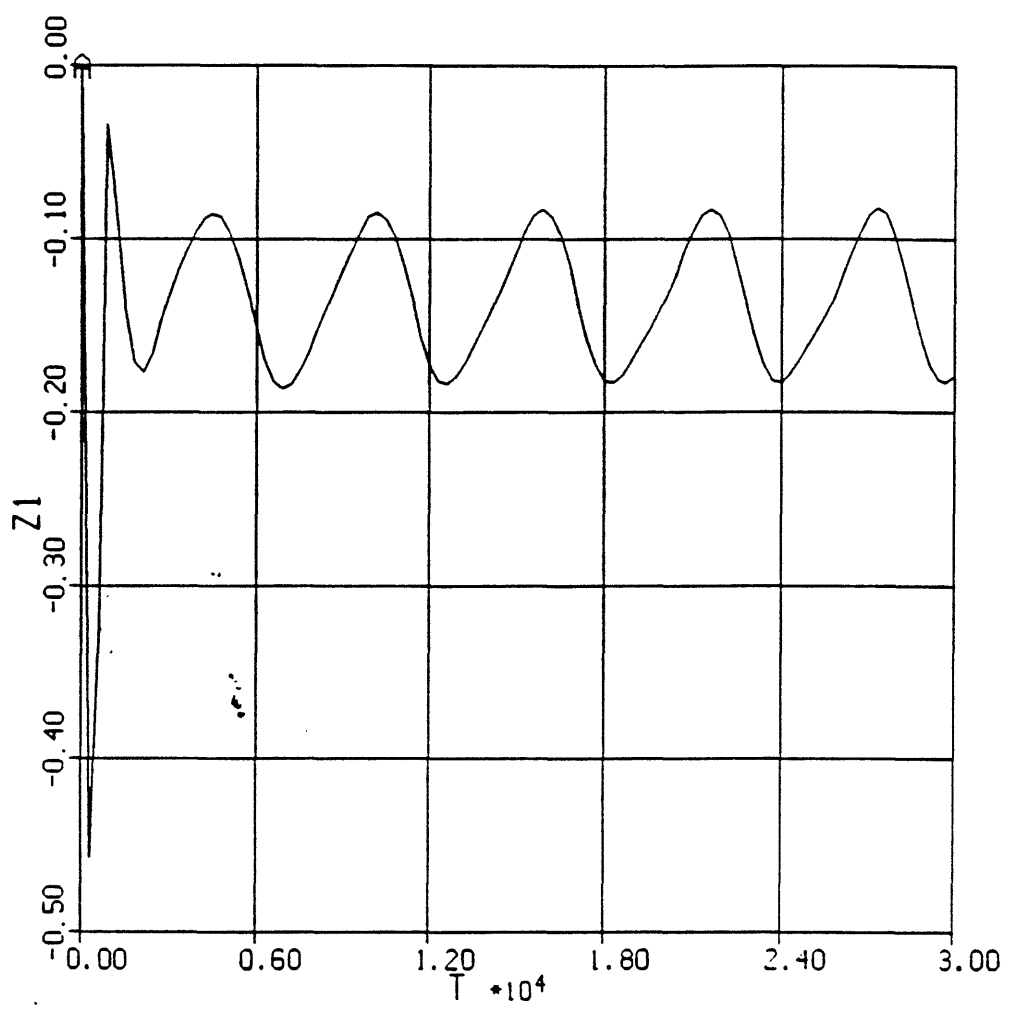


Fig. B.16 Pitch axis CMG control torque (ft.lb) v.s Time (sec)

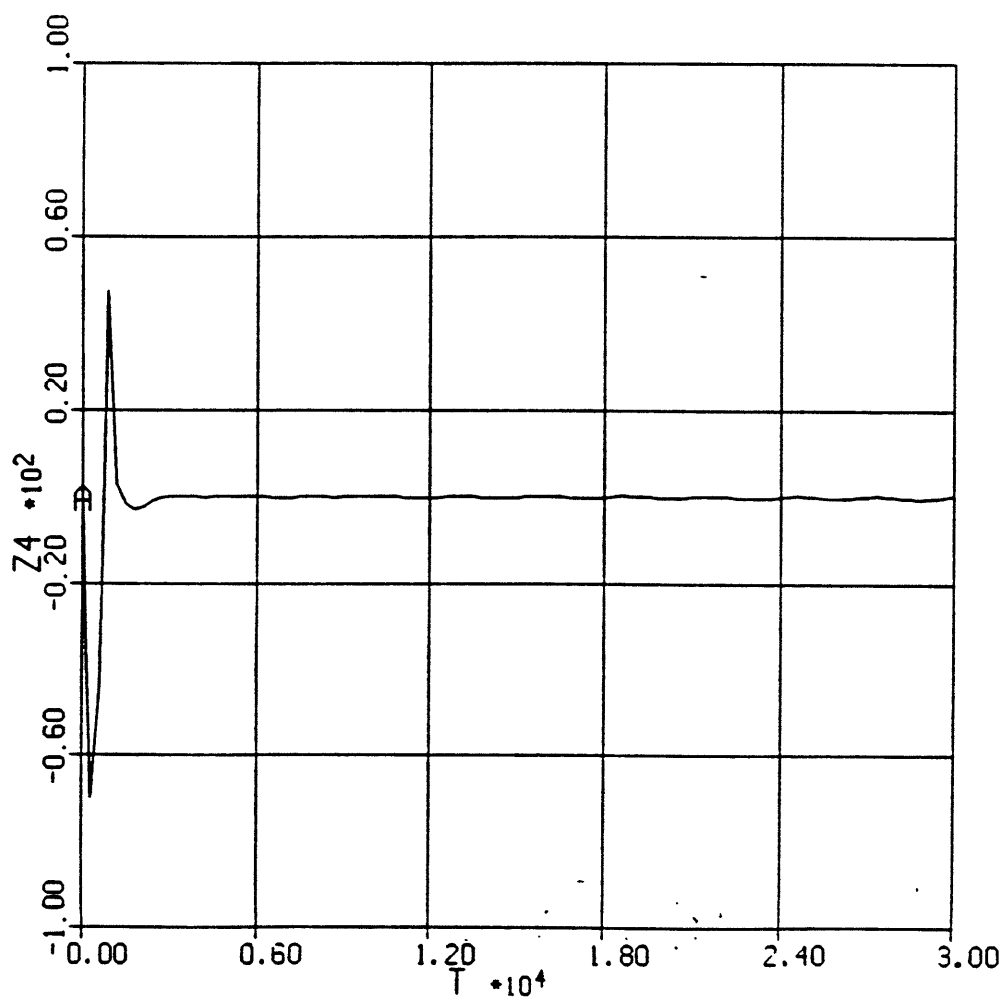


Fig. B.15 Pitch axis integral of momentum (ft.lb) v.s Time (sec)

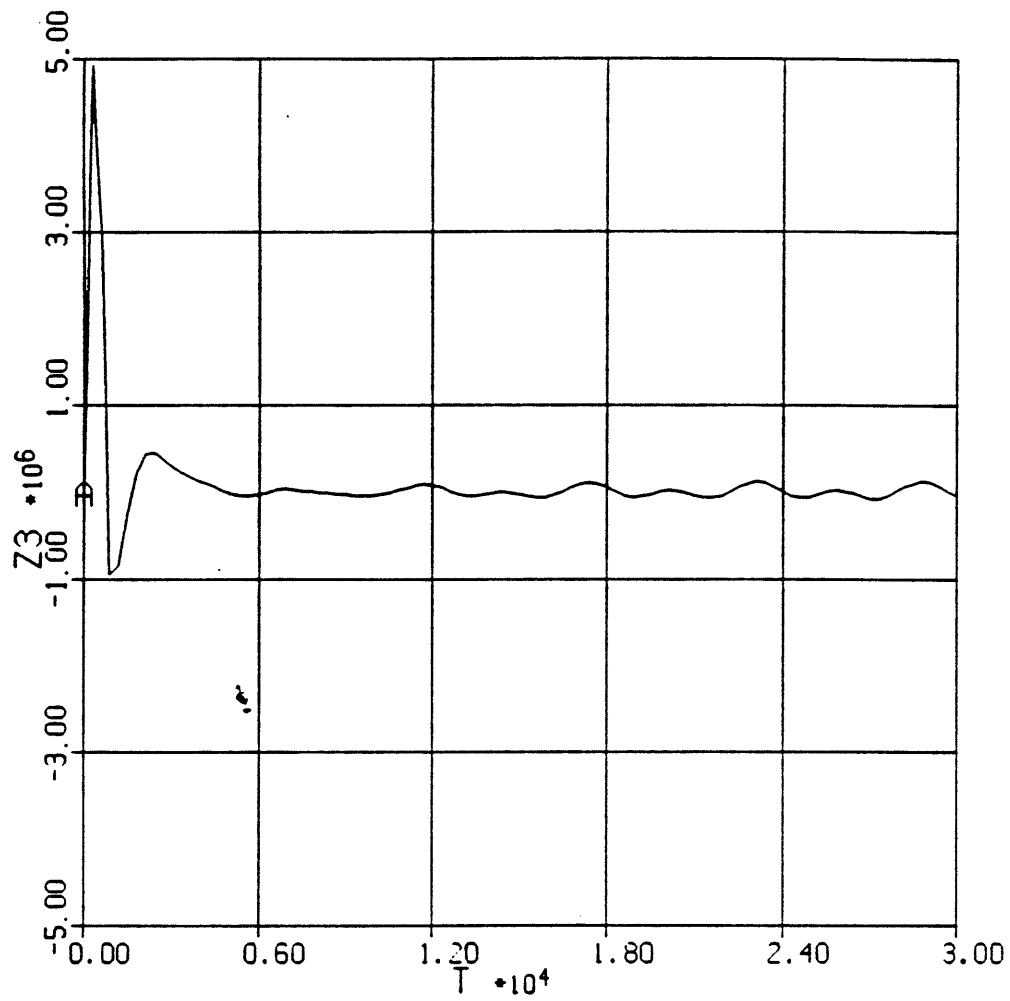




Fig. B.18 Yaw angle (rad) v.s Time (sec)

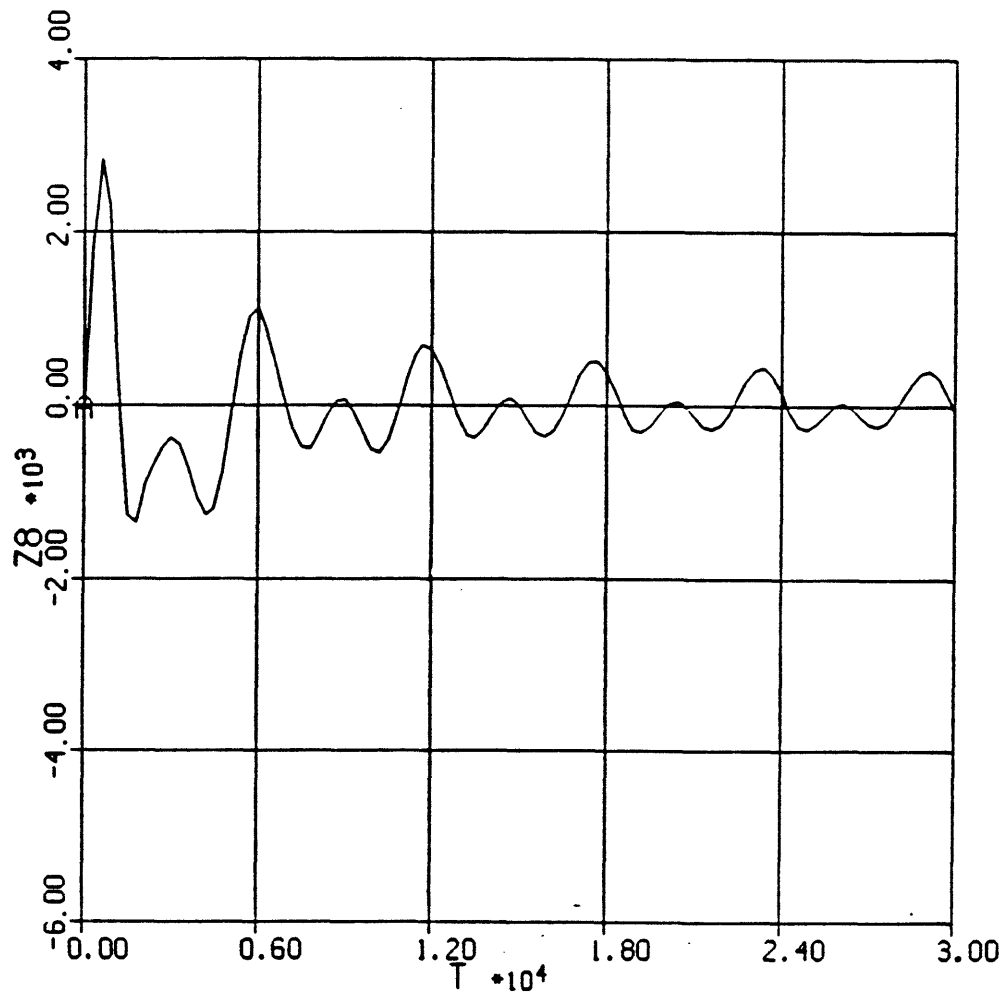


Fig. B.17 Roll angle (rad) v.s Time (sec)

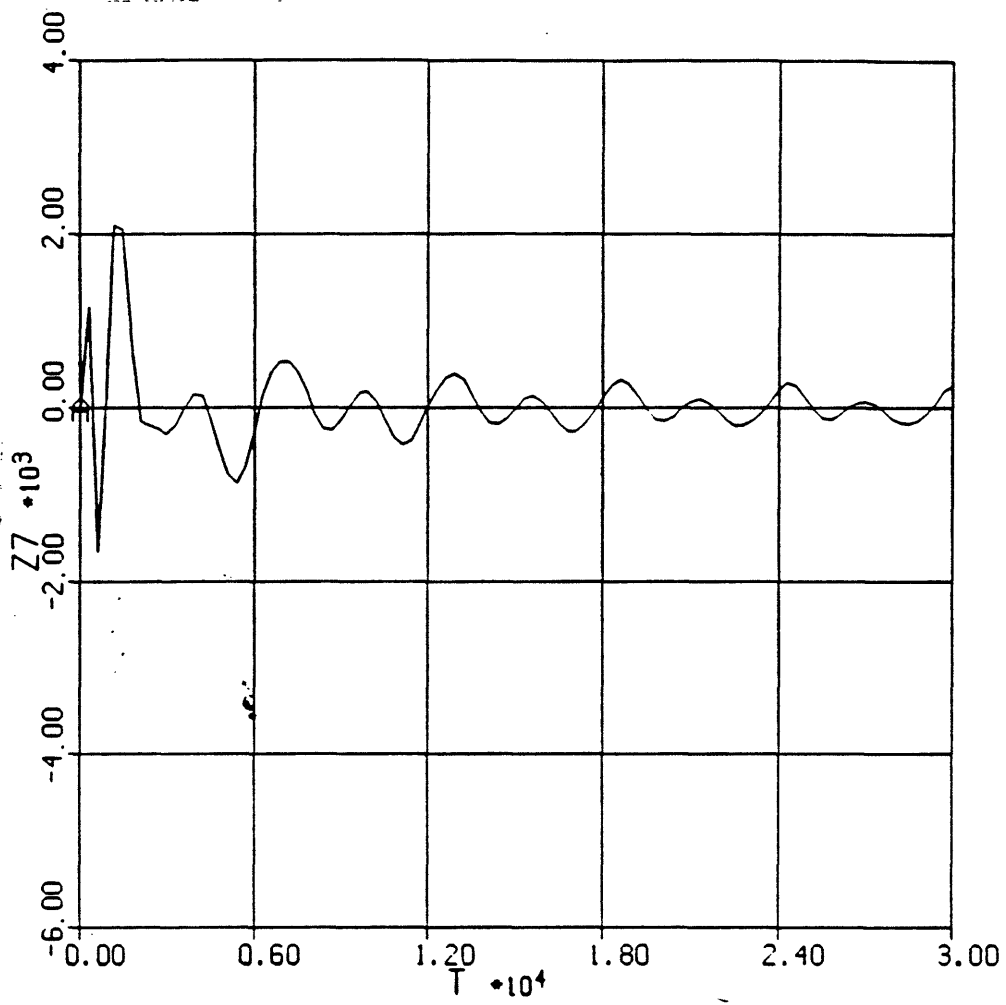


Fig. B.20 Yaw axis momentum (ft.lb.sec) v.s Time (sec)

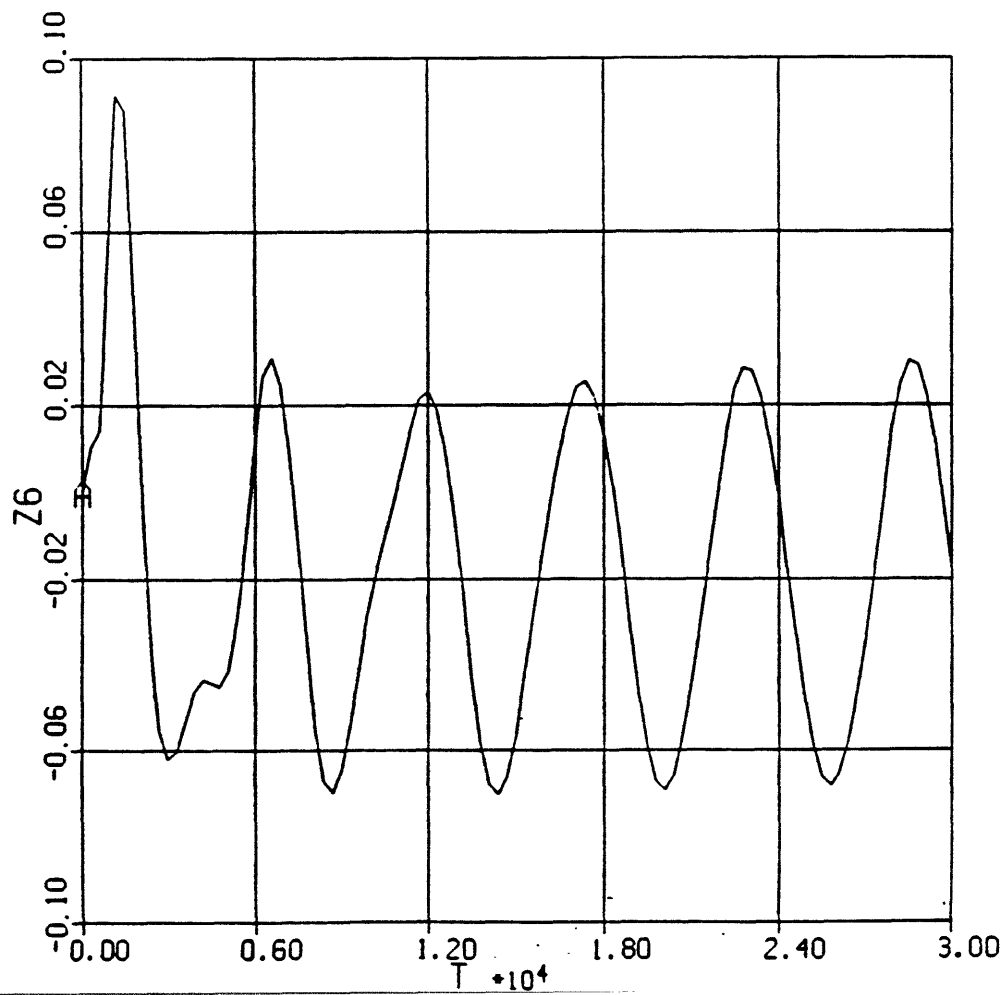


Fig. B.19 Roll axis momentum (ft.lb.sec) v.s Time (sec)

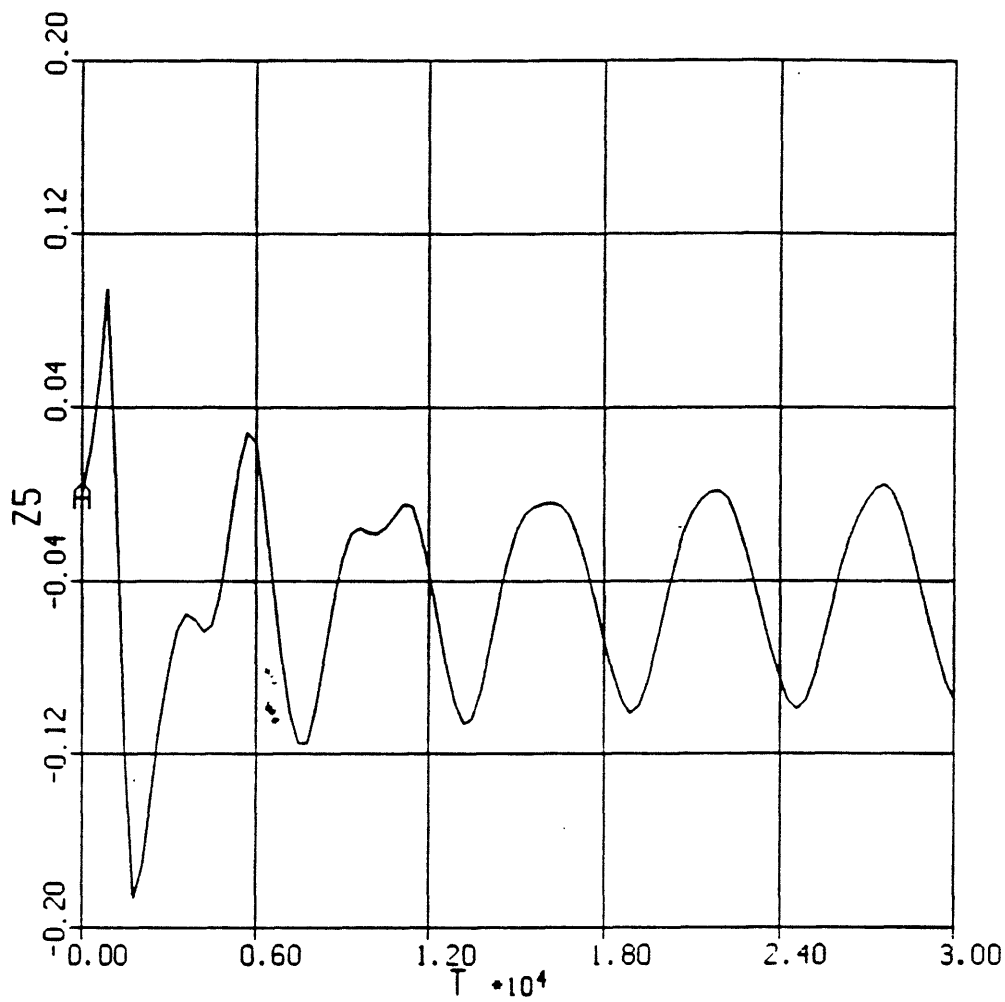


Fig. B.22 Yaw axis integral of momentum (ft.lb) v.s Time (sec)

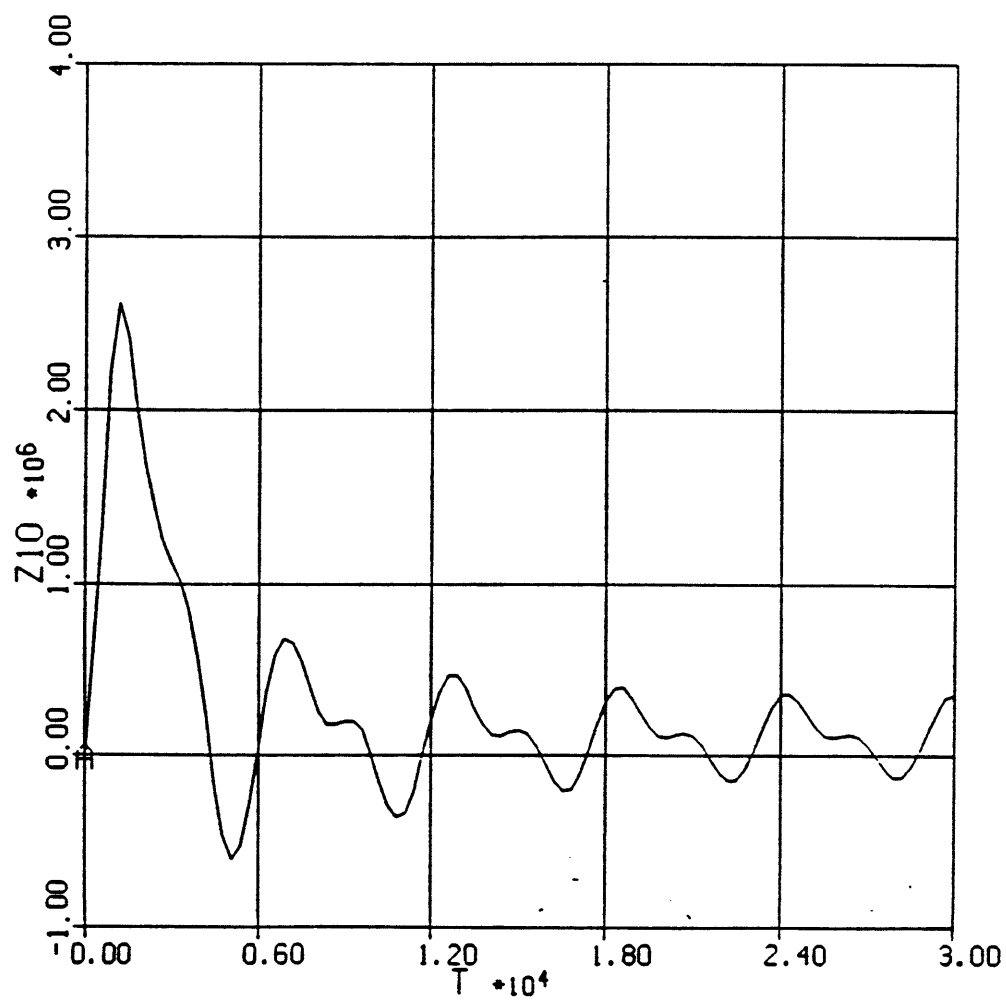


Fig. B.21 Roll axis integral of momentum (ft.lb) v.s Time (sec)

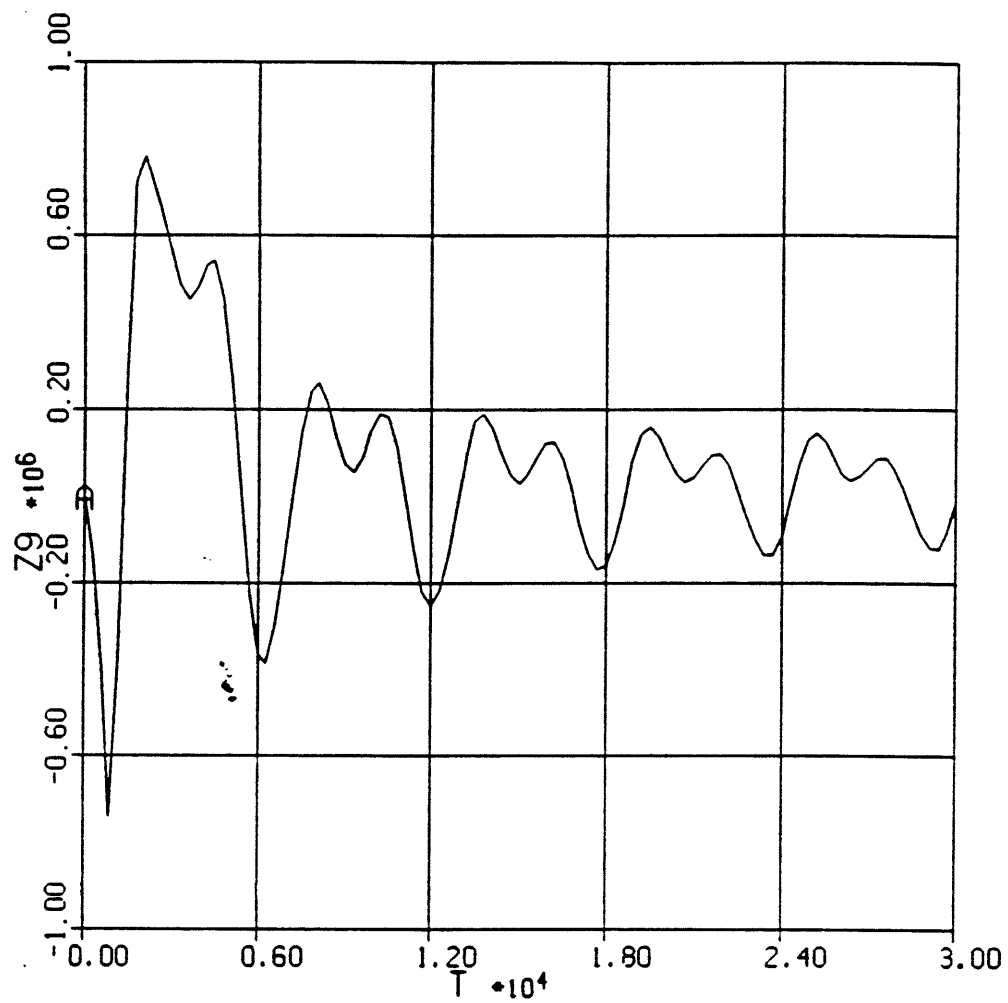


Fig. B.23 Roll axis CMG control torque (ft.lb) v.s Time (sec)

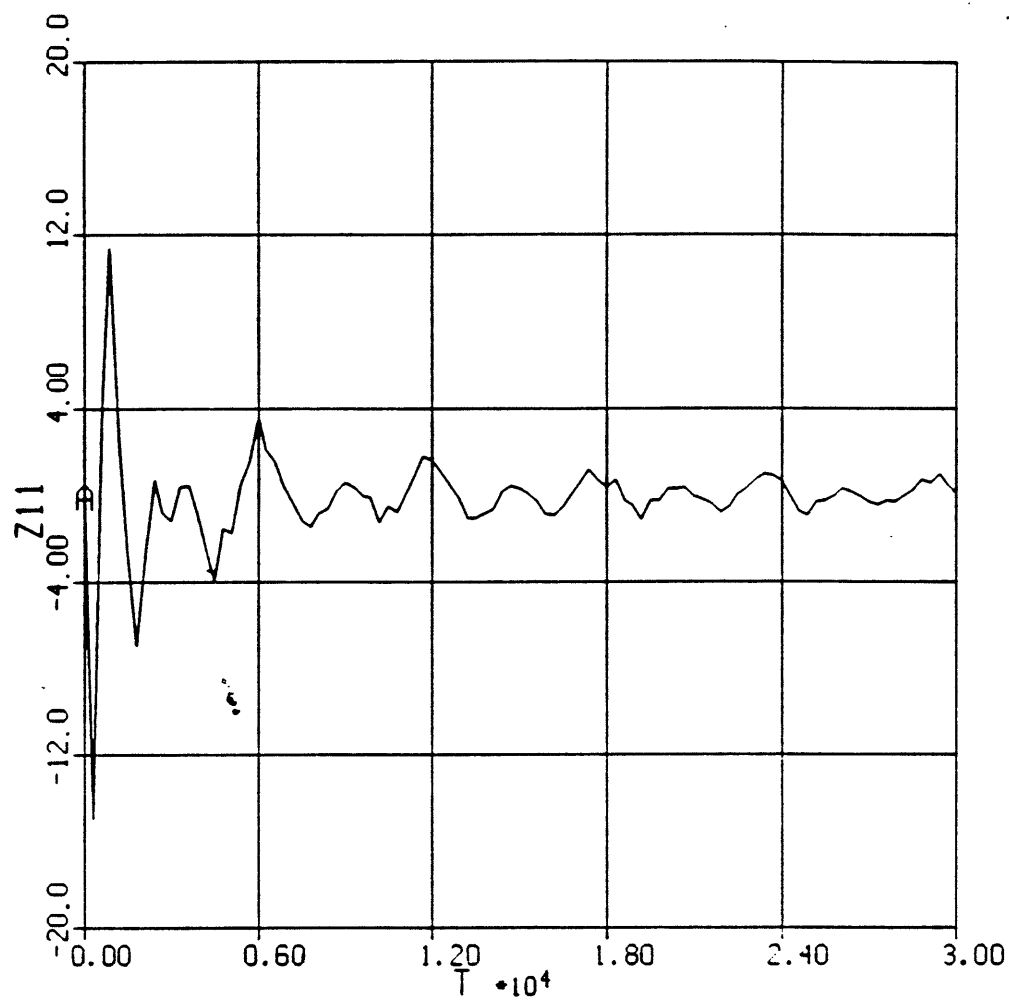
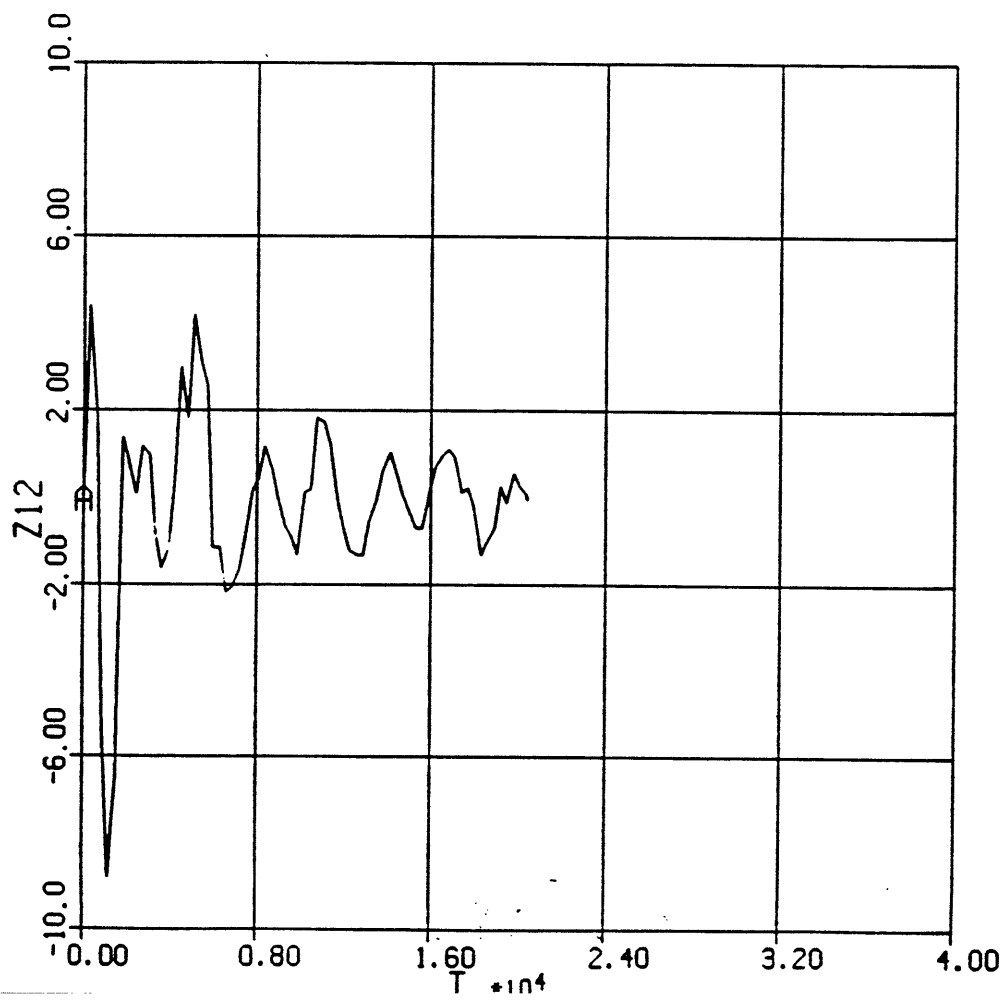


Fig. B.24 Yaw axis CMG control torque (ft.lb) v.s Time (sec)



## **APPENDIX C**

### **FREQUENCY RESPONSE**

## **BODE PLOTS**

Fig. C.1  $\frac{\theta_2}{\omega_2}(j\omega)$  v.s frequency (rad/sec)

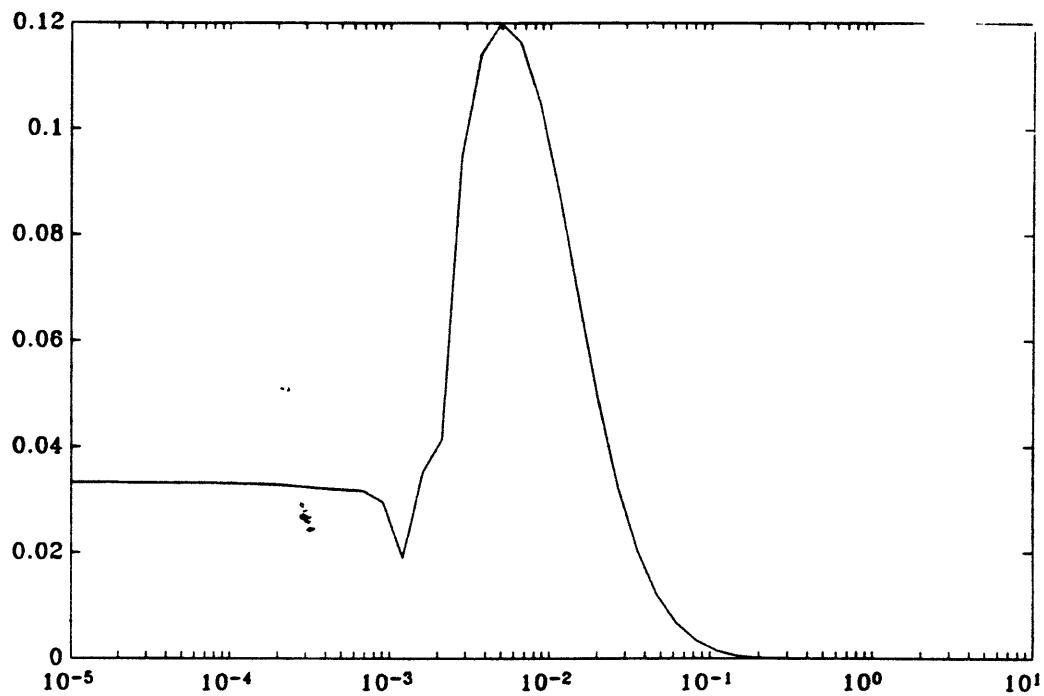


Fig. C.2  $\frac{h_2}{\omega_2}(j\omega)$  v.s frequency (rad/sec)

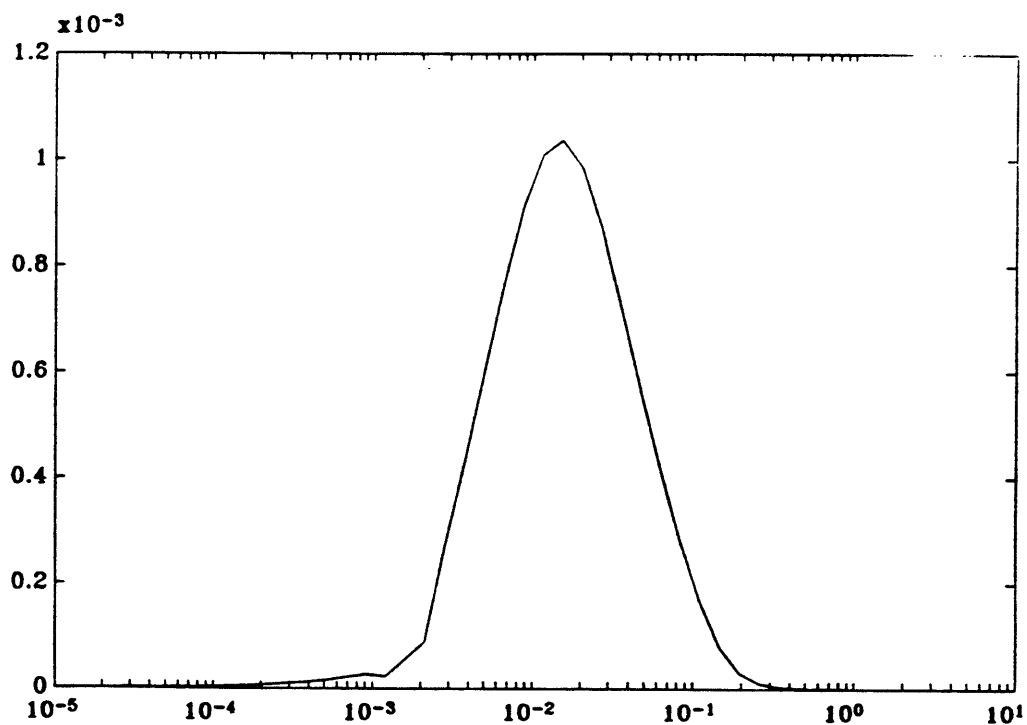


Fig. C.3  $\frac{h_1}{w_3}(j\omega)$  v.s frequency (rad/sec)

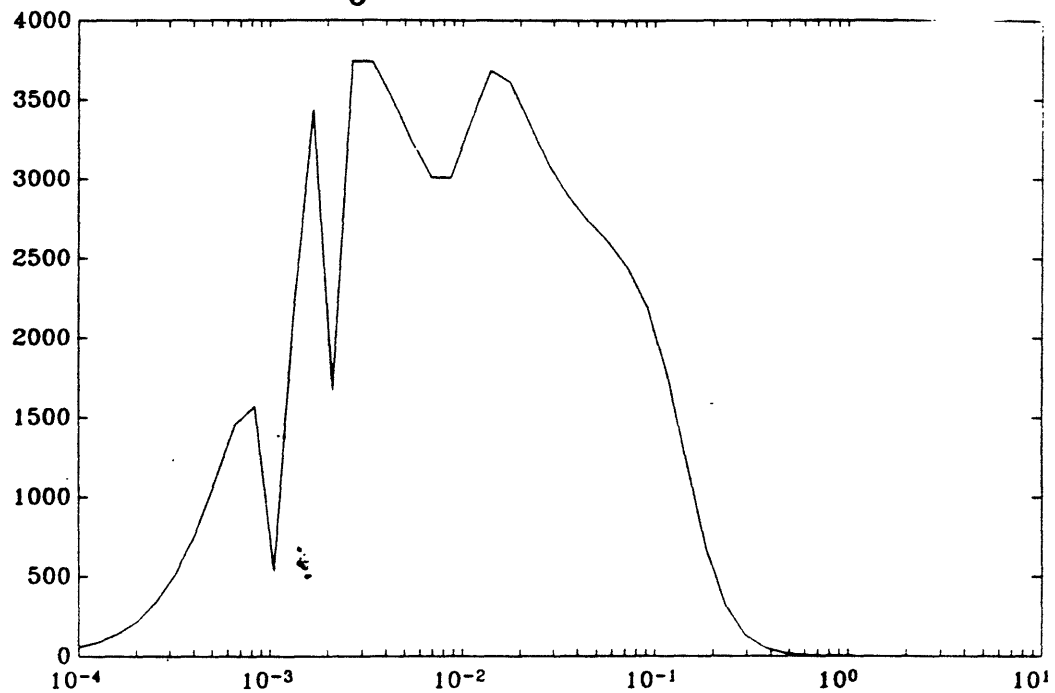


Fig. C.4  $\frac{h_1}{w_1}(j\omega)$  v.s frequency (rad/sec)

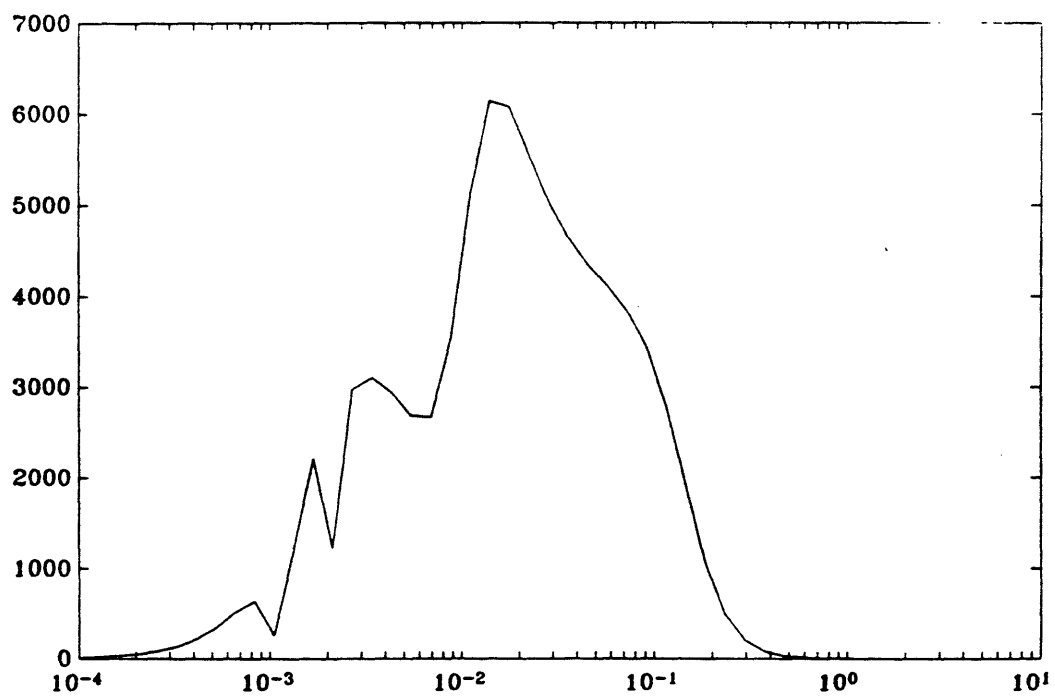




Fig. C.5  $\frac{h_3}{w_1}(j\omega)$  v.s frequency (rad/sec)

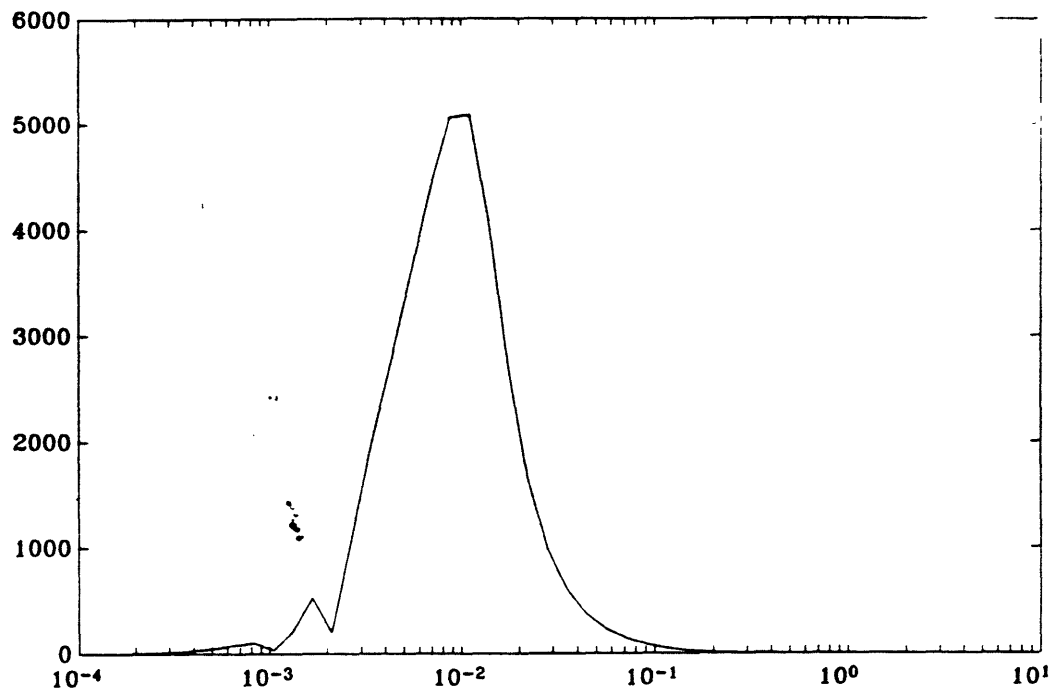


Fig. C.6  $\frac{h_3}{w_3}(j\omega)$  v.s frequency (rad/sec)

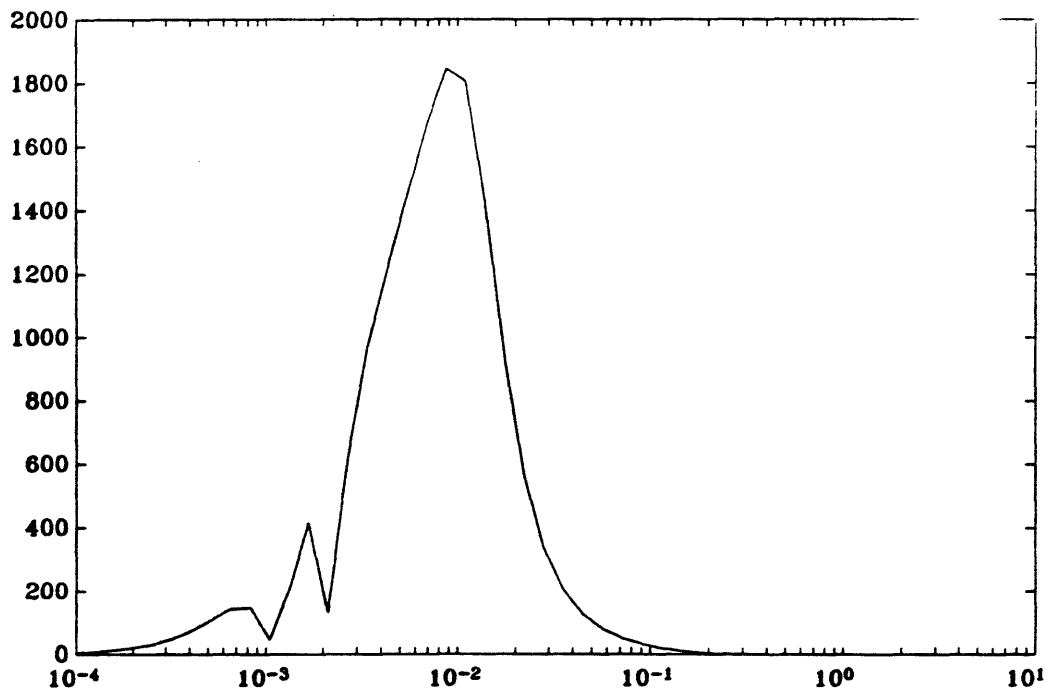


Fig. C.7  $\frac{\theta_1}{\omega_1}(j\omega)$  v.s frequency (rad/sec)

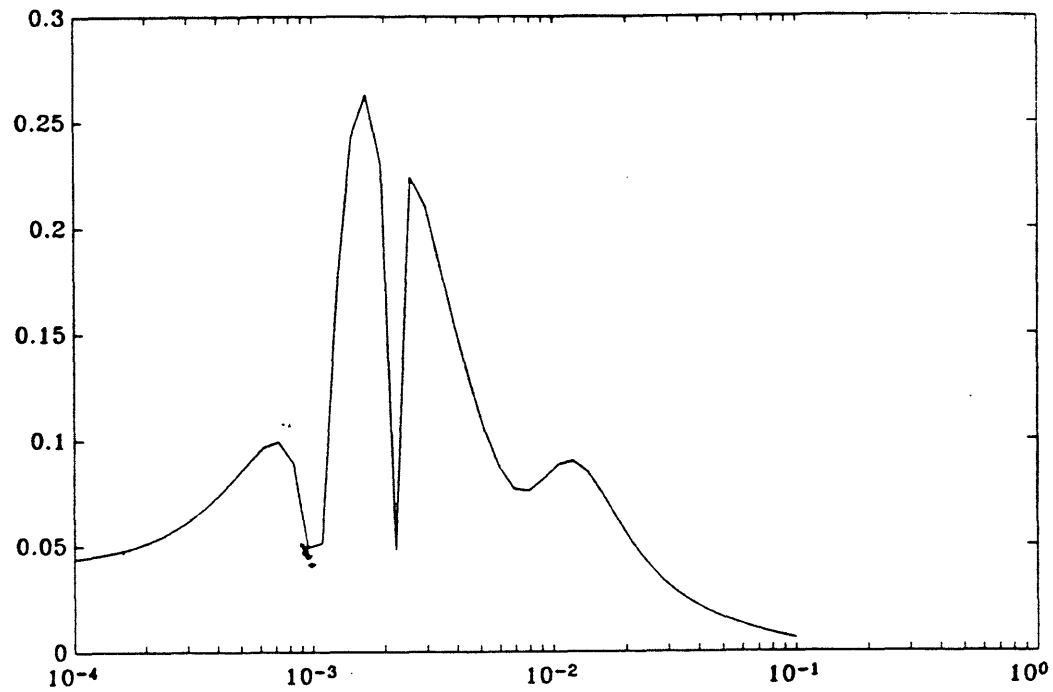


Fig. C.8  $\frac{\theta_1}{\omega_3}(j\omega)$  v.s frequency (rad/sec)

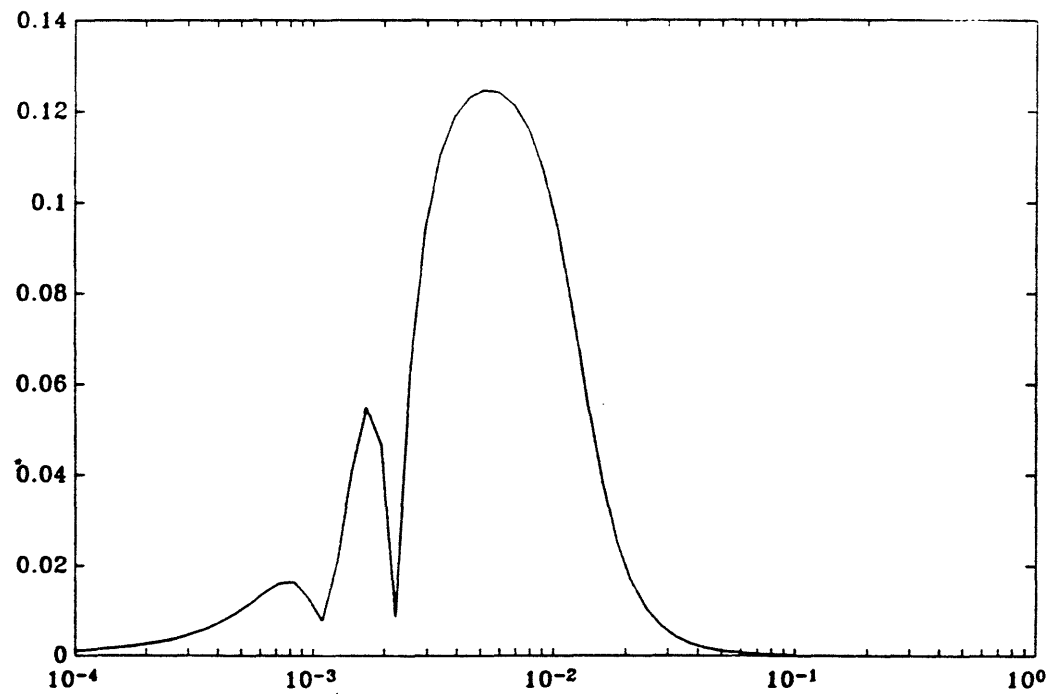


Fig. C.9  $\frac{\theta_3}{\omega_1}(j\omega)$  v.s frequency (rad/sec)

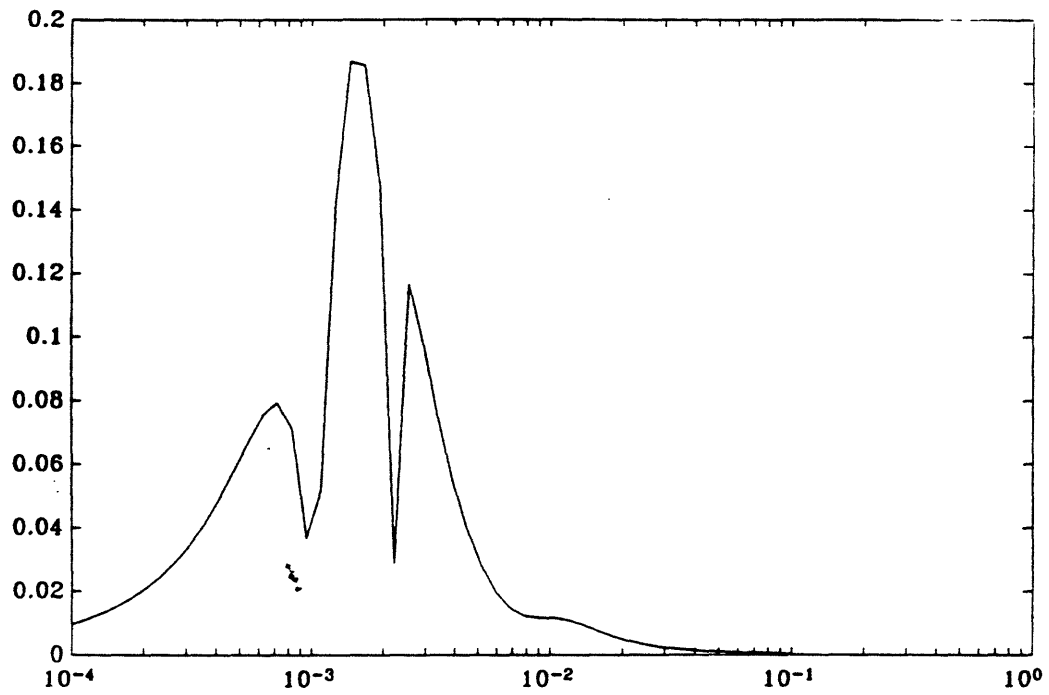
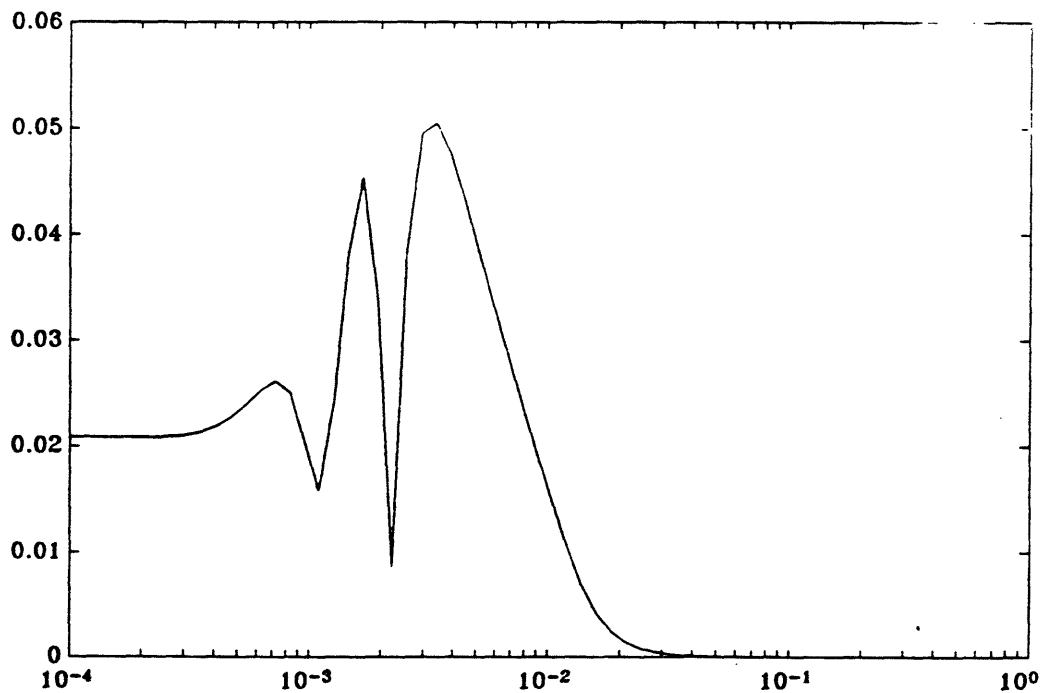


Fig. C.10  $\frac{\theta_3}{\omega_3}(j\omega)$  v.s frequency (rad/sec)



## **SINGULAR VALUE PLOTS**

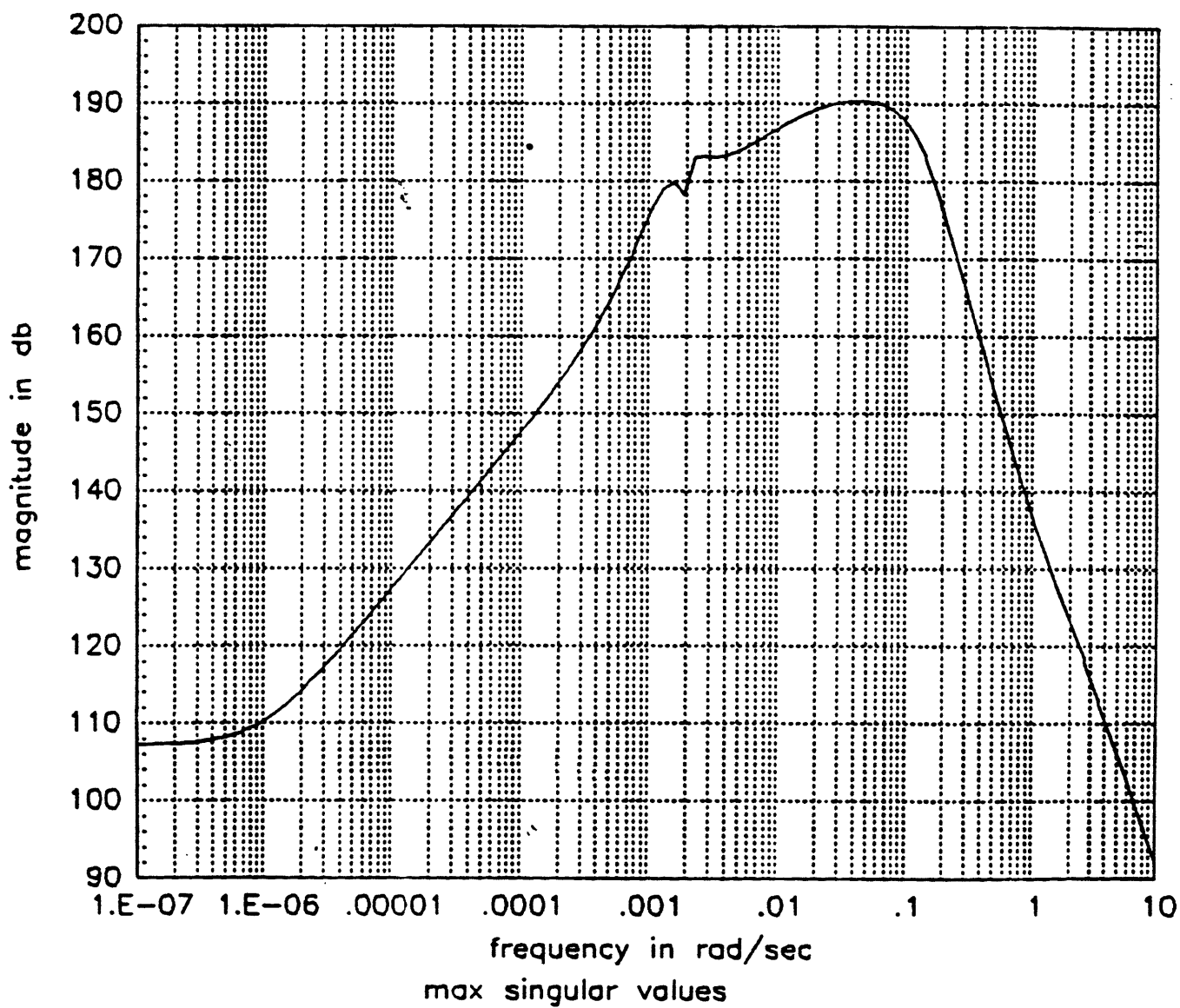


Fig. C.11  $\sigma_{\max}[H_{zw}(j\omega)]$  v.s frequency (rad/sec)  
pitch

Fig. C.12  $\sigma_{\max} \left[ \frac{\theta_2}{\text{dist}} (j \omega) \right]$  v.s frequency (rad/sec)

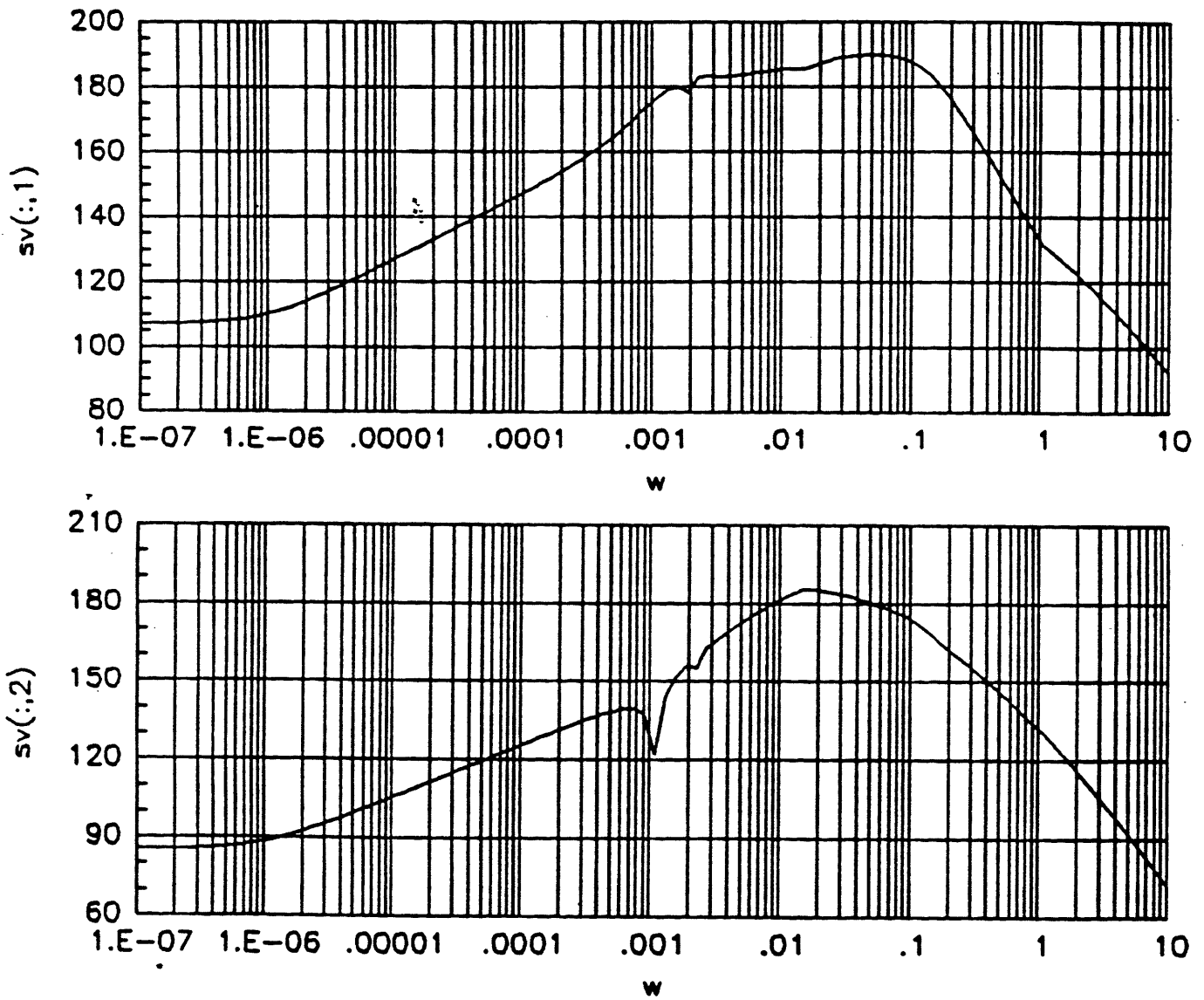


Fig. C.13  $\sigma_{\max} \left[ \frac{h_2}{\text{dist}} (j \omega) \right]$  v.s frequency (rad/sec)

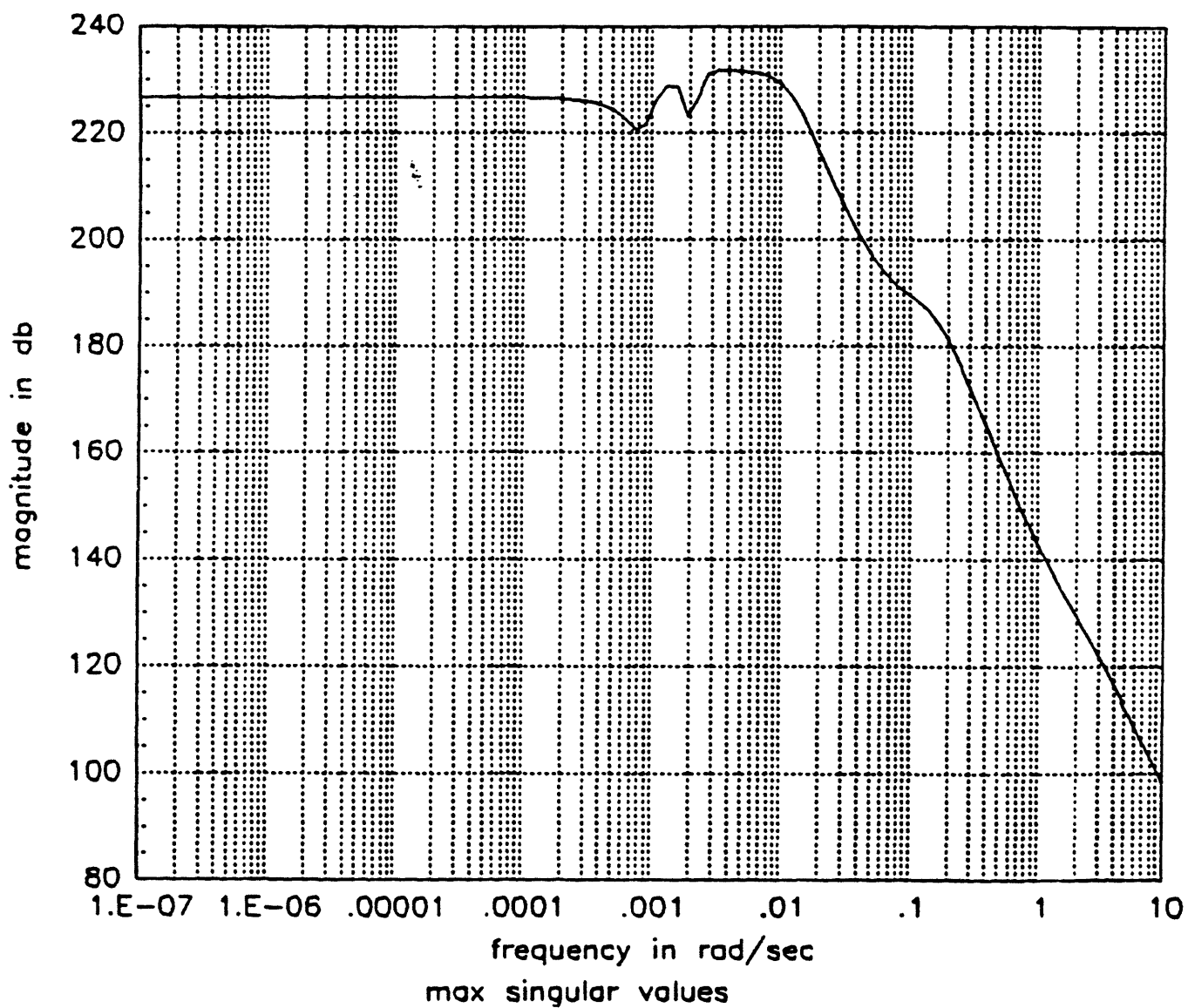


Fig. C.14  $\sigma_{\max}[H_{zw}(j\omega)]_{\text{roll/yaw}}$  v.s frequency (rad/sec)

Fig. C.15  $\sigma_{\max} \left[ \frac{\theta_1}{\text{dist}} (j \omega) \right]$  v.s frequency (rad/sec)

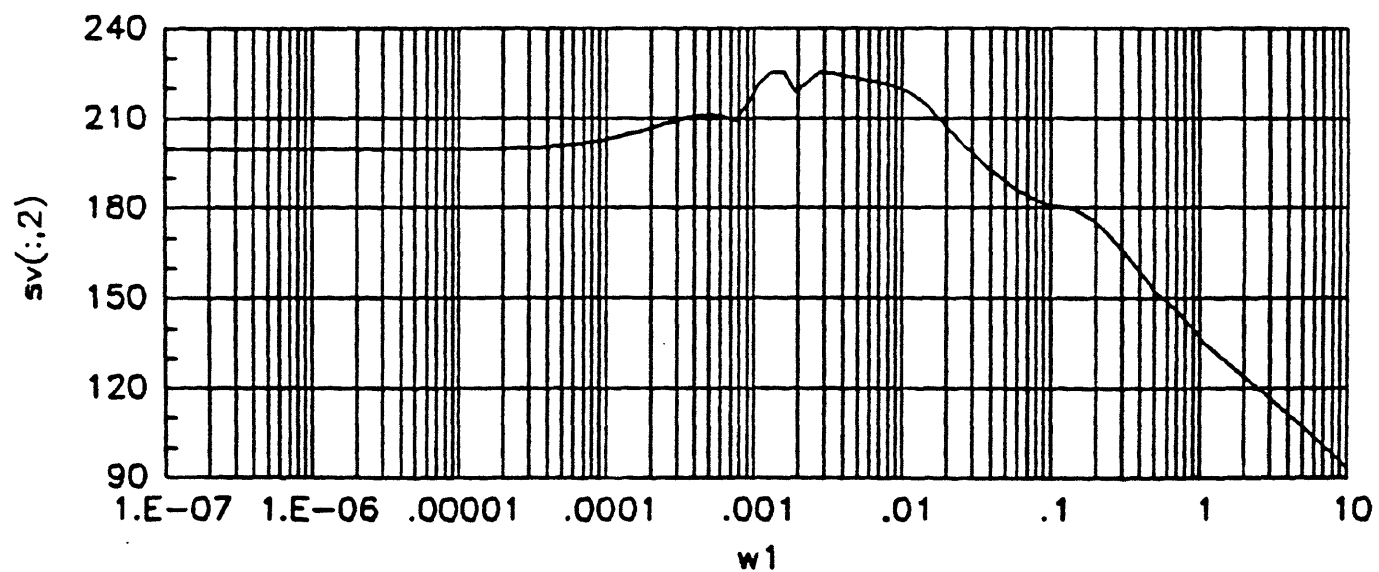
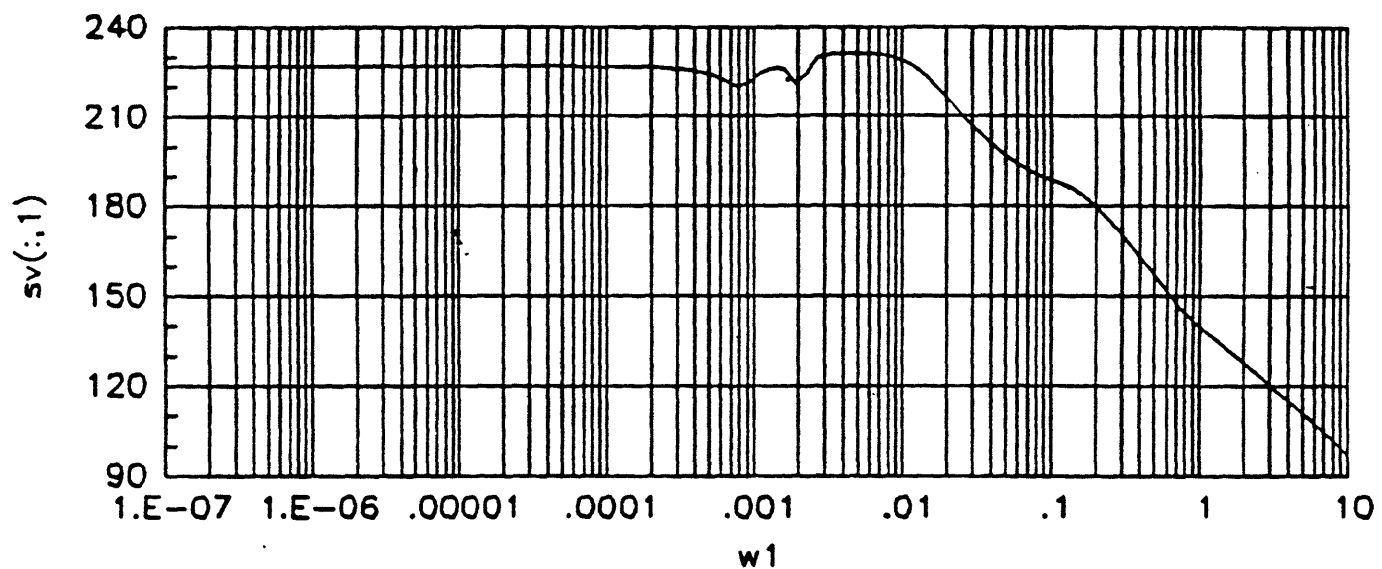


Fig. C.16  $\sigma_{\max} \left[ \frac{\theta_3}{\text{dist}} (j \omega) \right]$  v.s frequency (rad/sec)



Fig. C.17  $\sigma_{\max} \left[ \frac{h_1}{\text{dist}} (j \omega) \right]$  v.s frequency (rad/sec)

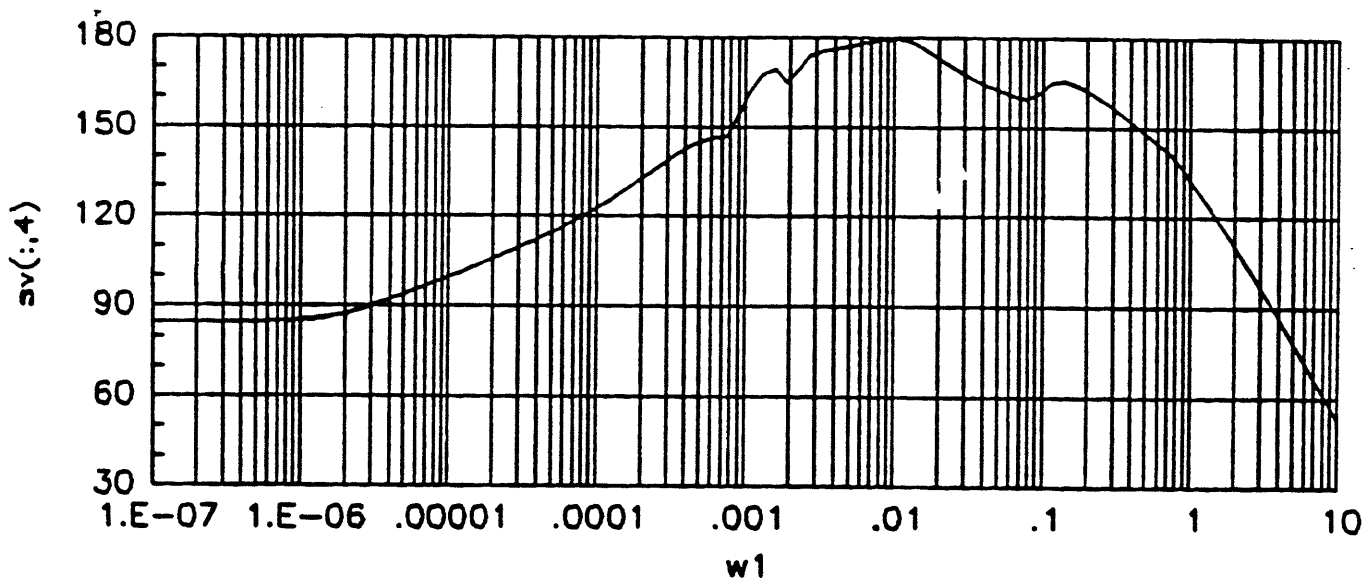
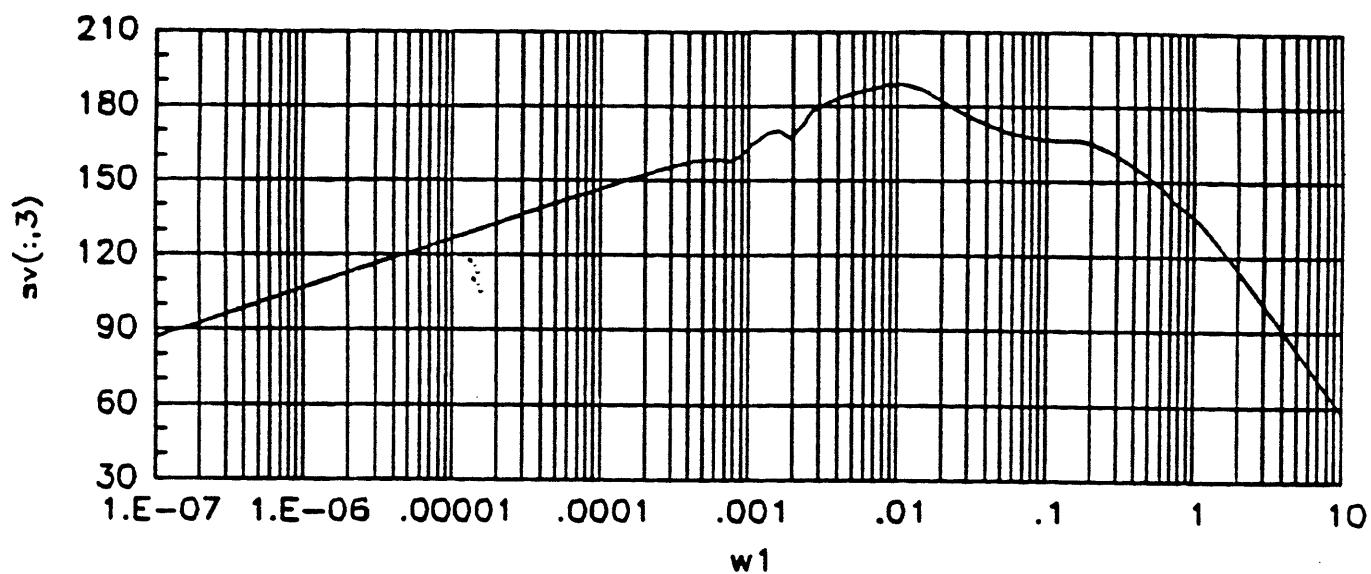


Fig. C.18  $\sigma_{\max} \left[ \frac{h_3}{\text{dist}} (j \omega) \right]$  v.s frequency (rad/sec)

Fig. C.19  $\sigma_{\max} \left[ \frac{\int h_1}{\text{dist}} (j \omega) \right]$  v.s frequency (rad/sec)

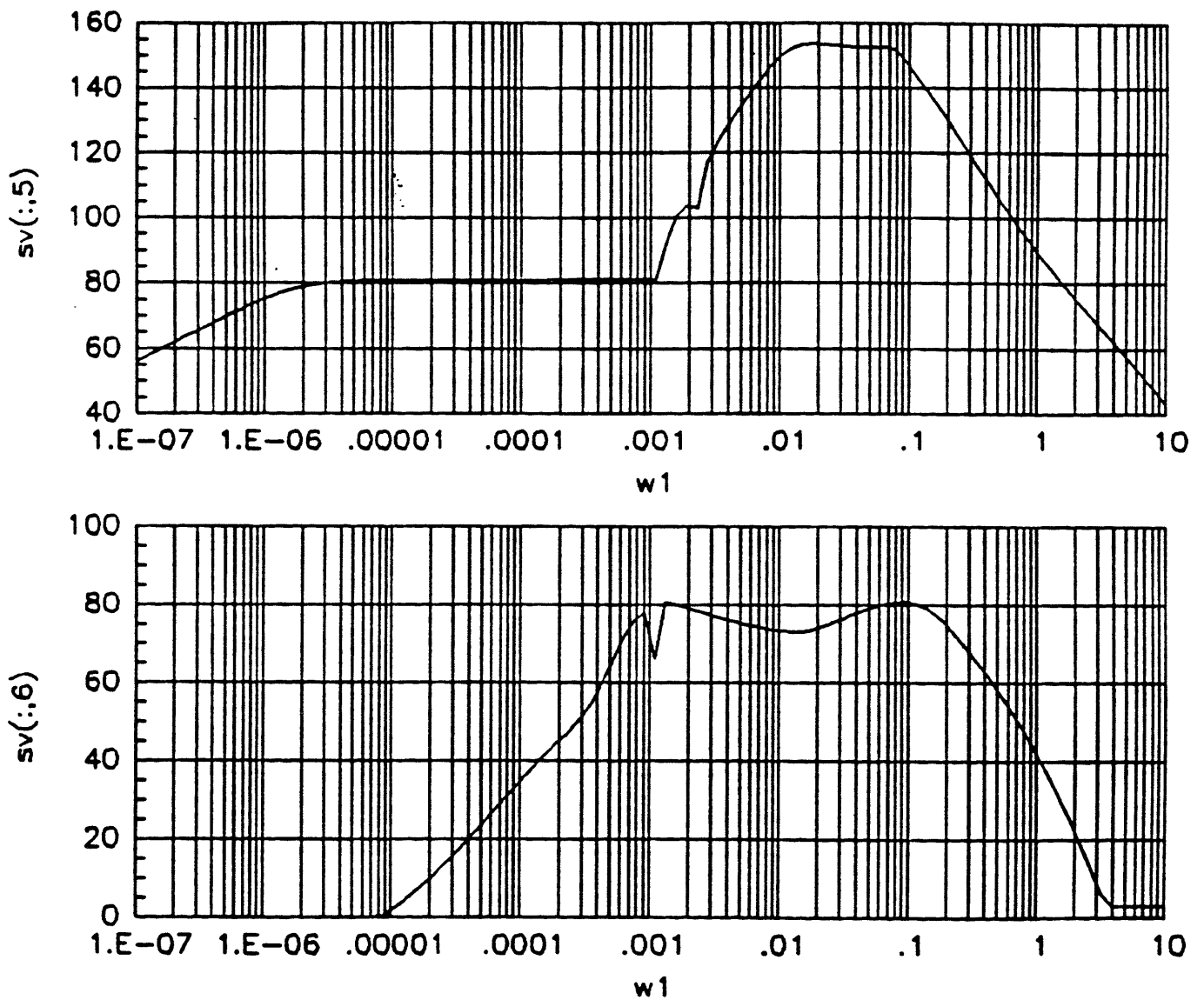


Fig. C.20  $\sigma_{\max} \left[ \frac{\int h_3}{\text{dist}} (j \omega) \right]$  v.s frequency (rad/sec)

Fig. C.21  $\sigma_{\max} \left[ \frac{u_1}{\text{dist}} (j \omega) \right]$  v.s frequency (rad/sec)

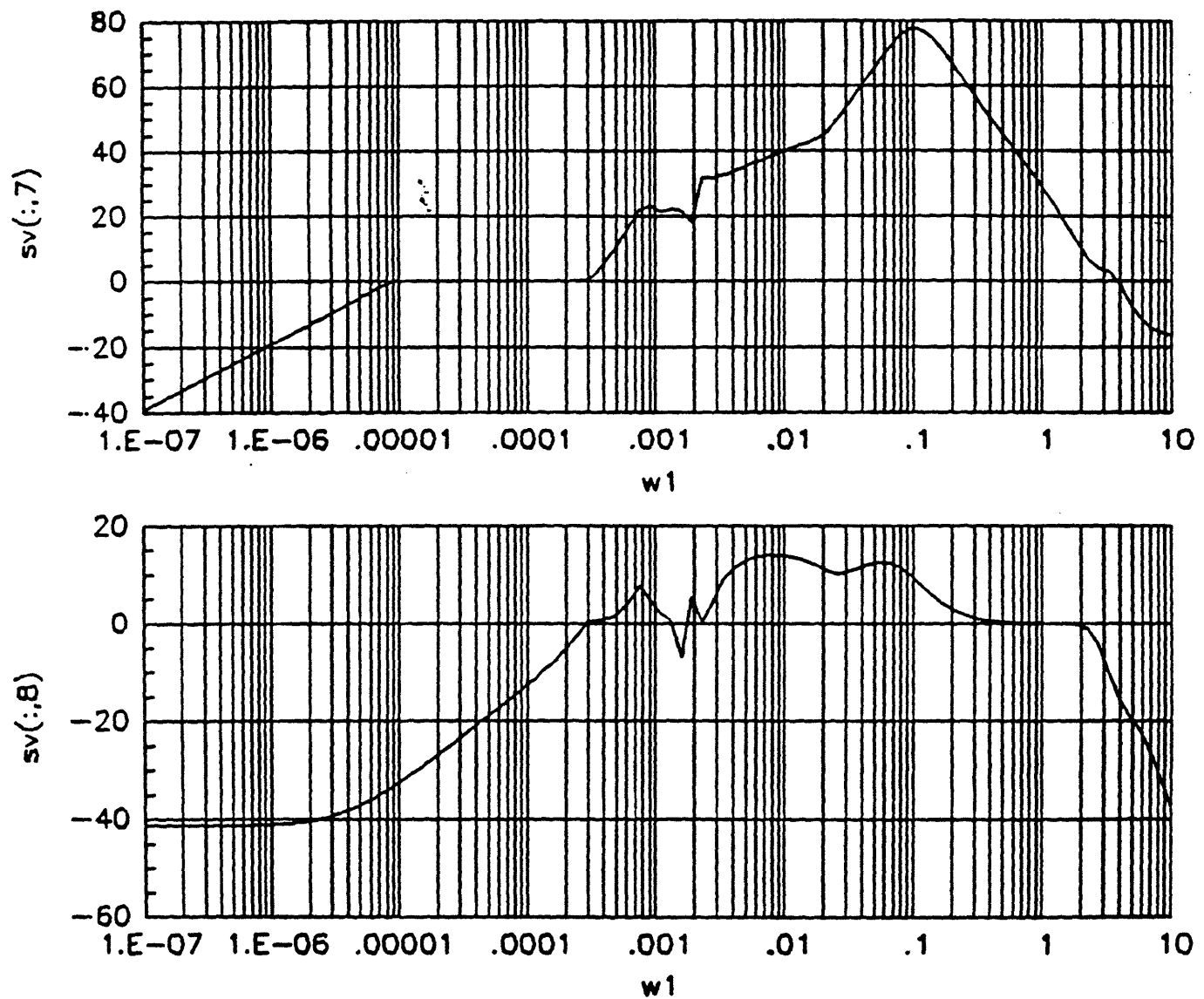


Fig. C.22  $\sigma_{\max} \left[ \frac{u_3}{\text{dist}} (j \omega) \right]$  v.s frequency (rad/sec)